AD-A278 158

Technical Report 1636
November 1993

The Effects of a Multipath Channel and Interference on Coherent *M*-PSK Digital Communication Systems

R. C. North
R. A. Axford
D. Bryan

DTIC
ELECTE
APR 13 1994
S G D

94-11233

DTIC QUALITY INSPECTED 3

Approved for public release; distribution is unlimited.

94 4 12 156

Technical Report 1636
November 1993

The Effects of a Multipath Channel and Interference on Coherent *M*-PSK Digital Communication Systems

R. C. North
R. A. Axford
D. Bryan

Accesion For		
NTIS CRA&I		☒
DTIC TAB		☐
Unannounced		☐
Justification		
By		
Distribution /		
Availability Codes		
Dist	Avail and / or Special	
A-1		

NAVAL COMMAND, CONTROL AND OCEAN SURVEILLANCE CENTER
RDT&E DIVISION
San Diego, California 92152–5001

K. E. EVANS, CAPT, USN
Commanding Officer

R. T. SHEARER
Executive Director

ADMINISTRATIVE INFORMATION

This work was performed during FY 1993. The work was performed under project RC32W11 of the Communications and Networking Block Program (CS2B). This Block Program is managed by Naval Command, Control and Ocean Surveillance Center, RDT&E Division (NRaD) under the guidance and direction of the Chief of Naval Research. The work was funded under program elements 0602232N and 0602234N (work unit number 804–P876–01), and performed by members of the Communication Technology and Systems Branch (Code 824), Electro-Optic Systems Branch, (Code 843), and the Undersea AI and Robotics Branch (Code 563), NRaD.

Released by
J. B. Rhode, Head
Communication Technology
and Systems Branch

Under authority of
R. J. Kochanski, Head
Communications Systems
Engineering and Integration
Division

MA

SUMMARY

This report derives expressions for the average probability of symbol error of a coherent M-ary phase-shift-keyed (M-PSK) communication system operating under the following nonideal conditions:

1. time-invariant multipath channel consisting of a direct path and a single multipath,
2. intentional/unintentional interference consisting of either a continuous wave (CW) signal or a bandpass-filtered white Gaussian noise signal (bandwidth is variable), and
3. additive white Gaussian noise.

In particular, the effect each of these nonidealities, individually and in combination, has on the performance of M-PSK communication systems is analyzed. The techniques used to derive these results are not new; however, this particular application, which is common to line-of-sight (LOS) radio is thought to be original. This report can be thought of as a follow-on report to NRaD Technical Report 1510, "Effects of CW- and BPSK-Signal Interference on a Standard BPSK Digital Communications System," written by Roy A. Axford in August 1992.

One particular example, LOS ultrahigh frequency (UHF) radio, is used extensively to exercise the derived expressions and illustrate typical system performance. The average probability of symbol error is plotted as a function of M, transmit power, magnitude of the multipath, data rate and interference power, bandwidth, and carrier offset frequency. It is found that for the "frequency nonselective multipath" condition, the effects of the multipath on system performance oscillate between constructively adding and destructively adding with the direct path. However, for the "frequency selective multipath" condition, the effects of the multipath result in mostly destructive only addition with the direct path. It is also shown that finite bandwidth interference can cause more performance degradation than CW interference for the same signal-to-interference ratio. Finally, it is shown that for constant data rates, the sensitivity to channel nonidealities increases dramatically as M increases even though the symbol rate decreases as M increases.

It should be emphasized that these results pertain to a receiver with no means of compensation for the nonideal channel conditions. The authors are presently investigating methods of compensation for multipath and interference, like adaptive equalization, beamforming, spatial diversity, and multichannel adaptive equalization. In addition, the authors are also analyzing a time-varying multipath channel.

CONTENTS

1. INTRODUCTION 1-1

2. SIGNAL AND CHANNEL MODEL 2-1

2.1 SIGNAL MODEL 2-1

2.2 FIR CHANNEL MODELS FOR MULTIPATH ENVIRONMENTS 2-2

2.3 TWO-PATH CHANNEL MODEL 2-3

2.4 SIGNAL STATISTICS 2-6

3. PERFORMANCE ANALYSIS OF BPSK SIGNAL 3-1

3.1 MATCHED-FILTER DETECTION OF BPSK WITH CW INTERFERENCE 3-2

3.2 TERMS IN EQ. (3.4) 3-3

3.3 MATCHED-FILTER DETECTION OF BPSK WITH FINITE BANDWIDTH INTERFERENCE 3-4

3.4 SUMMARY AND EXAMPLES 3-7

4. PERFORMANCE ANALYSIS OF *M*-PSK SIGNAL 4-1

4.1 MATCHED-FILTER DETECTION OF *M*-PSK WITH CW INTERFERENCE 4-2

4.2 TERMS IN EQS. (4.4) AND (4.5) 4-7

4.3 MATCHED-FILTER DETECTION OF *M*-PSK WITH FINITE BANDWIDTH INTERFERENCE 4-8

4.4 SUMMARY AND EXAMPLES 4-10

5. CONCLUSION 5-1

6. REFERENCES 6-1

APPENDICES:

A. COMPLEX BASEBAND REPRESENTATION A-1

B. PERFORMANCE ANALYSIS OF BPSK SIGNAL FOR $\tau_\Delta > T$ B-1

C. PERFORMANCE ANALYSIS OF *M*-PSK SIGNAL FOR $\tau_\Delta > T$ C-1

D. DERIVATIONS D-1

FIGURES

2.1 Generation of bandpass-transmitted signal. 2-2

2.2 Multipath band-limited channel model with additive interference and noise. 2-3

2.3 Continuous-time, bandpass model of communication channel. 2-4

2.4 Differential path length and delay spread for a two-path channel. 2-5

CONTENTS (continued)

2.5 Channel impulse response and channel frequency response for a two-path channel with $\tau_\Delta = 5\ nsec$ 2–6

2.6 Channel group delay and phase response for the two-path channel in figure 2.5. 2–6

2.7 Spectrum of finite bandwidth interference at bandpass. 2–7

2.8 Components of eq. (2.21) for $f_c\tau_\Delta \in \{1, 2, ...\}$ and (a) $\tau_\Delta = 2.5\ T$, (b) $\tau_\Delta = T$, (c) $\tau_\Delta = 0.5\ T$. 2–8

3.1 Correlator implementation of matched-filter receiver for BPSK signals. 3–1

3.2 Desired and interfering baseband signals in $[0, T]$, $0 \le \tau_\Delta \le T$, $a_k = +1, a_{k-1} = -1$ (from [1]). 3–2

3.3 Possible demodulated bits during the interval $[0, T]$ for a two-path channel with $0 \le \tau_\Delta \le T$. 3–7

3.4 Effect of CW interference on the demodulated bits during the interval $[0, T]$. 3–8

3.5 Generation of the average probability of bit error for a BPSK signal transmitted through a two-path channel with $0 < \tau_\Delta \le T$, CW interference and AWGN. 3–9

3.6 Generation of the average probability of bit error for a BPSK signal transmitted through a two-path channel with $0 < \tau_\Delta \le T$, finite bandwidth interference and AWGN. 3–9

3.7 Effects of multipath on BPSK, $\tau_\Delta = 0.0077\ T$. 3–12

3.8 Effects of multipath on BPSK, (a) $\tau_\Delta = 0.25\ T$, (b) $\tau_\Delta = 0.5\ T$, (c) $\tau_\Delta = 1.0\ T$. 3–13

3.9 System performance of a BPSK signal transmitted through a multipath channel, $\tau_\Delta = 5\ \eta$sec, for 1,10,50,100,150,200 Mbps data rates. 3–14

3.10 System performance as a function of data rate for a BPSK signal transmitted through a multipath channel, $\tau_\Delta = 5\ \eta$sec. 3–15

3.11 BPSK probability of bit error for (a) CW interferer with no multipath, (b) and (c) CW interferer with multipath, $\tau_\Delta = 0.0077\ T$. 3–16

3.12 BPSK probability of bit error for (a) and (b) CW or finite bandwidth interferer with no multipath, (c) CW or finite bandwidth interferer with multipath, $\tau_\Delta = 0.0077\ T$. 3–17

3.13 BPSK probability of bit error as a function of (a) interference bandwidth and (b) interference offset frequency for the case of no multipath. 3–18

4.1 Correlator implementation of matched-filter receiver for M-PSK signals. 4–1

4.2 8-PSK (a) constellation with decision boundaries, (b) bit-mapping using Gray encoding. 4–2

CONTENTS (continued)

4.3 Possible demodulated symbols during the interval [0, T] for a QPSK signal transmitted through a two-path channel with $0 \leq \tau_\Delta \leq T$. 4–10

4.4 Generation of the average probability of symbol error for an M-PSK signal transmitted through a two-path channel model with $0 \leq \tau_\Delta \leq T$ and AWGN. 4–12

4.5 Comparison of exact (dashed) and upper bound (solid) expressions for probability of symbol error. 4–12

4.6 Generation of the average probability of symbol error for an M-PSK signal transmitted through a two-path channel model with $0 \leq \tau_\Delta \leq T$, additive CW interference and AWGN. 4–14

4.7 Generation of the average probability of symbol error for an M-PSK signal transmitted through a two-path channel model with $0 \leq \tau_\Delta \leq T$, additive finite bandwidth interference and AWGN. 4–15

4.8 Effects of multipath as a function of carrier frequency for (a) QPSK S=5 dB, (b) 8–PSK S=10 dB, (c) 16–PSK S=20 dB and $\tau_\Delta = 0.0077\ T$. 4–16

4.9 Performance of M-PSK for fixed data rate of 1.544 Mbps and (a) no multipath, (b) $H_2 = -0.4, \tau_\Delta = 5\ \eta$sec, (c) $H_2 = -0.8, \tau_\Delta = 5\ \eta$sec. 4–17

4.10 Performance of M-PSK for fixed data rate of 10 Mbps and (a) no multipath, (b) $H_2 = -0.4, \tau_\Delta = 5\ \eta$sec, (c) $H_2 = -0.8, \tau_\Delta = 5\ \eta$sec. 4–18

4.11 Performance of M-PSK for fixed data rate of 50 Mbps and (a) no multipath, (b) $H_2 = -0.4, \tau_\Delta = 5\ \eta$sec, (c) $H_2 = -0.8, \tau_\Delta = 5\ \eta$sec. 4–19

4.12 Performance of M-PSK for fixed data rate of 100 Mbps and (a) no multipath, (b) $H_2 = -0.4, \tau_\Delta = 5\ \eta$sec, (c) $H_2 = -0.8, \tau_\Delta = 5\ \eta$sec. 4–20

4.13 Performance of M-PSK for fixed data rate of 200 Mbps and (a) no multipath, (b) $H_2 = -0.4, \tau_\Delta = 5\ \eta$sec, (c) $H_2 = -0.8, \tau_\Delta = 5\ \eta$sec. 4–21

4.14 Performance of M-PSK for increasing interference power and –20-dB noise power (a) CW Interference, (b) B = 1-Hz interference, (c) B = 10-MHz interference. 4–22

4.15 Performance of M-PSK for increasing carrier offset frequency (a) CW interference, (b) 1-Hz bandwidth interference, (c) 10-MHz bandwidth interference. 4–23

TABLE

4.1. Data rate, symbol rate, and τ_Δ/T for M = 2, 4, 8, 16 and $\tau = 5\ \eta$sec. 4–13

CONTENTS (continued)

FIGURES–APPENDICES

A.1 Continuous-time, complex baseband model of the communication channel. A–2

A.2 Spectrum of finite bandwidth interference at baseband. A–4

B.1 Desired and interfering baseband signals in $[0, T]$, $\gamma T \leq \tau_\Delta \leq (\gamma + 1)T$, $a_{k-\gamma} = +1, a_{k-(\gamma+1)} = -1$. B–2

B.2 Generation of the average probability of bit error for a transmitted BPSK signal through the two-path channel model with $\tau_\Delta > T$ and additive CW interference and AWGN. B–5

B.3 Generation of the average probability of bit error for a transmitted BPSK signal through the two-path channel model with $\tau_\Delta > T$ and additive finite bandwidth interference and AWGN. B–5

C.1 Generation of the average probability of symbol error for a transmitted M-PSK signal through the two-path channel model with $\tau_\Delta > T$ and AWGN. C–4

C.2 Generation of the average probability of symbol error for a transmitted M-PSK signal through the two-path channel model with $\tau_\Delta > T$, additive C interference and AWGN. C–5

C.3 Generation of the average probability of symbol error for a transmitted M-PSK signal through the two-path channel model with $\tau_\Delta > T$, additive finite bandwidth interference and AWGN. C–5

1. INTRODUCTION

This report derives expressions for the average probability of symbol error of a coherent M-ary phase-shift-keyed (M-PSK) communication system operating under the following nonideal conditions:

1. time-invariant multipath channel consisting of a direct path and a single multipath,
2. intentional/unintentional interference consisting of either a CW or a bandpass filtered white Gaussian noise signal (bandwidth is variable), and
3. additive white Gaussian noise.

In particular, the effect each of these nonidealities, individually and in combination, has on the performance of M-PSK communication systems is analyzed. Let the reader be forewarned, the techniques required to derive these results can get long and tedious. Every effort has been made to present the results in a concise and readable form. While all steps are either shown explicitly or described in the text, the unfamiliar reader might first start with [1]. This report is meant to be a follow-on to "Effects of CW- and BPSK-Signal Interference on a Standard BPSK Digital Communications System" by Roy A. Axford.

The text is organized as follows. Chapter 2 introduces the signal model and the finite impulse response (FIR) filter channel model. The FIR filter channel model is an intuitively good choice for a multipath environment due to its similarity to the physical propagation modes in the channel. However, the FIR filter channel model is not a physical propagation model (sometimes called an atmospheric model), but instead is meant only to describe the (possibly time-varying) frequency response of the channel over the bandwidth of interest [2]. The interrelation between the two types of models is not addressed here.

Chapter 3 derives expressions for the average probability of bit error for a coherent binary phase-shift-keyed (BPSK) signal and a delay spread less than the bit/symbol duration, $0 \le \tau_\Delta \le T$. Appendix B extends these results for $\tau_\Delta > T$. Chapter 4 and appendix C derive expressions for the average probability of symbol error for a coherent M-PSK signal with $0 \le \tau_\Delta \le T$ and $\tau_\Delta > T$ respectively. The problem of accurately computing the error probability of a digital communication system with intersymbol interference (ISI) has been addressed frequently over the past 25 years (see for example [3] for an excellent overview). Since the number of terms for I symbols of corruption in a M-ary system is $O(M^I)$, in general either error bounds (see for example [4]) or approximations (see for example [5]) must be made for tractable solutions.

The method used in this report is to treat the time-invariant two-path channel, thus I=1, with additive interference and additive white Gaussian noise (AWGN). While real channels will be time-variant, this model provides tractable solutions as well as being valid over short time intervals in a slowly fading channel. Future work will concentrate on removing the time-invariant channel restriction. Exact solutions are derived in chapter 3 for coherent BPSK while both exact and upper bound solutions (shown to be tighter than the Chernoff bound) are presented in chapter 4 for coherent M-PSK. Finally, chapter 5 contains a summary of the important results.

It is expected that the information contained in this report can be applied to any time-invariant two-path M-PSK communication channel with or without interference, for example HF, VHF, UHF, or SHF LOS communication systems. One particular example, UHF LOS radio, is used extensively throughout the text to support the UHF high data rate LOS communication project currently in

progress at NRaD. A delay spread of $\tau_\Delta = 5\ \eta$ sec is found in chapter 2 to be a reasonable value for LOS communication between two ships and, thus, this value is used in many of the examples. To fully exercise the τ_Δ/T dependence of the derived expressions in the UHF LOS examples, the value of the symbol rate, $R = 1/T$, is increased while the delay spread, $\tau_\Delta = 5\ \eta$ sec , is kept constant. However, for a delay spread of $\tau_\Delta = 5\ \eta$ sec, the data rate must get very large to illustrate the τ_Δ/T dependence, for example when $\tau_\Delta = T$, $R = 200$ Msps. These extremely large symbol rates are ***only*** possible with the assumptions made in this report, most notably, perfectly coherent demodulation and a time-invariant channel. In practice, these conditions cannot be met exactly and will no doubt limit the achievable symbol rates.

2. SIGNAL AND CHANNEL MODEL

This chapter discusses the typical characteristics of multipath communication channels and introduces some techniques used to accurately model these characteristics for the performance analysis presented in chapters 3 and 4.

2.1 SIGNAL MODEL

The received signal in a communication system is accurately expressed as being convolved through the impulse responses of the transmitter, the channel, and the antenna receiver. In this text, the effects of the transmitter, channel, and receiver are lumped into a single aggregate "channel" impulse response, $H(t)$. Thus, the real bandpass received signal, $R(t)$, can be written as

$$R(t) = H(t) * S(t) + I(t) + N(t), \tag{2.1}$$

where $S(t)$, $I(t)$, and $N(t)$ are the bandpass transmitted signal, interference signal, and additive noise respectively. In a multipath environment, the channel-induced distortion creates ISI, which can be thought of as correlated interference.

The transmitted communication signal can be written as

$$S(t) = a(t)\ cos(2\pi f_c t + \theta(t)), \tag{2.2}$$

where the real envelope of $S(t)$, $a(t)$, and the phase of $S(t)$, $\theta(t)$ bear the transmitted information and f_c is the carrier frequency. Eq. (2.2) can be rewritten using a trigonometric identity as

$$\begin{aligned} S(t) &= a(t)\ cos(\theta(t))\ cos(2\pi f_c t) - a(t)\ sin(\theta(t))\ sin(2\pi f_c t) \\ &= x(t)\ cos(2\pi f_c t) - y(t)\ sin(2\pi f_c t), \end{aligned} \tag{2.3}$$

where $x(t) = a(t)\cos(\theta(t))$ is called the in-phase component and $y(t) = a(t)\sin(\theta(t))$ is called the quadrature component. Both $x(t)$ and $y(t)$ are real baseband signals, that is, each has a spectrum that is symmetric about $f = 0$, and $s(t) = x(t) + j\ y(t)$, sometimes called the complex envelope, is a complex baseband signal. Using eq. (2.3), the transmitted signal can be generated by the block diagram in figure 2.1. The spectrum-shaping filter is typically a Nyquist pulse-shaping filter that has the property that at the ideal sampling instants, there are no contributions from data pulses other than the one being detected [3].

For digital communication, the complex baseband transmitted signal is described by,

$$s(t) = \sqrt{2S} \sum_k s_k\ P_T(t - kT) \tag{2.4}$$

where S is the average transmitted signal power, $\{s_k\}$ is a sequence of symbols transmitted at the symbol rate of $R = 1/T$ symbols per second, and $P_T(t)$ is a pulse with band-limited baseband frequency response. The binary data sequence is encoded to form the symbol sequence, $\{s_k\}$, by any of numerous digital-modulation techniques like M-PSK and M-ary Quadrature Amplitude Modulation (M-QAM). Thus, each symbol represents $\log_2 M$ bits of information. Each modulation technique is defined by its discrete alphabet (or constellation) of complex numbers.

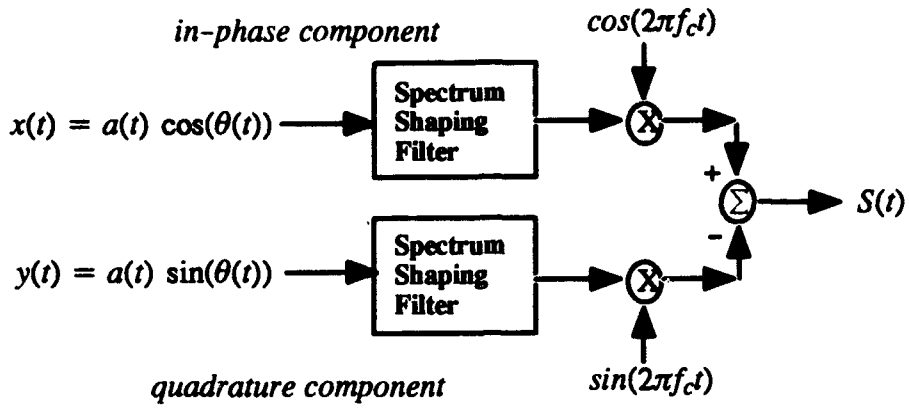

Figure 2.1. Generation of bandpass-transmitted signal.

2.2 FIR CHANNEL MODELS FOR MULTIPATH ENVIRONMENTS

All real world communication channels are nonideal. Sources of channel nonidealities are numerous. They include:

1. frequency dependent channel
2. antenna spatial patterns
3. multiple propagation paths
4. additive interference and noise
5. transmitter and receiver equipment-induced distortions
6. receiver synchronization errors

This section will discuss methods of modeling common nonidealities induced by a multipath communication channel.

A multipath channel with discrete and undistorted propagation paths can be modeled at time t as an FIR filter with impulse response

$$H(t) = \sum_{i=1}^{N} H_i(t)\ \delta(t - \tau_i) \tag{2.5}$$

for N separate propagation paths [6]. Figure 2.2 shows the N propagation path channel model with additive interference and AWGN. The tap-gain weights, $H_i(t)$, are typically modeled as either:

1. constants
2. time-varying deterministic variables, or
3. stochastic random variables.

Such a channel model is valid for *band-limited channels over short time intervals* only. The FIR channel model is an intuitively good choice for a multipath environment due to its similarity to the physical propagation modes in the channel.

The model described by eq. (2.5) is valid for *narrowband* signals only because each propagation path is subjected to an (possibly time-varying) ideal filter response (filter response of a single tap-gain weight), which is incapable of introducing any frequency-dependent amplitude or phase distortions on the individual propagation path. The accumulation of individual propagation paths introduces frequency-dependent channel distortions. Each propagation path of a *broadband* signal can undergo additional amplitude and phase distortions requiring modification of the model previously introduced (see [6] for more details).

The model described by eq. (2.5) is valid for *short time intervals* because each propagation delay, τ_i, is assumed to be a constant. This is only approximately true during short time intervals and, in general, the propagation delays are also time-varying.

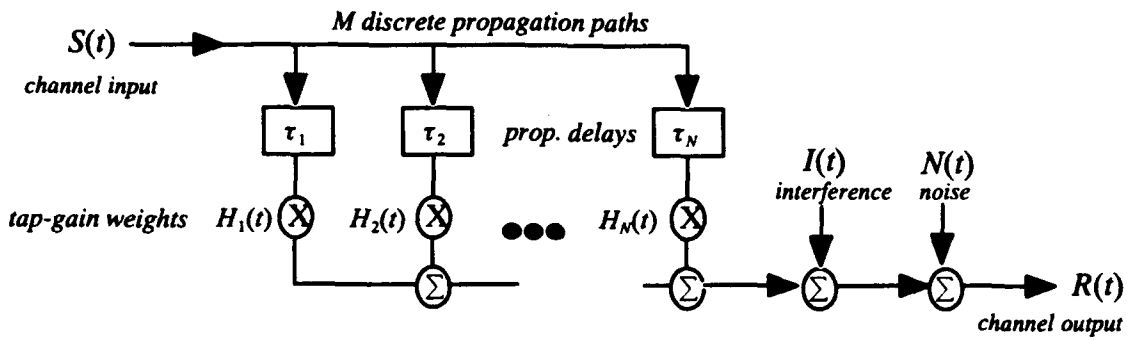

Figure 2.2. Multipath band-limited channel model with additive interference and noise.

2.3 TWO-PATH CHANNEL MODEL

This report will consider a channel consisting of two dominant propagation paths in a stationary, deterministic channel environment shown in figure 2.3. Such a channel is frequently observed in LOS radio and is called the "two-path" channel model ([2], [6] and [7]). This simplified model will allow for the derivation of closed form solutions of performance measures in chapters 3 and 4. In addition, it will provide insight into the mechanisms creating performance degradation due to multipath. Future work will concentrate on the N-path channel model with stochastic tap-gain weights. The channel impulse response given by eq. (2.5) for $N = 2$ can be rewritten with respect to the shortest path (called the direct path) as

$$\begin{aligned} H(t) &= H_1\delta(t) + H_2\,\delta\left(t - (\tau_2^{multi} - \tau_1^{direct})\right) \\ &= H_1\delta(t) + H_2\,\delta(t-\tau_\Delta), \end{aligned} \tag{2.6}$$

where $\tau_\Delta = \tau_2^{multi} - \tau_1^{direct}$ is called the delay spread. By taking the Fourier transform of eq. (2.6), we find the channel frequency response equal to

$$H(f) = \int_{-\infty}^{\infty} H(t)\, e^{-j2\pi ft} dt = H_1 + H_2\, e^{-j2\pi f\tau_\Delta}. \tag{2.7}$$

Recall that the power spectral density of the channel output is related to the power spectral density of the channel input by,

$$PSD_{H*S}(f) = |H(f)|^2 \, PSD_S(f) \tag{2.8}$$

where for real tap-gain weights,

$$|H(f)|^2 = H_1^2 + H_2^2 + 2 \, H_1 H_2 \cos(2 \pi f \tau_\Delta). \tag{2.9}$$

The spectral nulls in eq. (2.9) are characteristic of a multipath channel. The depth of the spectral null in the channel's frequency response increases as the value of H_2 approaches the value of H_1. The distance between spectral nulls decreases as the delay spread, τ_Δ, increases. For signals having large bandwidths (where "large" signal bandwidth will be qualified in example 2.3 as $BW \approx 2R \gtrsim 1/\tau_\Delta$), the spectral nulls in the channel frequency response can result in distortion of the transmitted symbols in the time domain.

The phase, $\measuredangle H(f)$, and group delay, $g(f) \equiv -\frac{1}{2\pi} \frac{d \measuredangle H(f)}{df}$, of the channel frequency response in eq. (2.9) are given by (derived in appendix D)

$$\measuredangle H(f) = \tan^{-1}\left[\frac{-H_2 \sin(2 \pi f \tau_\Delta)}{H_1 + H_2 \cos(2 \pi f \tau_\Delta)}\right] \qquad g(f) = H_2 \tau_\Delta \left[\frac{H_2 + H_1 \cos(2 \pi f \tau_\Delta)}{H_1^2 + H_2^2 + 2 \, H_1 H_2 \cos(2 \pi f \tau_\Delta)}\right] \tag{2.10}$$

The nonlinear phase (and nonconstant group delay) introduces delay distortion in the received signal that can create detection difficulties for angle-modulated data.

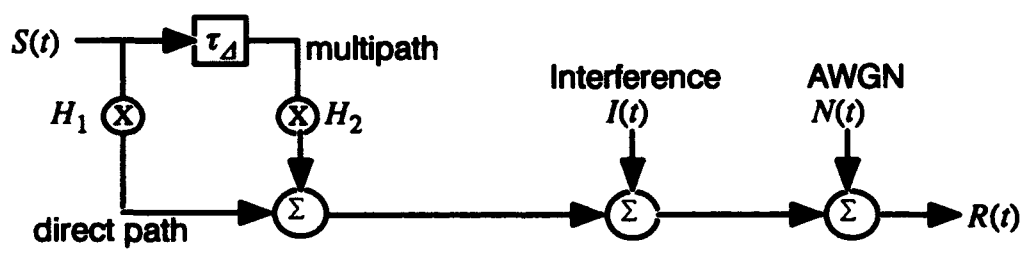

Figure 2.3. Continuous-time, bandpass model of communication channel.

The following examples will help to add physical insight into the characteristics of the two-path channel model described above:

Example 2.1 Ideal Channel

It's easy to show that an ideal channel is modeled by eq. (2.5) with N=1 and $H_1(t)$ equal to a constant (or by eq. (2.6) with $H_2 = 0$). An ideal channel is distortionless in that the frequency response of the channel has constant magnitude and linear phase (constant group delay) over the frequency bandwidth of the transmitted signal. Its impulse response and frequency response are given by

$$H(t) = H_1 \, \delta(t - \tau_1) \qquad\qquad H(f) = H_1 \, e^{-j2\pi f \tau_1} \tag{2.11}$$

where $H(f) = |H(f)| \, e^{j \measuredangle H(f)}$. Thus, we find that the distortionless channel has $|H(f)| = H_1$, $\measuredangle H(f) = -2 \pi f \tau_1$, and $g(f) = \tau_1$ for all frequencies of interest.

Example 2.2 Two-Path Over-the-Water LOS Channel

Consider the over-the-water LOS communication channel where the transmit and the receive antenna are at equal heights above the water. Figure 2.4a shows a ray diagram of the two most probable propagation paths. This channel clearly fits the two-path channel model given by eq. (2.6). Using the Pythagorean theorem and a flat earth approximation, it can be shown that the differential path length is

$$d_\Delta = d_{multi} - d_{direct} = 2\sqrt{\frac{r^2}{4} + h^2} - r \tag{2.12}$$

where r is the range between the antennas and equal to the length of the direct path. The delay spread is simply $\tau_\Delta = d_\Delta / c$, *where* $c \approx 3\text{x}10^8$ *m/s is the speed of the communication signal. Figure 2.4b plots the differential path length in meters and the delay spread in nanoseconds for h = 45 meters (≈150 feet). Note that the delay spread decreases with range. Figures 2.5 and 2.6 demonstrate the characteristics of the two-path channel model for* $H_1 = 1.0$, $H_2 = -0.8$, *and* $\tau_\Delta = 5$ *ηsec. From eq. (2.9), it's apparent that the null separation in the channel frequency response*

$$\textit{null separation} = \frac{1}{\tau_\Delta}\ (Hz) \tag{2.13}$$

is a function of range in this example.

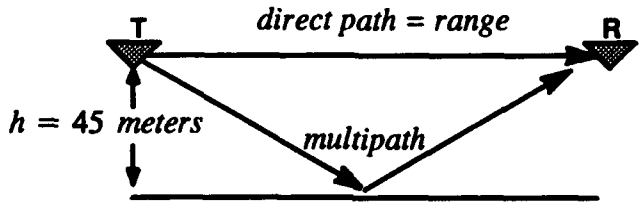

1 meter = 3.28 feet
1 nautical mile = 1852 meters

(a)

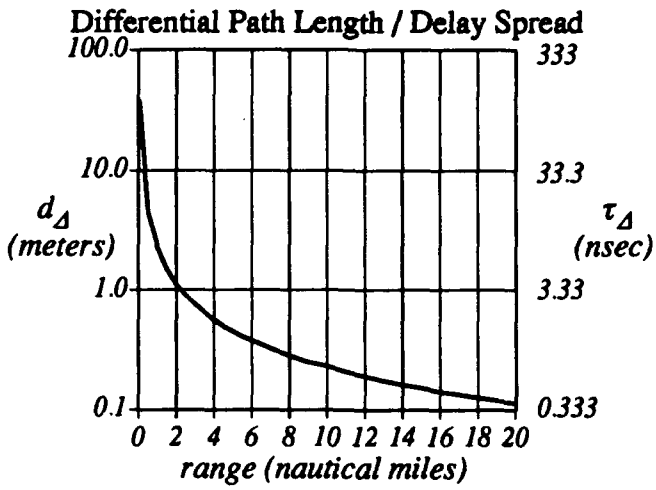

(b)

Figure 2.4. Differential path length and delay spread for a two-path channel.

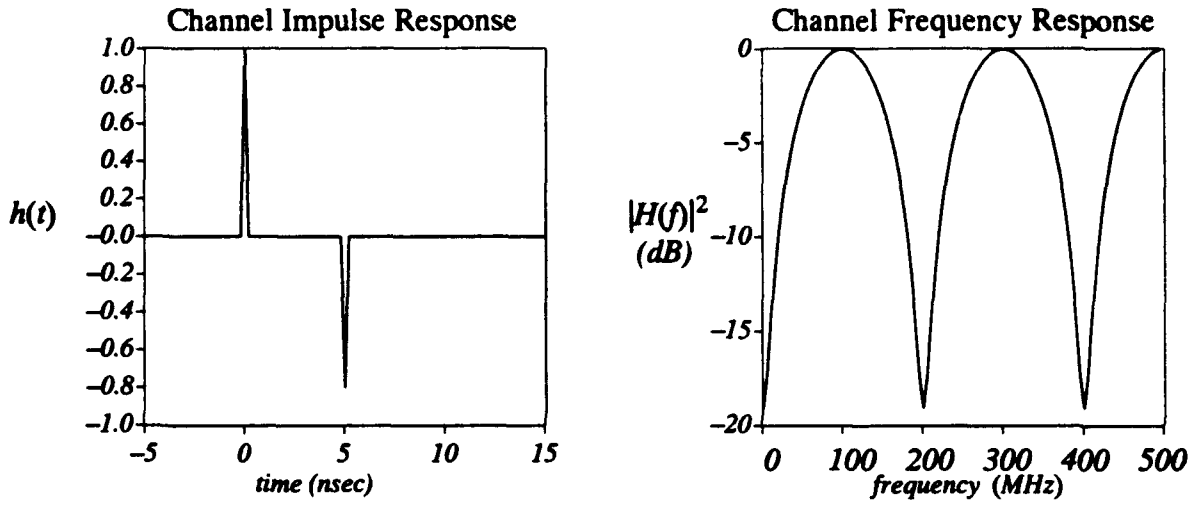

Figure 2.5 Channel impulse response and channel frequency response for a two-path channel with $\tau_{\Delta} = 5\ nsec$.

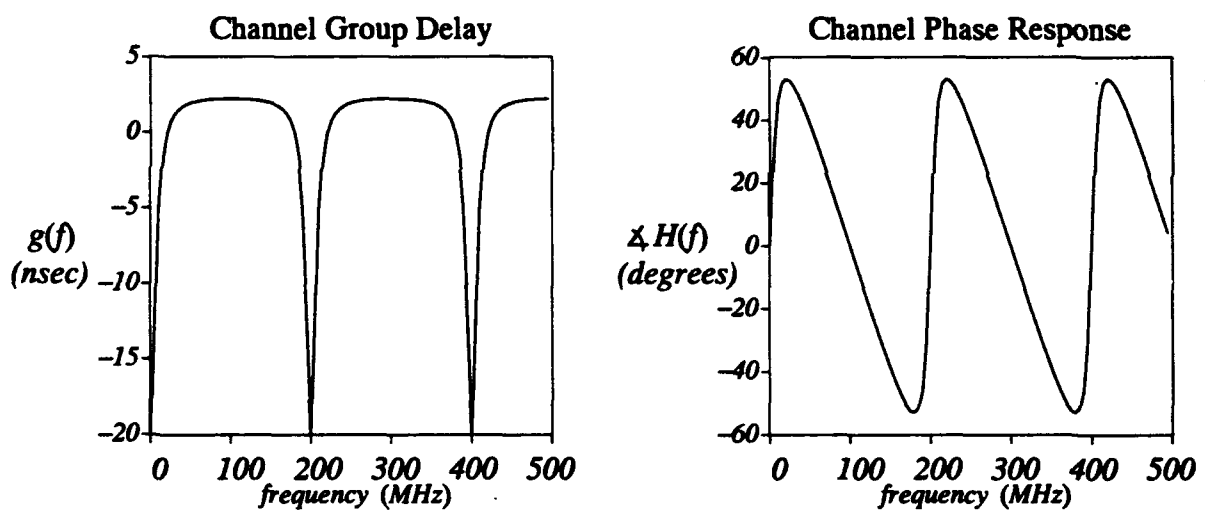

Figure 2.6. Channel group delay and phase response for the two-path channel in figure 2.5.

2.4. SIGNAL STATISTICS

Recall that the autocorrelation of a sum of signals can be written as the sum of the autocorrelation of each signal when each signal is mutually uncorrelated. With this assumption, we can write the autocorrelation of eq. (2.1) as

$$\phi_{R,R}(\tau) \equiv E\left[R(t)\ R^{*}(t-\tau)\right] = \phi_{H^{*}S,H^{*}S}(\tau) + \phi_{I,I}(\tau) + \phi_{N,N}(\tau) \qquad (2.14)$$

To proceed in evaluating these equations requires that some assumptions be made about the received signal components.

The channel impulse response to be considered in this paper is the two-path channel model with time-invariant, discrete paths, normalized to the delay of the direct path as described in section 2.3. With this channel model, it can be shown that

$$\phi_{H*S,H*S}(\tau) = H_1H_2\,\phi_{S,S}(\tau + \tau_\Delta) + (H_1^2 + H_2^2)\,\phi_{S,S}(\tau) + H_1H_2\,\phi_{S,S}(\tau - \tau_\Delta) \quad (2.15)$$

where for $P_T(t) = 1$ in the interval [0,T] and 0 elsewhere,

$$\phi_{S,S}(\tau) = \phi_{x,x}(\tau)\cos(2\pi f_c\tau) \quad (2.16)$$

and

$$\phi_{x,x}(\tau) = \begin{cases} S\left(1 - \frac{|\tau|}{T}\right) & -T \le \tau \le T \\ 0 & \text{otherwise} \end{cases} \quad (2.17)$$

$\phi_{x,x}(\tau)$ is the autocorrelation of the in-phase signal component, T is the symbol duration, [illegible] s the transmitted signal power. Eqs. (2.16) and (2.17) have explicitly assumed that the power s[illegible]tra of $S(t)$ is symmetric about $f=f_c$ (as is typical for double sideband communication systems) and thus, it can be shown that $\phi_{x,y}(\tau) = 0 = \phi_{y,x}(\tau)$ (see section 3.1 of [3]).

Two types of interference will be analyzed in this paper. The first is a CW interference given by, $I(t) = \sqrt{2I}\cos(2\pi(f_c + f_\Delta)t + \phi)$, where I, f_Δ, ϕ are the power, carrier offset frequency, and phase of the interference respectively. The autocorrelation of the CW interference is found to be,

$$\phi_{I,I}(\tau) = I\cos(2\pi(f_c + f_\Delta)\tau). \quad (2.18)$$

The second type of interference is bandpass white Gaussian noise with power spectral density shown in figure 2.7 and defined by

$$PSD_I(f) = \begin{cases} \frac{N_B}{2} & f_c + f_\Delta - \frac{B}{2} \le |f| \le f_c + f_\Delta + \frac{B}{2} \\ 0 & \text{otherwise} \end{cases}. \quad (2.19)$$

Its autocorrelation can be computed by taking the inverse Fourier transform of eq. (2.19)

$$\phi_{I,I}(\tau) = N_B B\left(\frac{\sin(\pi B\tau)}{\pi B\tau}\right)\cos(2\pi(f_c + f_\Delta)\tau). \quad (2.20)$$

This interference model encompasses both narrowband and broadband interference with a single parameter, the bandwidth B. For very small, but finite B, eq. (2.20) reduces to eq. (2.18) where $I = N_B B$ is equal to the total baseband interferer power.

Finally, the additive noise is assumed to come from a white Gaussian process with power spectral density $PSD_N(f) = N_0/2$ for all frequency resulting in its autocorrelation function being equal to $\phi_{N,N}(\tau) = \sigma_N^2\,\delta(\tau) = N_0/2\,\delta(\tau)$.

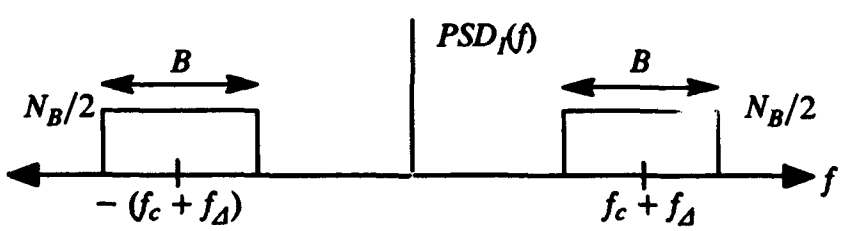

Figure 2.7. Spectrum of finite bandwidth interference at bandpass.

Example 2.3 Classification of Multipath Channels

Insight into the classification of multipath channels can be found from the autocorrelation of the output of the two-path channel model. Using eqs. (2.16) and (2.17) in eq. (2.15), we find

$$
\begin{aligned}
\phi_{H^rS,H^rS}(\tau) &= (H_1H_2)\,\phi_{x,x}(\tau+\tau_\Delta)\cos(2\pi f_c(\tau+\tau_\Delta)) + (H_1^2+H_2^2)\,\phi_{x,x}(\tau)\cos(2\pi f_c\tau) \\
&\quad + (H_1H_2)\,\phi_{xx}(\tau-\tau_\Delta)\cos(2\pi f_c(\tau-\tau_\Delta)) \\
&= \Big[(H_1H_2)\,S\Big(1-\frac{|\tau+\tau_\Delta|}{T}\Big)\cos(2\pi f_c\tau_\Delta) + (H_1^2+H_2^2)\,S\Big(1-\frac{|\tau|}{T}\Big) \\
&\qquad + (H_1H_2)\,S\Big(1-\frac{|\tau-\tau_\Delta|}{T}\Big)\cos(2\pi f_c\tau_\Delta)\Big]\cos(2\pi f_c\tau) \\
&\quad - \Big[(H_1H_2)\,S\Big(1-\frac{|\tau+\tau_\Delta|}{T}\Big)\sin(2\pi f_c\tau_\Delta) \\
&\qquad - (H_1H_2)\,S\Big(1-\frac{|\tau-\tau_\Delta|}{T}\Big)\sin(2\pi f_c\tau_\Delta)\Big]\sin(2\pi f_c\tau)
\end{aligned}
\tag{2.21}
$$

where the same notation as in eq. (2.17) is implied. Figure 2.8 plots the components of $\phi_{H^rS,H^rS}(\tau)$ given in eq. (2.21) for $H_1 = 1.0$, $H_2 = -0.8$ and for the special case when $f_c\tau_\Delta \in \{1, 2, ...\}$. Note that the case when the delay spread is greater than the inverse of the signal bandwidth, $\tau_\Delta \geq \frac{1}{2R} = \frac{T}{2}$, or equivalently the null separation in the channel frequency response is less than the signal bandwidth, $\frac{1}{\tau_\Delta} \leq 2R = \frac{2}{T}$, is typically called "resolvable multipath" or "frequency selective multipath" [3]. This condition implies that the multipath channel may affect disjoint parts of the signal spectrum in different ways. Thus, all figures in figure 2.8 are cases of "frequency selective multipath" with figure 2.8 (c) equal to the limiting case. For the case when $\tau_\Delta < \frac{1}{2R} = \frac{T}{2}$, the channel is called "frequency nonselective multipath" or "flat multipath." This condition implies that the multipath channel will affect all parts of the signal spectrum in a similar way.

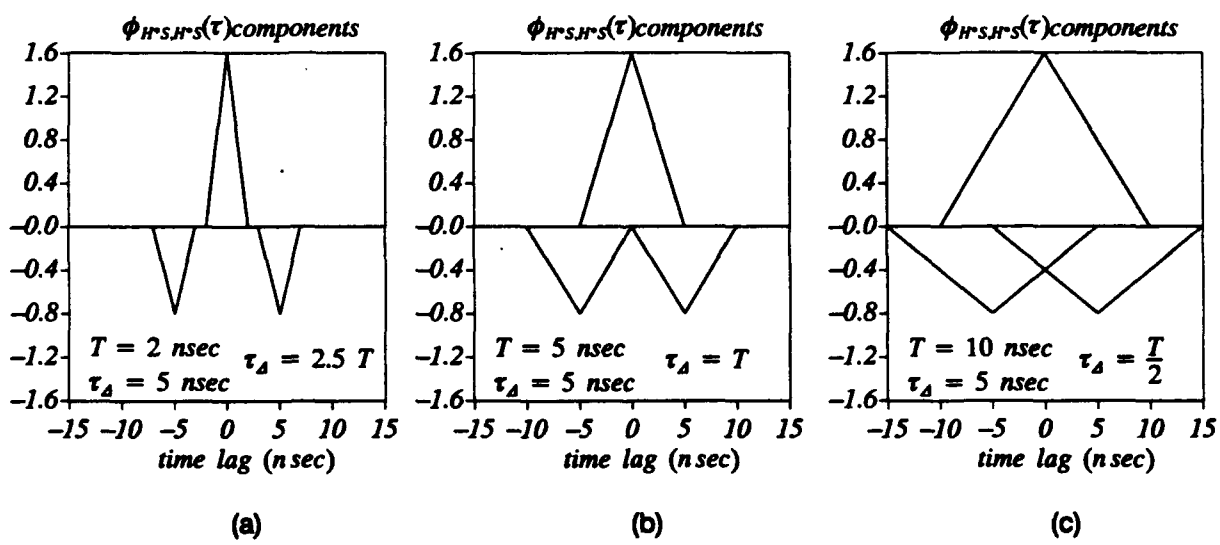

Figure 2.8. Components of eq. (2.21) for $f_c\tau_\Delta \in \{1, 2, ...\}$ and (a) $\tau_\Delta = 2.5\ T$, (b) $\tau_\Delta = T$, (c) $\tau_\Delta = 0.5\ T$.

3. PERFORMANCE ANALYSIS OF BPSK SIGNAL

This chapter presents an analysis of the average probability of bit error for a BPSK signal transmitted through the channel shown in figure 2.3 and received by the coherent matched filter shown in figure 3.1. The receiver model consists of a correlator implementation of a coherent matched-filter receiver for BPSK. While the analysis technique is well known, the particular example used in this text is thought to be unique (see [8], [1] for closely related examples).

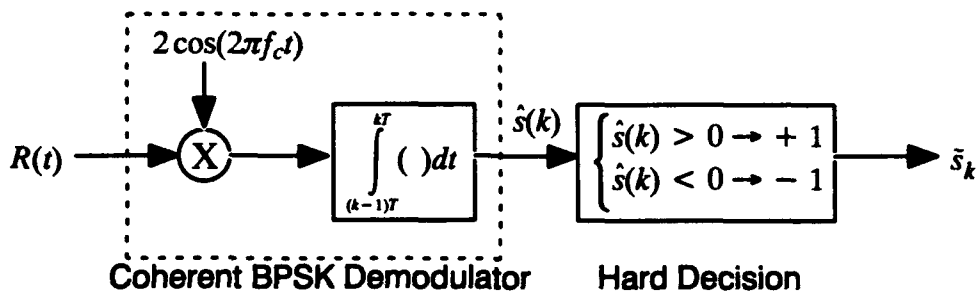

Figure 3.1. Correlator implementation of matched-filter receiver for BPSK signals.

Using the two-path multipath channel model described in section 2.3, $H(t) = H_1\,\delta(t) + H_2\,\delta(t-\tau_\Delta)$, the received signal can be expressed as

$$R(t) = H_1 S(t) + H_2 S(t-\tau_\Delta) + I(t) + N(t), \tag{3.1}$$

where

$$S(t) = \sqrt{2S} \sum_k a_k\, P_T(t - kT)\, \cos(2\pi f_c t) \tag{3.2}$$

is the BPSK transmitted bandpass signal, $a_k \in \{+1, -1\}$ is the *kth* bit, S is the transmitted signal power, and $P_T(t)$ the symbol pulse waveform. At most, one-bit transition of the multipath signal can take place in the interval $[0, T]$ of the direct path signal. The following analysis will consider only the case of $0 \le \tau_\Delta \le T$ as shown in figure 3.2. The case of $\tau_\Delta > T$ is a straight forward extension and detailed in appendix B. Using this assumption on the delay spread, the received signal during the interval [0,T] can be written as

$$\begin{aligned} R(t) &= H_1\sqrt{2S}\; a_k\, P_T(t)\, \cos(2\pi f_c t) + H_2\sqrt{2S}\; a_k\, P_T(t-\tau_\Delta)\, \cos(2\pi f_c(t-\tau_\Delta)) \\ &\quad + H_2\sqrt{2S}\; a_{k-1}\, P_T(t+T-\tau_\Delta)\, \cos(2\pi f_c(t+T-\tau_\Delta)) + I(t) + N(t) \\ &= \Big[H_1\sqrt{2S}\; a_k\, P_T(t) + H_2\sqrt{2S}\; a_k\, P_T(t-\tau_\Delta)\, \cos(2\pi f_c \tau_\Delta) \\ &\quad + H_2\sqrt{2S}\; a_{k-1}\, P_T(t+T-\tau_\Delta)\, \cos(2\pi f_c(\tau_\Delta - T))\Big]\, \cos(2\pi f_c t) + I(t) + N(t) \end{aligned} \tag{3.3}$$

using trigonometric identities and neglecting $\sin(2\pi f_c t)$ terms since they will be eliminated by the coherent BPSK demodulator in figure 3.1.

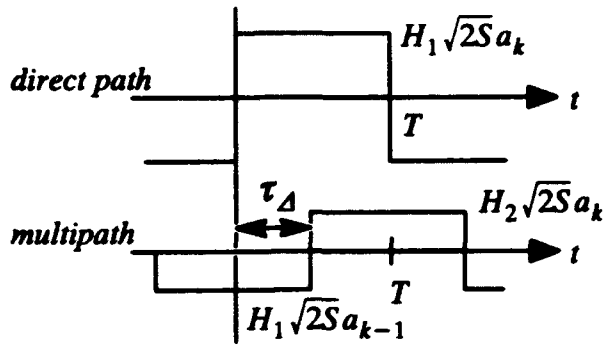

Figure 3.2. Desired and interfering baseband signals in $[0, T]$, $0 \le \tau_\Delta \le T$, $a_k = +1$, $a_{k-1} = -1$ (from [1]).

3.1 MATCHED-FILTER DETECTION OF BPSK WITH CW INTERFERENCE

This section derives the probability of symbol error for the received signal given by eq. (3.1) with CW interference, $I(t) = \sqrt{2I}\cos(2\pi(f_c + f_\Delta)t + \phi)$. Without loss of generality, consider the interval [0,T]. The decision variable, $\hat{s}(k)$, in figure 3.1 can be written as

$$\hat{s}(k) = \int_0^T R(t)\, 2\cos(2\pi f_c t)\, dt = a_k D(k) + a_k F_1(k) + a_{k-1} F_2(k) + I(k) + N(k) \quad (3.4)$$

where the terms in eq. (3.4) will be defined in section 3.2. The conditional probability of bit error, given the parameters of the channel model and interference parameters, is given by,

$$P_e(H_1,H_2,\tau_\Delta,I,f_\Delta,\phi) = \tfrac{1}{2}P_e(+1|H_1,H_2,\tau_\Delta,I,f_\Delta,\phi) + \tfrac{1}{2}P_e(-1|H_1,H_2,\tau_\Delta,I,f_\Delta,\phi) \quad (3.5)$$

for equal probabilities of transmitting +1 and –1 bit. For the case when $0 \le \tau_\Delta \le T$

$$\begin{aligned} P_e(+1|H_1,H_2,\tau_\Delta,I,f_\Delta,\phi) &= \tfrac{1}{2}\Pr\big(\hat{s}(k) < 0 \mid a_{k-1} = -1, a_k = +1\big) \\ &+ \tfrac{1}{2}\Pr\big(\hat{s}(k) < 0 \mid a_{k-1} = +1, a_k = +1\big). \end{aligned} \quad (3.6)$$

$$\begin{aligned} P_e(-1|H_1,H_2,\tau_\Delta,I,f_\Delta,\phi) &= \tfrac{1}{2}\Pr\big(\hat{s}(k) > 0 \mid a_{k-1} = -1, a_k = -1\big) \\ &+ \tfrac{1}{2}\Pr\big(\hat{s}(k) > 0 \mid a_{k-1} = +1, a_k = -1\big). \end{aligned} \quad (3.7)$$

For the case when $\tau_\Delta > T$, eqs. (3.6) and (3.7) each contain 4 components since the two data bits in the multipath are not correlated with the data bit in the direct path, a_k, during the interval $[0,T]$. This is presented in appendix B.

The only random term in eq. (3.4) that is not being conditioned on is the Gaussian random variable, $N(k)$. Thus, the decision variable, $\hat{s}(k)$, will be a conditionally Gaussian random variable with variance σ_N^2, which will be calculated below. Recall that the cumulative distribution function of a random variable X is defined in terms of its probability density function,

$cdf(x) = \Pr(X \le x) \equiv \int_{-\infty}^{x} pdf_X(t)\ dt$. For a zero mean, unity variance, Gaussian random variable X

$$Pr(X \le x) = \frac{1}{\sqrt{2\pi}} \int_{-\infty}^{x} e^{-t^2/2}\ dt \equiv \Phi(x). \tag{3.8}$$

Thus, rewriting eqs. (3.6) and (3.7) so that the Gaussian random variable has zero mean and unity variance, we find that eq. (3.5) can be written in terms of eq. (3.8) as

$$\begin{aligned} P_e(H_1,H_2,\tau_\Delta,I,f_\Delta,\phi) = {} & \frac{1}{4}\Phi\left(-\frac{+D(k)+F_1(k)-F_2(k)+I(k)}{\sigma_N}\right) \\ & + \frac{1}{4}\Phi\left(-\frac{+D(k)+F_1(k)+F_2(k)+I(k)}{\sigma_N}\right) \\ & + \frac{1}{4}\Phi\left(\frac{-D(k)-F_1(k)-F_2(k)+I(k)}{\sigma_N}\right) \\ & + \frac{1}{4}\Phi\left(\frac{-D(k)-F_1(k)+F_2(k)+I(k)}{\sigma_N}\right). \end{aligned} \tag{3.9}$$

3.2 TERMS IN EQ. (3.4)

$a_k\ D(k)$ is the desired signal term from the direct transmission path. It can be found from interpreting figure 3.1 as

$$a_k\ D(k) = \int_0^T H_1\sqrt{2S}\ a_k \cos(2\pi f_c t)\ 2\cos(2\pi f_c t)\ dt$$

for $P_T(t)$ equal to a rectangular pulse during the interval $[0,T]$. Solving for $D(k)$ we find

$$D(k) = H_1\sqrt{2S}T \tag{3.10}$$

since the high-frequency terms are removed by the integration.

$a_k\ F_1(k)$ and $a_{k-1}\ F_2(k)$ are coherent interference terms (ISI) created by the multipath. They are found to be

$$a_k\ F_1(k) = \int_{\tau_\Delta}^{T} H_2\sqrt{2S}\ a_k \cos(2\pi f_c \tau_\Delta)\ \cos(2\pi f_c t)\ 2\cos(2\pi f_c t)\ dt$$

$$a_{k-1}\ F_2(k) = \int_0^{\tau_\Delta} H_2\sqrt{2S}\ a_{k-1} \cos(2\pi f_c (T-\tau_\Delta))\ \cos(2\pi f_c t)\ 2\cos(2\pi f_c t)\ dt,$$

which can be reduced to

$$F_1(k) = H_2\sqrt{2S}\ (T - \tau_\Delta)\ \cos(2\pi f_c \tau_\Delta) \tag{3.11}$$

$$F_2(k) = H_2\sqrt{2S}\ (\tau_\Delta)\ \cos(2\pi f_c (T - \tau_\Delta)). \tag{3.12}$$

For the CW interference, $I(k)$ is given by

$$\begin{aligned} I(k) &= \int_0^T \sqrt{2I}\cos(2\pi(f_c + f_\Delta)t + \phi)\ 2\cos(2\pi f_c t)\ dt \\ &= \sqrt{2I}\ \frac{\left[\sin(2\pi f_\Delta T + \phi) - \sin(\phi)\right]}{2\pi f_\Delta} \end{aligned} \tag{3.13}$$

$N(k)$ is the Gaussian noise term defined as

$$N(k) = \int_0^T N(t)\ 2\cos(2\pi f_c t)\ dt.$$

Since this term is a Gaussian random variable, it will be necessary to compute the first and second moments of $N(k)$. The mean is zero since $E[N(t)] = 0$. The variance is given by

$$\begin{aligned} \sigma_N^2 &= \int_0^T\int_0^T E[N(t_1)N(t_2)]\ 2\cos(2\pi f_c t_1)\ 2\cos(2\pi f_c t_2)\ dt_1 dt_2 \\ &= \int_0^T\int_0^T \sigma_{\mathcal{N}}^2\ \delta(t_1 - t_2)\ 4\cos(2\pi f_c t_1)\ \cos(2\pi f_c t_2)\ dt_1 dt_2 \\ &= 4\sigma_{\mathcal{N}}^2 \int_0^T \cos^2(2\pi f_c t)\ dt \\ &= N_0 T \end{aligned} \tag{3.14}$$

since $\sigma_{\mathcal{N}}^2 = N_0/2$.

Thus, the conditional probability of bit error for a BPSK signal transmitted through a two-path channel with additive CW interference and white Gaussian noise is given by using eqs. (3.10) – (3.14) in eq. (3.9). For the simplified case, of only a single channel, $H_2 = 0$, this expression reduces to eq. (11) of [1].

3.3 MATCHED-FILTER DETECTION OF BPSK WITH FINITE BANDWIDTH INTERFERENCE

The previous results are now extended to include a finite bandwidth interference. In particular, the interference is generated by passing white Gaussian noise through an ideal bandpass filter resulting in the spectrum displayed in figure 2.7. In this case, both the interference and the noise are assumed to be uncorrelated, Gaussian random variables. Thus, eq. (3.9) can be modified to find the conditional probability of bit error, given the parameters of the channel model and interference parameters as

$$P_e(H_1,H_2,\tau_\Delta,N_B,f_\Delta,B) = \frac{1}{2}\Phi\left(-\frac{+D(k)+F_1(k)-F_2(k)}{\sigma_{I+N}}\right) + \frac{1}{2}\Phi\left(-\frac{+D(k)+F_1(k)+F_2(k)}{\sigma_{I+N}}\right) \tag{3.15}$$

where

$$\sigma_{I+N}^2 = \sigma_I^2 + \sigma_N^2 \tag{3.16}$$

All that remains to be computed is σ_I^2 since $\sigma_N^2 = N_0T$ was computed in eq. (3.14).

Let the received bandpass interference be written in terms of its in-phase baseband signal, $x(t)$, and its quadrature baseband signal, $y(t)$,

$$\begin{aligned} I(t) &= x(t)\cos(2\pi(f_c+f_\Delta)t) - y(t)\sin(2\pi(f_c+f_\Delta)t) \\ &= \left[x(t)\cos(2\pi f_\Delta t) - y(t)\sin(2\pi f_\Delta t)\right]\cos(2\pi f_c t) \\ &\quad -\left[x(t)\sin(2\pi f_\Delta t) + y(t)\cos(2\pi f_\Delta t)\right]\sin(2\pi f_c t). \end{aligned} \tag{3.17}$$

Then, the interference component of the decision variable can be written as,

$$\begin{aligned} I(k) &= \int_0^T \left[x(t)\cos(2\pi f_\Delta t) - y(t)\sin(2\pi f_\Delta t)\right]\cos(2\pi f_c t)\, 2\cos(2\pi f_c t)\, dt \\ &\quad - \int_0^T \left[x(t)\sin(2\pi f_\Delta t) + y(t)\cos(2\pi f_\Delta t)\right]\sin(2\pi f_c t)\, 2\cos(2\pi f_c t)\, dt \\ &= \int_0^T \left[x(t)\cos(2\pi f_\Delta t) - y(t)\sin(2\pi f_\Delta t)\right] dt \end{aligned} \tag{3.18}$$

since high-frequency terms are removed by the integration. The mean of eq. (3.18) will be zero since $E[x(t)] = E[y(t)] = 0$. Before proceeding to compute σ_I^2, we first make several observations from chapter 2 that will simplify the analysis (note that a similar analysis was completed in [9] for $f_\Delta = 0$). First, note that $\phi_{x,y}(\tau) = 0 = \phi_{y,x}(\tau)$ for all τ since the bandpass Gaussian noise is symmetric about $f = f_c + f_\Delta$. Second, $\phi_{x,x}(\tau) = \phi_{y,y}(\tau)$ since the bandpass Gaussian noise is assumed to be stationary. Thus, the two nonzero terms of σ_I^2 reduce to,

$$\begin{aligned} \sigma_I^2 &= \int_0^T\int_0^T E[x(t_1)\,x(t_2)]\left[\cos(2\pi f_\Delta t_1)\cos(2\pi f_\Delta t_2)\right] \\ &\qquad + E[y(t_1)\,y(t_2)]\left[\sin(2\pi f_\Delta t_1)\sin(2\pi f_\Delta t_2)\right] dt_1 dt_2 \\ &= \int_0^T\int_0^T N_B B\,\frac{\sin(\pi B\tau)}{\pi B\tau}\cos(2\pi f_\Delta \tau)\, dt_1 dt_2 \end{aligned} \tag{3.19}$$

using eq. (2.20) and $\tau = t_1 - t_2$. Applying trigonometric identities we find

$$\sigma_I^2 = \int_0^T \int_0^T \frac{N_B B}{2} \frac{\sin(\pi(B-2f_\Delta)\tau)}{\pi B \tau} dt_1 dt_2 + \int_0^T \int_0^T \frac{N_B B}{2} \frac{\sin(\pi(B+2f_\Delta)\tau)}{\pi B \tau} dt_1 dt. \tag{3.20}$$

Since both terms of eq. (3.20) will have similar solutions, only the details of the first term will be presented. By making the substitution $x = \pi(B - 2f_\Delta)\tau$ and consolidating terms, the first term of eq. (3.20) can be rewritten as

$$\begin{aligned} first_term &= \frac{N_B}{2\pi} \int_0^T \int_{\pi(B-2f_\Delta)(-t_2)}^{\pi(B-2f_\Delta)(T-t_2)} \frac{\sin(x)}{x} dx\, dt_2 \\ &= \frac{N_B}{2\pi} \int_0^T \left[Si(\pi(B-2f_\Delta)t_2) + Si(\pi(B-2f_\Delta)(T-t_2)) \right] dt_2 \end{aligned} \tag{3.21}$$

where eq. (3.21) has used the $Si(y)$ relationship defined by $Si(y) = \int_0^y \frac{\sin(x)}{x} dx$. To proceed, note that by using integration by parts with $u = Si(x)$ and $dv = dx$, it can be shown that $\int_A^B Si(x)\, dx = x\, Si(x) \,|_A^B - \int_A^B sin(x) dx$. Substituting $x = \pi(B - 2f_\Delta)t_2$ into the first term of eq. (3.21) and $x = \pi(B - 2f_\Delta)(T - t_2)$ into the second term of eq. (3.21) we find

$$\begin{aligned} first_term &= \frac{N_B}{2\pi} \frac{1}{\pi(B-2f_\Delta)} \left[\int_0^{\pi(B-2f_\Delta)T} Si(x)\, dx - \int_{\pi(B-2f_\Delta)T}^{0} Si(x)\, dx \right] \\ &= \frac{N_B}{\pi} \frac{1}{\pi(B-2f_\Delta)} \left[x\, Si(x) \,|_0^{\pi(B-2f_\Delta)T} - \int_0^{\pi(B-2f_\Delta)T} \sin(x)\, dx \right] \\ &= \frac{N_B}{\pi} T \left[Si(\pi(B-2f_\Delta)T) + \frac{\cos(\pi(B-2f_\Delta)T)-1}{\pi(B-2f_\Delta)T} \right]. \end{aligned} \tag{3.22}$$

Finally, we combine a similar result for the second term of eq. (3.20) to obtain the desired result

$$\begin{aligned} \sigma_I^2 = \frac{N_B}{\pi} T &\left[Si(\pi(B-2f_\Delta)T) + \frac{\cos(\pi(B-2f_\Delta)T) - 1}{\pi(B-2f_\Delta)T} \right] \\ + \frac{N_B}{\pi} T &\left[Si(\pi(B+2f_\Delta)T) + \frac{\cos(\pi(B+2f_\Delta)T)-1}{\pi(B+2f_\Delta)T} \right]. \end{aligned} \tag{3.23}$$

Thus, the conditional probability of error for a BPSK signal transmitted through a two-path channel with additive finite bandwidth interference and white Gaussian noise is given by using eqs. (3.10) - (3.12), (3.14) and (3.23) in eq. (3.15). For the simplified case, of only a single channel, $H_2 = 0$ and no offset frequency, $f_\Delta = 0$, this expression reduces to

$$P_e(H_1,N_B,B) = \Phi\left[-\frac{H_1\sqrt{2S}T}{\sqrt{N_0T + \frac{N_b}{\pi}\,2T\left[Si(\pi BT) + \frac{\cos(\pi BT)-1}{\pi BT}\right]}}\right]. \tag{3.24}$$

3.4. SUMMARY AND EXAMPLES

Before proceeding with an equation summary and some examples, it is useful to present a vector representation of the received baseband signal for both the two-path channel and CW interference to help develop some intuition into the performance characteristics displayed in the examples. The other channel combinations follow directly from these cases.

Figure 3.3 illustrates the vector diagram of the received baseband signal when the BPSK signal is transmitted through the time-invariant two-path channel. The two transmitted bits correspond to two vectors of length $H_1\sqrt{2S}$ originating at the origin and terminating at +1 and –1 on the in-phase axis. Since the multipath travels a longer distance than the direct path, its propagation time is longer than the direct path, which will result in a phase offset when the received signal is demodulated with respect to the direct path. Referring to figure 3.2, there can be two interfering bits from the multipath in the interval $[0,T]$, which results in two vectors of length $H_2\sqrt{2S}$ and with phase relative to the direct path of $\theta_1 = 2\pi f_c\tau_\Delta$ and $\theta_2 = 2\pi f_c(\tau_\Delta - T)$. For the case of $\tau_\Delta \le T$, the multipath bit in the interval of $[0,\tau_\Delta]$ can be either a +1 or a –1, which results in two vectors 180 degrees out of phase. However, the multipath bit in the interval of $[\tau_\Delta,T]$ is correlated with the transmitted direct path bit in the interval $[0,T]$, so its value is determined by the present transmitted bit, a_k, and a single vector is generated. The received demodulated bits can be found by vector addition resulting in a total of two possible bits demodulated in the interval $[0,T]$ for each transmitted bit. Note that only one of the possible demodulated bits represented in figure 3.3 exists at any one time. The duration of each bit is defined in figure 3.2. For the case of $\tau_\Delta > T$, the multipath bit in the interval of $[\tau_\Delta,T]$ is no longer correlated with the transmitted bit, so it too will generate two vectors 180 degrees out of phase resulting in the demodulation of four possible received bits for each transmitted bit.

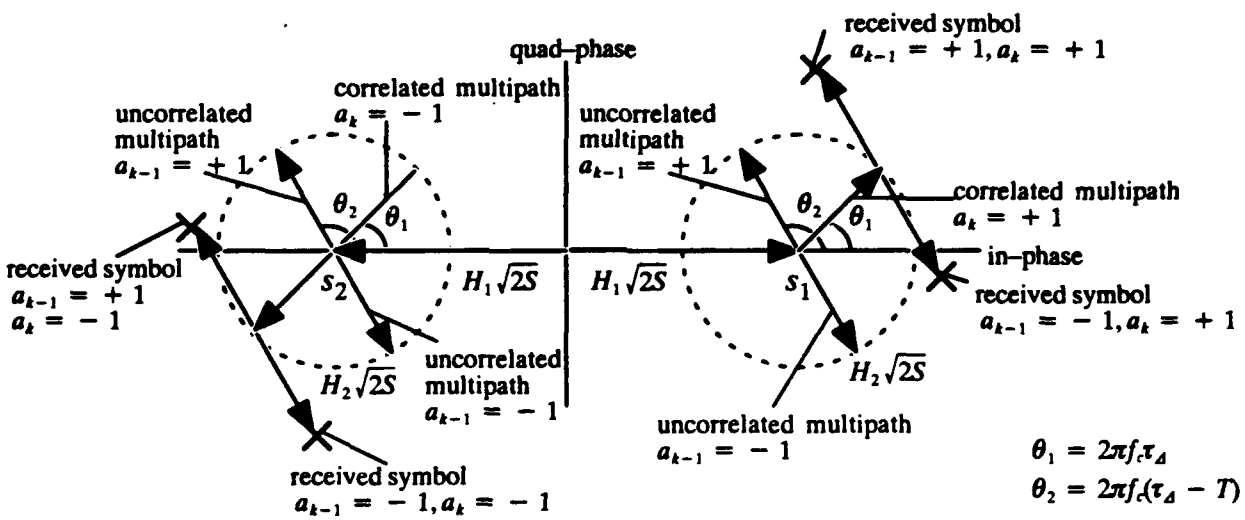

Figure 3.3. Possible demodulated bits during the interval $[0, T]$ for a two-path channel with $0 \le \tau_\Delta \le T$.

Figure 3.4 illustrates the vector diagram of the received baseband signal for the case of additive CW interference and no multipath. The figure is similar to figure 3.3. The CW interference creates a vector that spins about either of the two transmitted bit vectors with phase $\theta(t) = 2\pi f_\Delta t + \phi$ during the interval $[0,T]$. Of course, the detection depends on the integration between $[0,T]$, which determines the actual system performance. The finite bandwidth interferer is from a Gaussian random process and will not have a constant envelope or a constant phase as was the case for the CW interferer. Thus, its vector diagram will form a cluster of received symbols centered about the symbol mean values with radius determined by the variance of the interference.

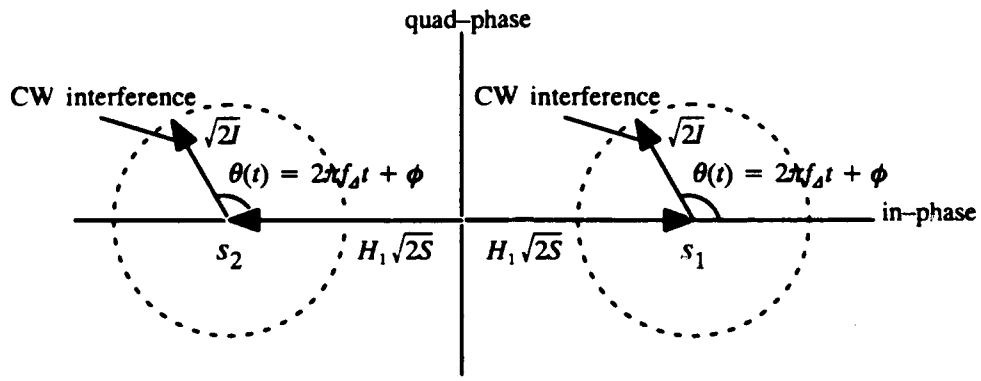

Figure 3.4. Effect of CW interference on the demodulated bits during the interval $[0, T]$.

The following examples will exercise the average probability of bit error equations derived in this chapter to highlight some of the characteristics exhibited by a multipath communication channel with additive interference. Specific input values are used corresponding to example 2.2; however, these values can be easily modified to fit any LOS radio communication system. Figures 3.5 and 3.6 summarize the equations required to compute the average probability of bit error for the CW interference and the finite bandwidth interference cases respectively for $0 \le \tau_\Delta \le T$. Appendix B presents results for $\tau_\Delta > T$.

$$D(k) = H_1\sqrt{2S}\,T$$
$$F_1(k) = H_2\sqrt{2S}\;(T - \tau_\Delta)\cos(2\pi f_c\tau_\Delta)$$
$$F_2(k) = H_2\sqrt{2S}\;(\tau_\Delta)\cos(2\pi f_c(\tau_\Delta - T))$$
$$I(k) = \sqrt{2I}\;\frac{[\sin(2\pi f_\Delta T + \phi) - \sin(\phi)]}{2\pi f_\Delta}$$
$$\sigma_N = \sqrt{N_0 T}$$
$$P_e = \frac{1}{4}\Phi\left(-\frac{+D(k) + F_1(k) - F_2(k) + I(k)}{\sigma_N}\right) + \frac{1}{4}\Phi\left(-\frac{+D(k) + F_1(k) + F_2(k) + I(k)}{\sigma_N}\right) + \frac{1}{4}\Phi\left(\frac{-D(k) - F_1(k) - F_2(k) + I(k)}{\sigma_N}\right) + \frac{1}{4}\Phi\left(\frac{-D(k) - F_1(k) + F_2(k) + I(k)}{\sigma_N}\right)$$

transmitted signal power $= S$
interference power $= I$
in-band noise power $= \left(\frac{2}{T}\right)\left(\frac{N_0}{2}\right) = \frac{N_0}{T}$

Figure 3.5. Generation of the average probability of bit error for a BPSK signal transmitted through a two-path channel with $0 < \tau_\Delta \le T$, CW interference and AWGN.

$$D(k) = H_1\sqrt{2S}\,T$$
$$F_1(k) = H_2\sqrt{2S}\;(T - \tau_\Delta)\cos(2\pi f_c\tau_\Delta)$$
$$F_2(k) = H_2\sqrt{2S}\;(\tau_\Delta)\cos(2\pi f_c(\tau_\Delta - T))$$
$$\sigma_N^2 = N_0 T$$
$$\sigma_I^2 = \frac{N_B}{\pi}\,T\left[Si(\pi(B - 2f_\Delta)T) + \frac{\cos(\pi(B - 2f_\Delta)T) - 1}{\pi(B - 2f_\Delta)T}\right] + \frac{N_B}{\pi}\,T\left[Si(\pi(B + 2f_\Delta)T) + \frac{\cos(\pi(B + 2f_\Delta)T) - 1}{\pi(B + 2f_\Delta)T}\right]$$
$$\sigma_{I+N} = \sqrt{\sigma_N^2 + \sigma_I^2}$$
$$P_e = \frac{1}{2}\Phi\left(-\frac{+D(k) + F_1(k) - F_2(k)}{\sigma_{I+N}}\right) + \frac{1}{2}\Phi\left(-\frac{+D(k) + F_1(k) + F_2(k)}{\sigma_{I+N}}\right)$$

transmitted signal power $= S$
interference power $= N_B B$
in-band noise power $= \left(\frac{2}{T}\right)\left(\frac{N_0}{2}\right) = \frac{N_0}{T}$

Figure 3.6. Generation of the average probability of bit error for a BPSK signal transmitted through a two-path channel with $0 < \tau_\Delta \le T$, finite bandwidth interference, and AWGN.

Example 3.1 BPSK Signal, Multipath and AWGN

Consider first the simplified case of a BPSK signal transmitted through a time-invariant two-path channel with additive white Gaussian noise. Figures 3.7 – 3.10 plot the performance of this system as a function of the magnitude of the multipath tap-gain and the data rate. Either summary of equations can be applied, figures 3.7 – 3.10 with I=0, or figure 3.6 with B = 0, since they both reduce to an identical set of equations for the case of no interference.

Figure 3.7 shows the effect of the magnitude of the multipath with respect to the direct path by varying H_2 between - 1.2 and 1.2 in 0.2 increments while keeping $H_1 = 1$. Note that the free-path propagation loss has been neglected without loss of generality. The delay spread is $\tau_\Delta = 5\ \eta$sec selected from previous examples and the data rate, $R = 1.544$ Mbps, resulting in $\tau_\Delta = 0.0077\ T$. From figure 3.7c, it can be seen that the effects of the multipath for these conditions are cyclic described by $\cos(2\pi f_c \tau_\Delta)$. This comes from the channel frequency response of the two-path channel given by eq. (2.9) and is reflected in the probability of bit error equations by the $F_1(k)$ term given by eq. (3.11). Note that when $\cos(2\pi f_c \tau_\Delta) = 0$ corresponding to $f_c = \frac{i}{4\tau_\Delta}$, $i \in \{1,3,5,...\}$ and $f_c = 250$ and 350 MHz in figure 3.7c, the multipath has no affect on system performance (see figure 3.7b), as might be expected for $\tau_\Delta = 0.0077\ T$. However, at all other carrier frequencies, the multipath has significant effects on system performance. In spectral nulls of the channel frequency response, the system performance degrades, corresponding to a reduction in received signal energy due to the multipath and the direct path adding destructively, ie $F_1(k) < 0$. For $H_2 < 0$, this is seen from figure 3.7c and 2.5 to take place when 0 MHz $< f_c <$ 50 MHz, 150 MHz $< f_c <$ 250 MHz, 350 MHz $< f_c <$ 450 MHz, etc. In spectral peaks of the channel frequency response, the system performance improves, corresponding to an increase in received signal energy due to the multipath and the direct path adding constructively, i.e., $F_1(k) > 0$. For $H_2 < 0$, this is seen from figures 3.7c and 2.5 to take place when 50 MHz $< f_c <$ 150 MHz, 250 MHz $< f_c <$ 350 MHz, etc. When $H_2 > 0$ these effects are exactly reversed.

Note that as $T \rightarrow \tau_\Delta$ corresponding to increasing the data rate for a fixed delay spread (or equivalently $\tau_\Delta \rightarrow T$ corresponding to increasing the delay spread for a fixed data rate), the coherent overlap region between the multipath and the direct path reduces (see figure 3.2) and the constructive/destructive addition becomes less of a factor in determining system performance. This is evident in figures 3.8 - 3.10. From figure 3.10 it can be seen that the carrier frequency dependence decreases approximately linearly as $T \rightarrow \tau_\Delta$ (for $\tau_\Delta = 5\ \eta$sec, $T = \tau_\Delta$ when $R = 200$ Mbps). For the special case when $\tau_\Delta = T$, figure 3.8c shows no carrier frequency dependence. For $\tau_\Delta \geq T$ the system degradation is blind to the sign of H_2 corresponding to the multipath being completely uncorrelated with the direct path during the interval $[0,T]$. It is interesting to observe that the system performance appears to be a strong function of the carrier frequency as long as $\tau_\Delta \leq 0.5\ T$, the so called "flat" or "frequency-nonselective" condition describing the characteristics of the multipath channel in example 2.3. Thus, these results suggest that if one is operating in a deep null and the "frequency-nonselective" channel conditions hold, then a change in carrier frequency by $1/(2\tau_\Delta)$ should dramatically improve performance.

Example 3.2 BPSK Signal, Multipath, Interference and AWGN

Consider now the case of a BPSK signal transmitted through a time-invariant two-path channel with additive interference and additive white Gaussian noise. The two interference models consider either the case of a deterministic CW interjerer or a stochastic finite bandwidth interference. Figure 3.11 plots the system performance with additive CW interference for interference power varying between –20 and +20dB. System performance is seen to degrade rapidly for signal-to-interference ratios on the order of –10 to 0 dB. Figure 3.11c also shows a similar carrier frequency dependence as was described in example 3.1. Figures 3.12 and 3.13 illustrate the effect of interference bandwidth on system performance. For finite bandwidth interference, system degradation is a more gradual function of the signal-to-interference ratio than is the CW interference. However, figure 3.12a shows that for signal power greater than about 3 dB, the finite bandwidth interferer can degrade performance more than the CW interferer of equal power. As the interference bandwidth increases above the data rate and its power, $N_B * B$, remains constant, the effects of the interference decreases as seen clearly in figure 3.13a. This is because the "in-band" interference power, $N_B * 2\ R$, decreases since N_B decreases.

In figure 3.13b, system performance is plotted as a function of interference carrier offset frequency. Performance is seen to be most severely effected when the the interference carrier offset frequency is zero. Local minimum occur for narrowband Gaussian interference in the nulls of the transmitted BPSK signal spectrum, $f_\Delta = R, 2R, \ldots$. As the bandwidth of the interference increases, the interference loses the ability to "hide" in the BPSK signal spectral nulls. Note that the deterministic CW interference has additional offset frequencies, $f_\Delta = \frac{R}{2}, R, \frac{3R}{2}, 2R, \ldots$, where it doesn't affect performance. These values can be found by examining the limiting cases of eq. (3.13)

$$
\begin{aligned}
I(k) &= \sqrt{2I} && \text{for } f_\Delta = 0\ ,\ \phi = 0 \\
I(k) &= \sqrt{2I}\ \cos(\phi) && \text{for } f_\Delta = 0\ ,\ \phi \neq 0 \\
I(k) &= \sqrt{2I}\ \frac{\sin(2\pi f_\Delta T)}{2\pi f_\Delta} && \text{for } f_\Delta \neq 0\ ,\ \phi = 0
\end{aligned}
\tag{3.25}
$$

and solving for f_Δ when $I(k) = 0$. The intermediate values of f_Δ for which system performance is not affected, i.e., $f_\Delta = \frac{R}{2}, \frac{3R}{2}, \ldots$, are an artifact of the integration of the deterministic, constant envelope, and constant phase CW interference that does not exist when the envelope and phase are stochastic (see for instance figure 6 of [1]).

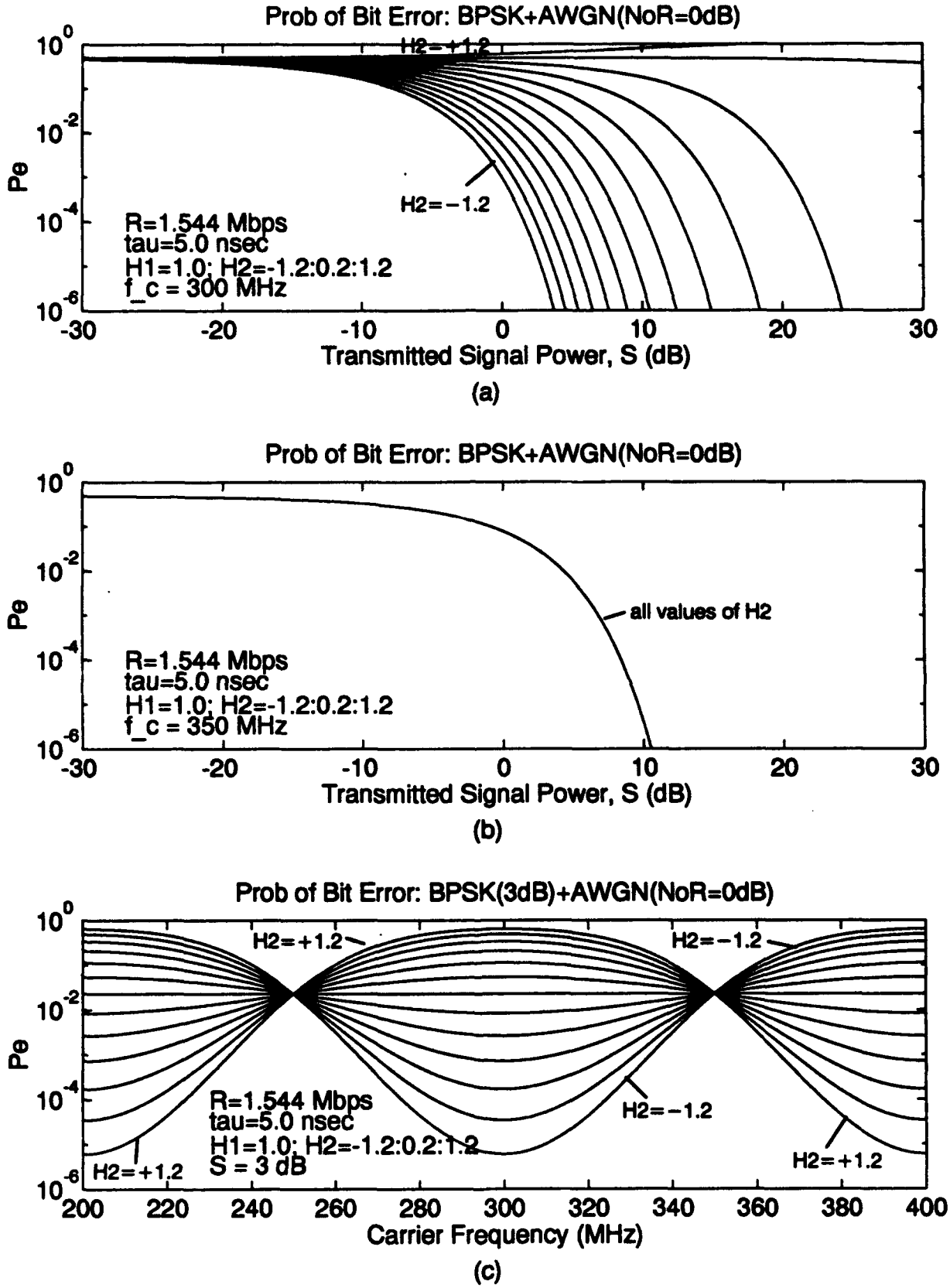

Figure 3.7. Effects of Multipath on BPSK, $\tau_{\Delta} = 0.0077\ T$.

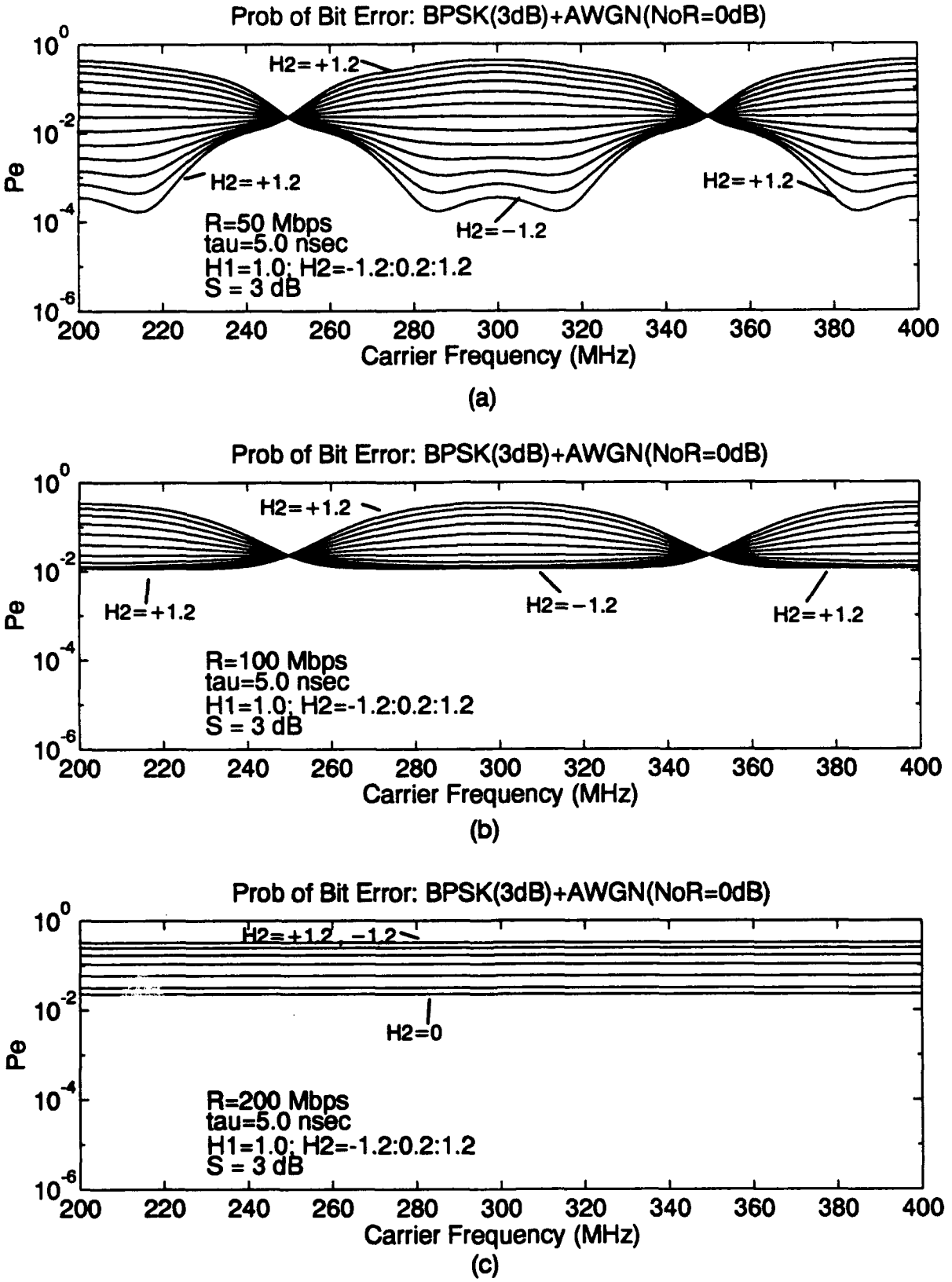

Figure 3.8. Effects of Multipath on BPSK, (a) $\tau_\Delta = 0.25\ T$, (b) $\tau_\Delta = 0.5\ T$, (c) $\tau_\Delta = 1.0\ T$.

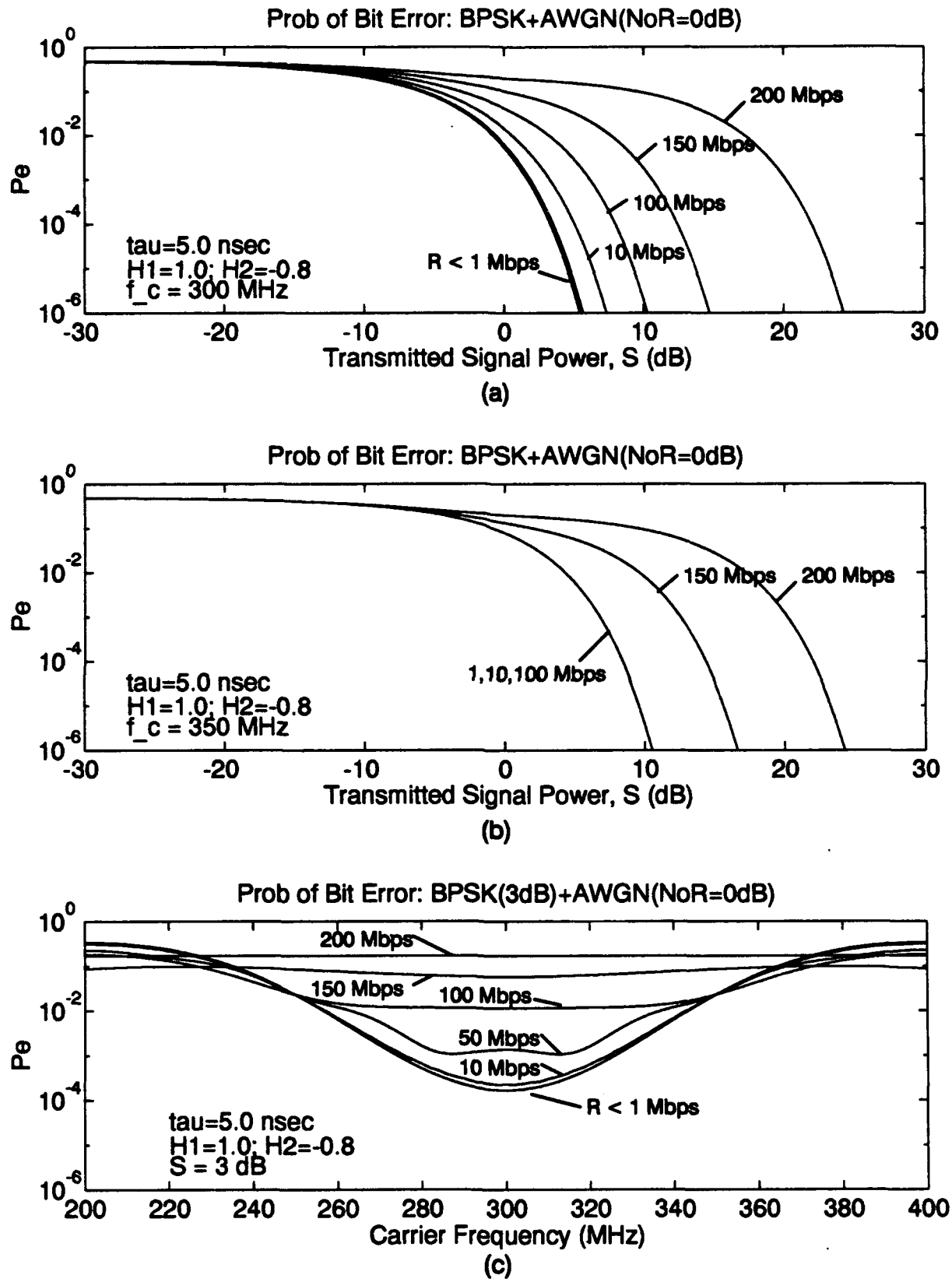

Figure 3.9. System performance of a BPSK signal transmitted through a multipath channel, $\tau_{\Delta} = 5\ \eta$sec, for 1,10,50,100,150,200 Mbps data rates.

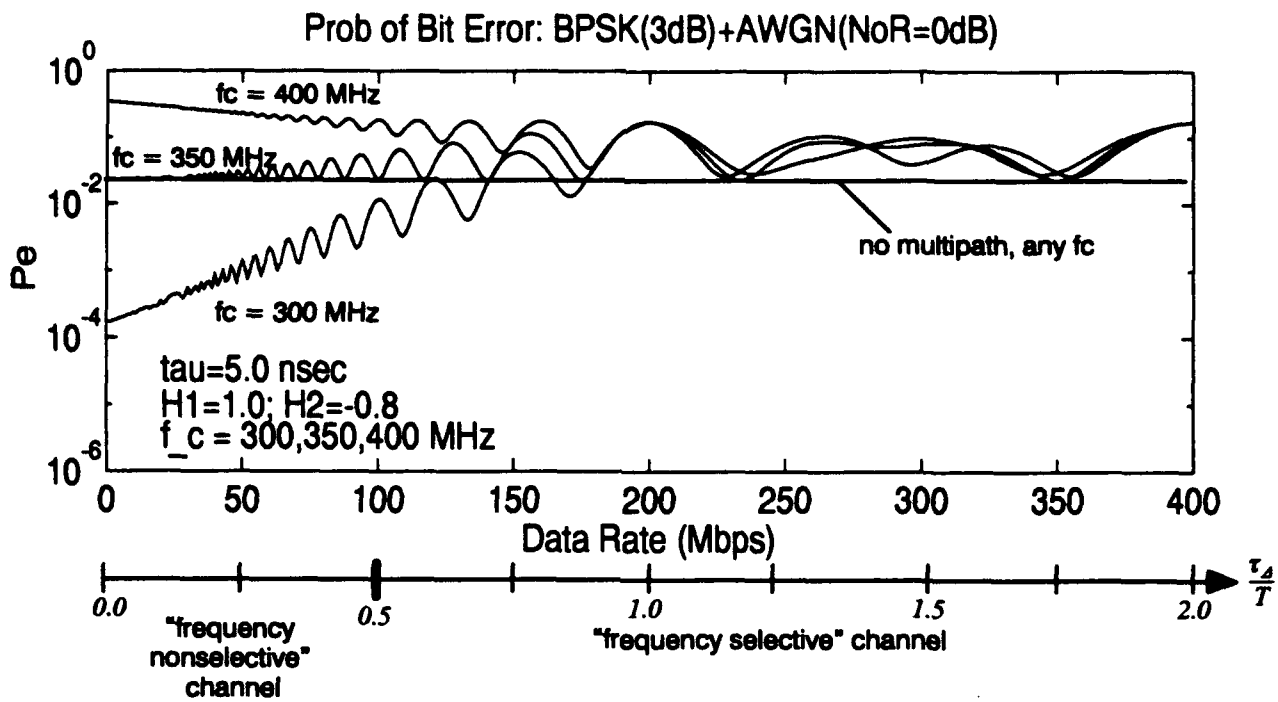

Figure 3.10. System performance as a function of data rate for a BPSK signal transmitted through a multipath channel, $\tau_\Delta = 5\ \eta$sec.

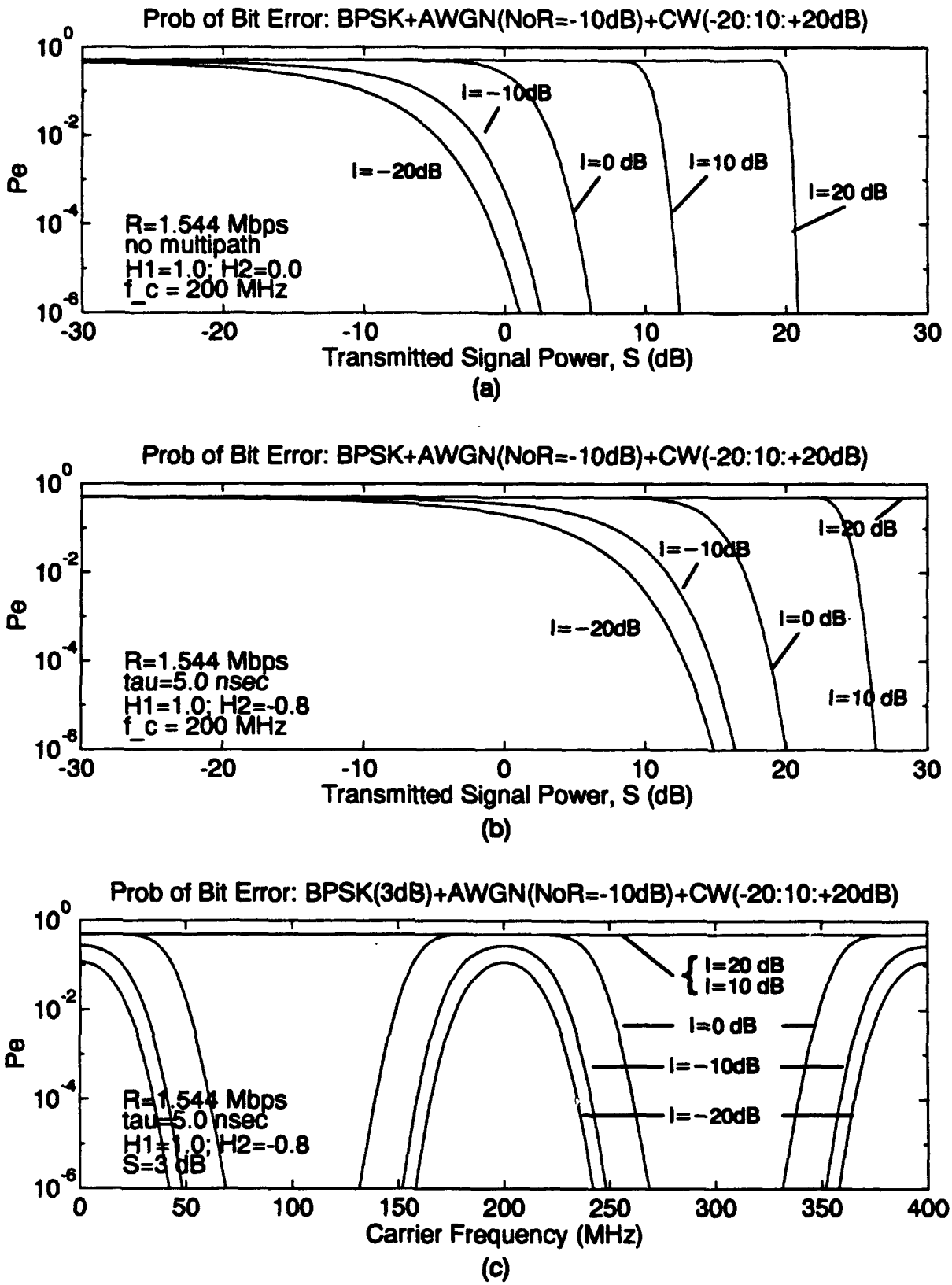

Figure 3.11. BPSK probability of bit error for (a) CW interferer with no multipath, (b) and (c) CW interferer with multipath, $\tau_{\Delta} = 0.0077\ T$.

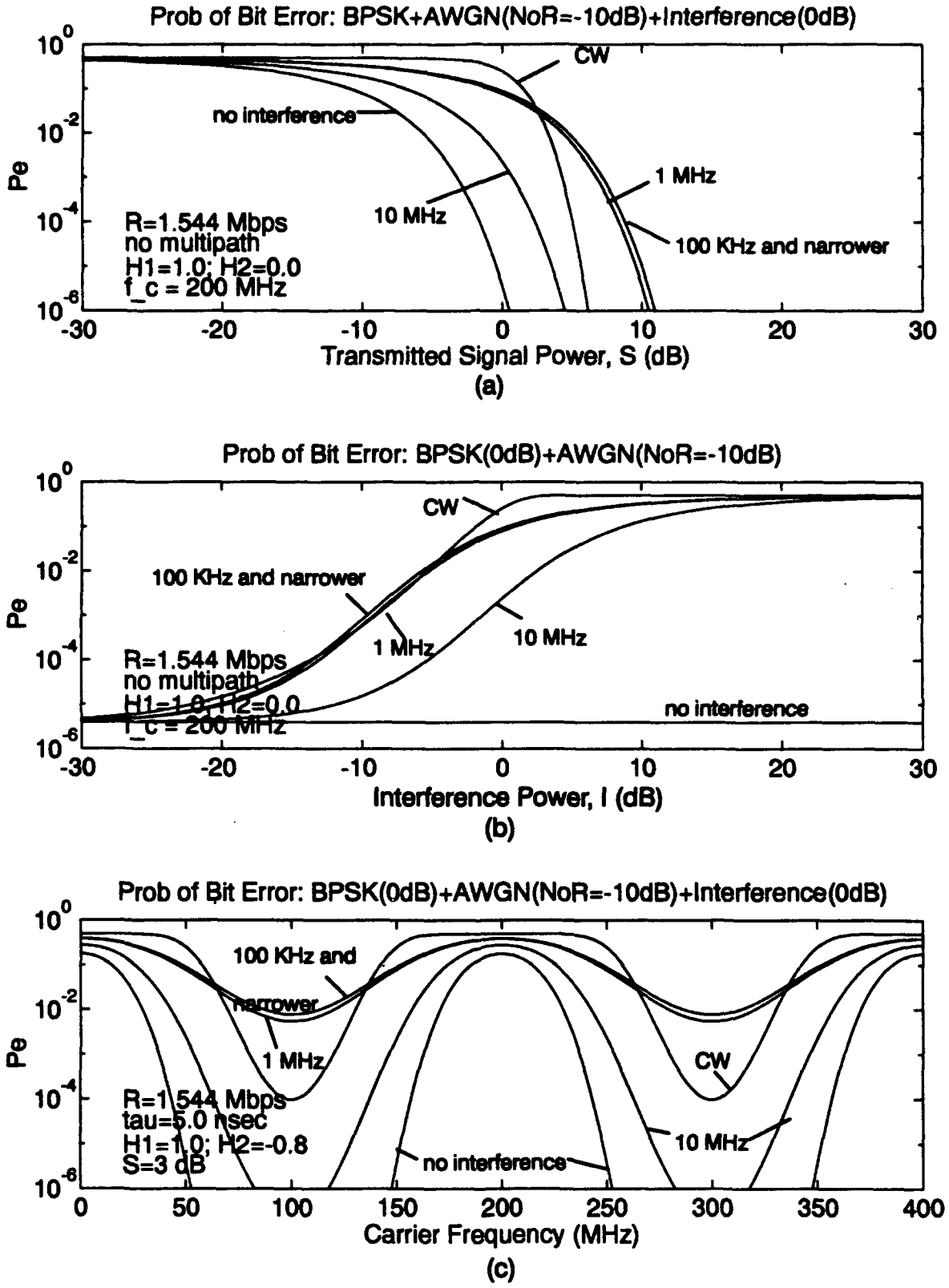

Figure 3.12. BPSK probability of bit error for (a) and (b) CW or finite bandwidth interferer with no multipath, (c) CW or finite bandwidth interferer with multipath, $\tau_{\Delta} = 0.0077\ T$.

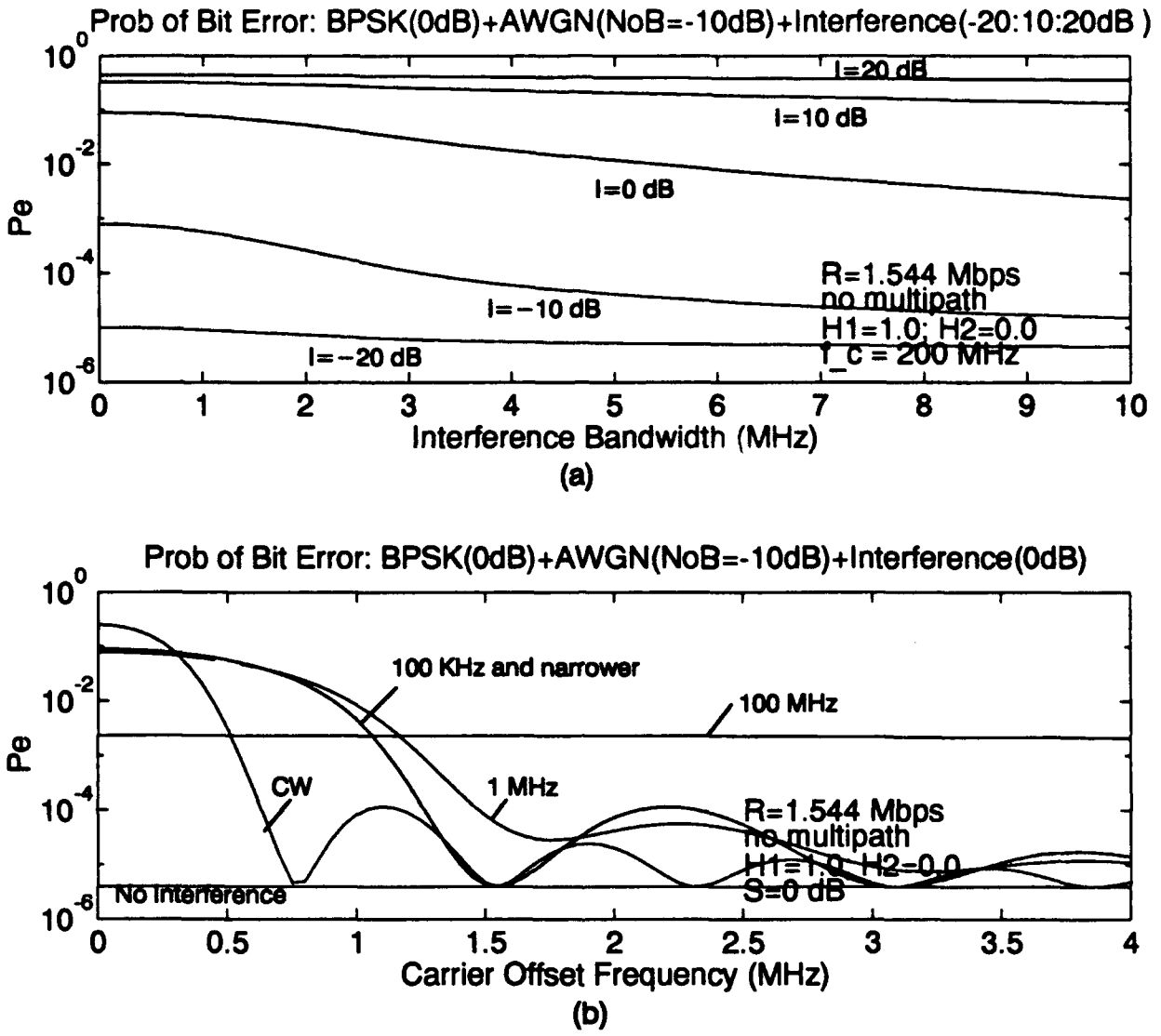

Figure 3.13. BPSK probability of bit error as a function of (a) interference bandwidth and (b) interference offset frequency for the case of no multipath.

4. PERFORMANCE ANALYSIS OF M-PSK SIGNAL

This chapter presents an analysis of the average probability of symbol error for a M-PSK signal transmitted through the channel shown in figure 2.3 and received by the coherent matched filter shown in figure 4.1. The receiver model consists of a correlator implementation of a coherent matched-filter receiver for M-PSK. Figure 4.2 shows the constellation of 8-PSK with its associated decision boundaries and a typical bit-to-symbol mapping called Gray encoding. Note that $\log_2(M)$ bits of information are transmitted with each M-PSK symbol. The material presented in this chapter is an extension of the analysis presented in chapter 3.

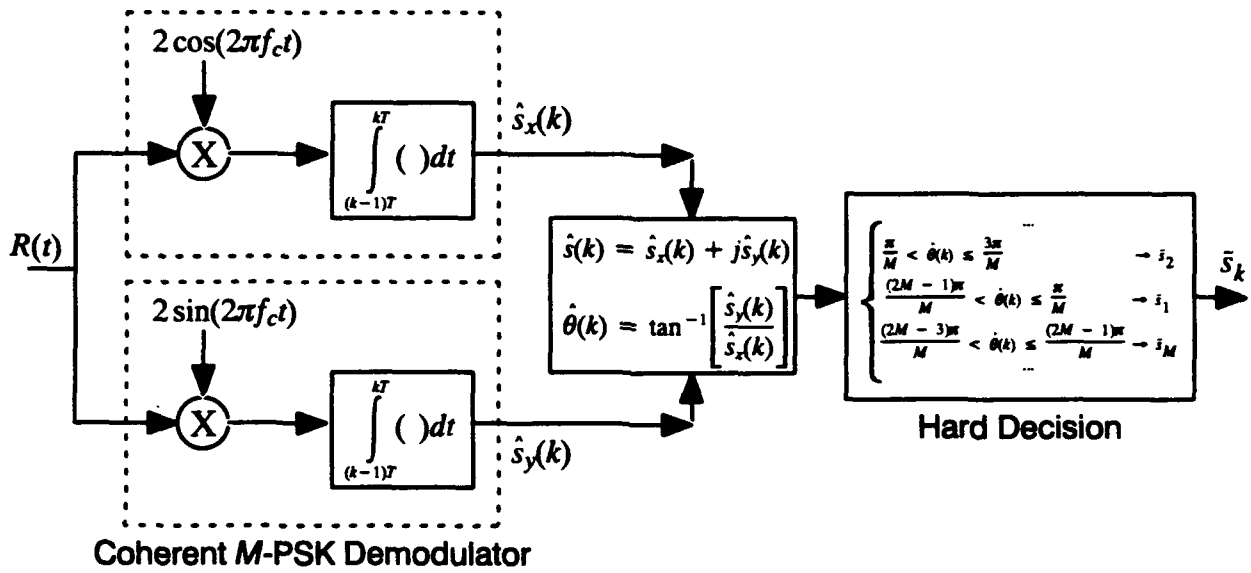

Figure 4.1. Correlator implementation of matched-filter receiver for M-PSK signals.

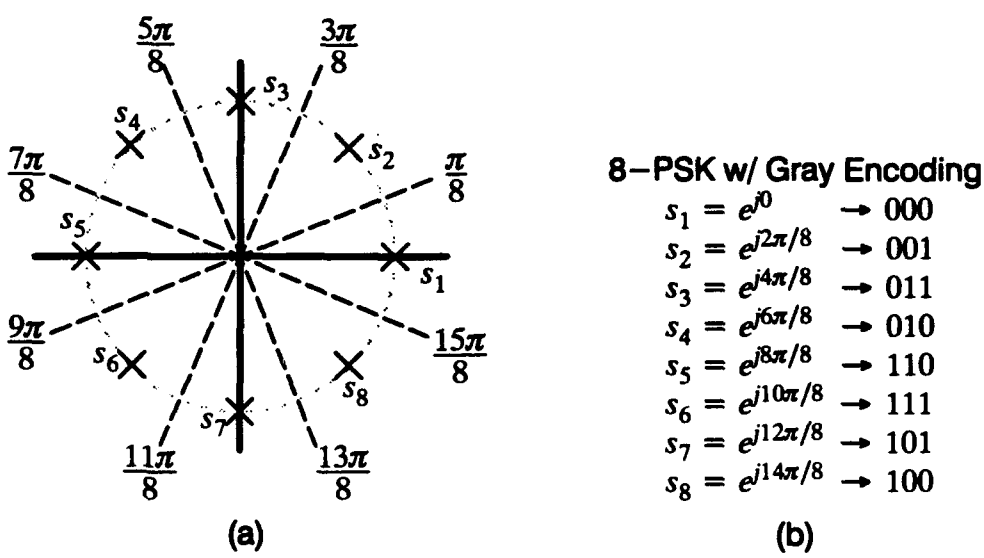

Figure 4.2. 8-PSK (a) constellation with decision boundaries, (b) bit-mapping using Gray encoding.

Using the two-path multipath channel model described in section 2.3, $H(t) = H_1\delta(t) + H_2\,\delta(t - \tau_\Delta)$, the received signal can be expressed as

$$R(t) = H_1 S(t) + H_2 S(t-\tau_\Delta) + I(t) + N(t). \tag{4.1}$$

The M-PSK transmitted bandpass signal can be written as,

$$\begin{aligned} S(t) &= \sqrt{2S} \sum_k P_T(t - kT) \cos(2\pi f_c t + \theta_k) \\ &= \sqrt{2S} \sum_k \left[a_k \cos(2\pi f_c t) - b_k \sin(2\pi f_c t)\right] P_T(t-kT), \end{aligned} \tag{4.2}$$

where $\theta_k \in \left\{\frac{2\pi}{M}\,(i-1)\right\}$ for $i = 1,\ldots,M$ is the phase of the kth M-PSK symbol, $a_k = \cos(\theta_k)$, $b_k = \sin(\theta_k)$, S is the transmitted signal power, and $P_T(t)$ the symbol pulse waveform. At most, one-symbol transition of the multipath signal can take place in the interval $[0, T]$ of the direct path signal. The following analysis will consider only the case of $0 \le \tau_\Delta \le T$. The case of $\tau_\Delta > T$ is a straightforward extension and presented in appendix C. With this assumption on the delay spread, the received signal during the interval $[0,T]$ can be written as

$$\begin{aligned} R(t) = {} & H_1\sqrt{2S}\left[a_k\cos(2\pi f_c t) - b_k\sin(2\pi f_c t)\right] P_T(t) \\ & + H_2\sqrt{2S}\left[a_k \cos(2\pi f_c(t - \tau_\Delta)) - b_k \sin(2\pi f_c(t - \tau_\Delta))\right] P_T(t - \tau_\Delta) \\ & + H_2\sqrt{2S}\left[a_{k-1} \cos(2\pi f_c(t + T - \tau_\Delta)) - b_{k-1} \sin(2\pi f_c(t + T - \tau_\Delta))\right] P_T(t + T - \tau_\Delta) \\ & + I(t) + N(t) \\ = {} & \Big[H_1\sqrt{2S}\; a_k\, P_T(t) + H_2\sqrt{2S}\left\{a_k \cos(2\pi f_c\tau_\Delta) + b_k \sin(2\pi f_c\tau_\Delta)\right\} P_T(t - \tau_\Delta) \\ & + H_2\sqrt{2S}\left\{a_{k-1}\cos(2\pi f_c(\tau_\Delta - T)) + b_{k-1}\sin(2\pi f_c(\tau_\Delta - T))\right\}P_T(t + T - \tau_\Delta))\Big] \cos(2\pi f_c t) \\ & - \Big[H_1\sqrt{2S}\; b_k\, P_T(t) + H_2\sqrt{2S}\left\{- a_k \sin(2\pi f_c\tau_\Delta) + b_k \cos(2\pi f_c\tau_\Delta)\right\} P_T(t - \tau_\Delta) \\ & + H_2\sqrt{2S}\left\{- a_{k-1}\sin(2\pi f_c(\tau_\Delta - T)) + b_{k-1}\cos(2\pi f_c(\tau_\Delta - T))\right\}P_T(t + T - \tau_\Delta))\Big] \sin(2\pi f_c t) \\ & + I(t) + N(t) \end{aligned} \tag{4.3}$$

using trigonometric identities. Note that for BPSK, M=2 and $\theta_k \in \{0°, 180°\}$, thus, $a_k \in \{+1, -1\}$ and $b_k = 0$ and eq. (4.3) reduces to eq. (3.3) when the $\sin(2\pi f_c t)$ terms are neglected.

4.1 MATCHED-FILTER DETECTION OF M-PSK WITH CW INTERFERENCE

This section derives the probability of symbol error for the received signal given by eq. (4.3) with CW interference, $I(t) = \sqrt{2I}\,\cos(2\pi(f_c + f_\Delta)t + \phi)$. Without loss of generality, consider the interval $[0,T]$. The output of the in-phase integrator, $\hat{s}_x(k)$, and the output of the quadrature integrator, $\hat{s}_y(k)$, in figure 4.1 can be written as

$$\hat{s}_x(k) = \int_0^T R(t)\ 2\cos(2\pi f_c t)\ dt$$

$$= a_k\ D(k) + a_k\ F_1(k) + b_k\ G_1(k) + a_{k-1}\ F_2(k) + b_{k-1}\ G_2(k) + I_x(k) + N_x(k), \qquad (4.4)$$

$$\hat{s}_y(k) = \int_0^T R(t)\ 2\sin(2\pi f_c t)\ dt$$

$$= b_k\ D(k) + b_k\ F_1(k) - a_k\ G_1(k) + b_{k-1}\ F_2(k) - a_{k-1}\ G_2(k) + I_y(k) + N_y(k) \qquad (4.5)$$

where the terms in eqs. (4.4) and (4.5) will be defined in section 4.2. The conditional probability of symbol error, given the parameters of the channel model and interference parameters, is given by

$$P_s(H_1, H_2, \tau_\Delta, I, f_\Delta, \phi) = \sum_{j=1}^{M} \frac{1}{M}\ P_s(s_j \mid H_1, H_2, \tau_\Delta, I, f_\Delta, \phi) \qquad (4.6)$$

for equal probabilities of transmitting each of the M symbols. Recall that the probability of detecting a symbol error, P_s, is equal to one minus the probability of detecting a correct symbol, P_c. Thus, for the case when $0 \le \tau_\Delta \le T$, we can express the conditional probability of symbol error given that the symbol s_j was transmitted as

$$P_s(s_j|H_1, H_2, \tau_\Delta, I, f_\Delta, \phi) = 1 - P_c(s_j|H_1, H_2, \tau_\Delta, I, f_\Delta, \phi)$$

$$= 1 - \sum_{i=1}^{M} \frac{1}{M}\ \Pr\left(\theta_1^j < \hat{\theta}(k) \le \theta_2^j \mid s_{k-1} = s_i\ ,\ s_k = s_j\right), \qquad (4.7)$$

where θ_1^j and θ_2^j are the angles of the lower and upper decision boundaries respectively. For example for $s_j = s_1 = e^{j0}$, we have $\theta_1^1 = -\frac{\pi}{M}$ and $\theta_2^1 = \frac{\pi}{M}$. Note that for M-ary signals, we must consider the possibility that one of M symbols was previously transmitted. For the case when $\tau_\Delta > T$, eq. (4.7) would contain M^2 components since the two symbols in the multipath are not correlated with the symbol in the direct path, s_k, during the interval $[0,T]$. This case is presented in appendix C.

When the probability of symbol error is the same for each symbol, eq. (4.6) can be simplified to

$$P_s(H_1, H_2, \tau_\Delta, I, f_\Delta, \phi) = P_s(s_1 \mid H_1, H_2, \tau_\Delta, I, f_\Delta, \phi). \qquad (4.8)$$

This can be shown to be true for either the case of multipath and AWGN or the case of multipath with additive finite bandwidth interference and AWGN (treated in section 4.3). However, it is not true for the case considered here. Hence, we will be forced to solve the general form of eq. (4.7).

To compute eq. (4.7), it will be necessary to derive the probability density function of $\hat{\theta}_k$ since $\Pr(\theta_1 < \hat{\theta}(k) \le \theta_2) \equiv \int_{\theta_1}^{\theta_2} pdf_{\hat{\theta}}(\theta)\ d\theta$. This will require the following steps:

(1) find the joint probability density function of $\hat{s}_x(k)$ and $\hat{s}_y(k)$ in rectangular coordinates, $pdf_{\hat{s}_x\hat{s}_y}(x,y)$, (2) transform $pdf_{\hat{s}_x\hat{s}_y}(x,y)$ into a joint probability density function in polar coordinates,

$pdf_{\hat{r},\hat{\theta}}(r,\theta)$, and (3) remove the radial dependence by integration, $pdf_{\hat{\theta}}(\theta) = \int_0^\infty pdf_{\hat{r},\hat{\theta}}(r,\theta)\, dr$. The following proceeds with each of these steps:

(1) Note that the only random term in eq. (4.4) that is not being conditioned on is the Gaussian random variable, $N_x(k)$. Thus, $\hat{s}_x(k)$ will be a conditionally Gaussian random variable with conditional mean and variance

$$\begin{aligned} m_{\hat{s}_x} &= a_k\, D(k) + a_k\, F_1(k) + b_k\, G_1(k) + a_{k-1}\, F_2(k) + b_{k-1}\, G_2(k) + I_x(k) \\ \sigma^2_{\hat{s}_x} &= \sigma^2_{N_x} = \sigma^2_N. \end{aligned} \tag{4.9}$$

Similarly, $\hat{s}_y(k)$ given by eq. (4.5) will be a conditionally Gaussian random variable uncorrelated with $\hat{s}_x(k)$ and with statistics given by

$$\begin{aligned} m_{\hat{s}_y} &= b_k\, D(k) + b_k\, F_1(k) - a_k\, G_1(k) + b_{k-1}\, F_2(k) - a_{k-1}\, G_2(k) + I_y(k) \\ \sigma^2_{\hat{s}_y} &= \sigma^2_{N_y} = \sigma^2_N. \end{aligned} \tag{4.10}$$

The terms in eqs. (4.9) and (4.10) will be calculated below in section 4.2. Since $\hat{s}_x(k)$ and $\hat{s}_y(k)$ are uncorrelated and Gaussian random variables they are also independent [10]. Thus, their joint probability density function is

$$\begin{aligned} pdf_{\hat{s}_x\hat{s}_y}(x,y) &= \left[\frac{1}{\sqrt{2\pi}\,\sigma_N}\, e^{-\frac{(x-m_x)^2}{2\sigma_N^2}}\right]\left[\frac{1}{\sqrt{2\pi}\,\sigma_N}\, e^{-\frac{(y-m_y)^2}{2\sigma_N^2}}\right] \\ &= \frac{1}{2\pi\sigma_N^2}\, e^{\frac{(x-m_x)^2+(y-m_y)^2}{2\sigma_N^2}}. \end{aligned} \tag{4.11}$$

(2) From figure 4.1, it is seen that the decision variable is $\hat{\theta}(k) = \tan^{-1}\left[\frac{\hat{s}_y(k)}{\hat{s}_x(k)}\right]$, thus the probability density function of eq. (4.11) must be changed into a probability density function involving magnitude and phase (see section 2.11 of [10]). This is accomplished by a change of variables, $r = \sqrt{x^2 + y^2}$ and $\theta = \tan^{-1}\left[\frac{y}{x}\right]$ resulting in

$$\begin{aligned} pdf_{\hat{r},\hat{\theta}}(r,\theta) &= pdf_{\hat{s}_x\hat{s}_y}(x,y) \begin{vmatrix} \frac{\partial x}{\partial r} & \frac{\partial x}{\partial \theta} \\ \frac{\partial y}{\partial r} & \frac{\partial y}{\partial \theta} \end{vmatrix}_{x=r\cos(\theta),\, y=r\sin(\theta)} \\ &= \frac{r}{2\pi\sigma_N^2}\, e^{\frac{r^2-2r\{m_x\cos(\theta)+m_y\sin(\theta)\}+m_x^2+m_y^2}{2\sigma_N^2}} \end{aligned} \tag{4.12}$$

(3) The final step requires removal of the r dependence in eq. (4.12) by integration. Proceeding by completing the square in the exponent term and letting $\beta = m_x\cos(\theta) + m_y\sin(\theta)$ we find

$$pdf_{\hat{\theta}}(\theta) = \int_0^\infty pdf_{\hat{r},\hat{\theta}}(r,\theta)\, dr$$

$$= \frac{1}{2\pi\sigma_N^2}\, e^{-\frac{-\beta^2+m_x^2+m_y^2}{2\sigma_N^2}} \int_0^\infty r\, e^{-\frac{(r-\beta)^2}{2\sigma_N^2}}\, dr. \tag{4.13}$$

Let $t = (r-\beta)/\sigma_N$, we can rewrite eq. (4.13) as

$$pdf_{\hat{\theta}}(\theta) = \frac{1}{2\pi\sigma_N^2}\, e^{-\frac{-\beta^2+m_x^2+m_y^2}{2\sigma_N^2}} \int_{-\beta/\sigma_n}^\infty \sigma_N \left[t\,\sigma_N + \beta\right] e^{-\frac{t^2}{2}}\, dt$$

$$= \frac{1}{2\pi\sigma_N^2}\, e^{-\frac{-\beta^2+m_x^2+m_y^2}{2\sigma_N^2}} \left\{ \sigma_N^2 \int_{-\beta/\sigma_n}^\infty t\, e^{-\frac{t^2}{2}}\, dt + \sigma_N\,\beta \int_{-\beta/\sigma_n}^\infty e^{-\frac{t^2}{2}}\, dt \right\}. \tag{4.14}$$

The first integration in eq. (4.14) is straightforward while the second integration can be found from eq. (3.8) noting that $\Phi(-x) = 1 - \Phi(x)$. Thus, evaluating eq. (4.14),

$$pdf_{\hat{\theta}}(\theta) = \frac{1}{2\pi\sigma_N^2}\, e^{-\frac{-\beta^2+m_x^2+m_y^2}{2\sigma_N^2}} \left\{ -\sigma_N^2\, e^{-\frac{t^2}{2}} \Big|_{t=-\beta/\sigma_n}^{t=\infty} + \sqrt{2\pi}\,\sigma_N\,\beta\,\Phi\left(\frac{\beta}{\sigma_n}\right) \right\}$$

$$= \frac{1}{2\pi}\, e^{-\frac{m_x^2+m_y^2}{2\sigma_N^2}} + \frac{\beta}{\sqrt{2\pi}\,\sigma_N}\, e^{-\frac{-\beta^2+m_x^2+m_y^2}{2\sigma_N^2}}\, \Phi\left(\frac{\beta}{\sigma_n}\right). \tag{4.15}$$

Plugging β into eq. (4.15) and rewriting the exponent in the second term we finally arrive at

$$pdf_{\hat{\theta}}(\theta) = \frac{1}{2\pi}\, e^{-\frac{m_x^2+m_y^2}{2\sigma_N^2}} + \frac{m_x\cos(\theta) + m_y\sin(\theta)}{\sqrt{2\pi}\,\sigma_N}\, e^{-\frac{(m_x\sin(\theta)-m_y\cos(\theta))^2}{2\sigma_N^2}}\, \Phi\left(\frac{m_x\cos(\theta) + m_y\sin(\theta)}{\sigma_n}\right) \tag{4.16}$$

Thus, the conditional probability of symbol error is given by

$$P_s(s_j|H_1,H_2,\tau_\Delta,I,f_\Delta,\phi) = 1 - \sum_{i=1}^{M} \frac{1}{M} \int_{\theta_1^j}^{\theta_2^j} pdf_{\hat{\theta}}\left(\theta \mid s_{k-1} = s_i\,,\ s_k = s_j\right) d\theta \tag{4.17}$$

using eq. (4.16) to compute $pdf_{\hat{\theta}}(\theta)$, and eqs. (4.9) and (4.10) to compute m_x and m_y respectively. Note that m_x and m_y are dependent on the symbols s_k and s_{k-1}. In general, the integral in eq. (4.17) must be evaluated by numerical methods (at least as far as the authors are aware of). However, we can make use the following upper bound (see p. 264 of [3])

$$\Phi(-x) \equiv \frac{1}{\sqrt{2\pi}} \int_x^\infty e^{-t^2/2}\, dt$$

$$\leq \frac{1}{\sqrt{2\pi}} \int_x^\infty \frac{1+t^2}{t^2}\, e^{-t^2/2}\, dt \quad \text{since } \frac{1+t^2}{t^2} > 0 \quad \text{for } t > 0$$

$$\leq \frac{1}{\sqrt{2\pi}} \frac{1}{x}\, e^{-x^2/2} \quad \text{for } x > 0. \tag{4.18}$$

Before continuing, it should be noted that the upper bound in eq. (4.18) is much tighter than the Chernoff Bound, $\Phi(-x) \leq e^{-x^2/2}$ for $x > 0$, derived in appendix D. Modifying eq. (4.18) slightly by noting that $\Phi(x) = 1 - \Phi(-x)$, we obtain

$$\Phi(x) \leq 1 - \frac{1}{\sqrt{2\pi}\, x}\, e^{-x^2/2} \quad \text{for } x > 0, \tag{4.19}$$

which can be used to remove the phi function in eq. (4.16) and evaluate the integral in eq. (4.17). Using eq. (4.19) in eq. (4.15) we find the following

$$pdf_{\dot{\theta}}(\theta) \leq \frac{1}{2\pi}\, e^{-\frac{m_x^2+m_y^2}{2\sigma_N^2}} + \frac{\beta}{\sqrt{2\pi}\,\sigma_N}\, e^{-\frac{-\beta^2+m_x^2+m_y^2}{2\sigma_N^2}} \left(1 - \frac{1}{\sqrt{2\pi}} \frac{\sigma_n}{\beta}\, e^{-\frac{\beta^2}{2\sigma_N^2}}\right)$$

$$\leq \frac{\beta}{\sqrt{2\pi}\,\sigma_N}\, e^{\frac{-\beta^2+m_x^2+m_y^2}{2\sigma_N^2}} \quad \text{for } \left[m_x\cos(\theta) + m_y\sin(\theta)\right] > 0. \tag{4.20}$$

Now, evaluating just the integral in eq. (4.17) and using eq. (4.20) with β plugged back in and letting $t = \left(m_x\sin(\theta) - m_y\cos(\theta)\right)/\sigma_N$, we have

$$\int_{\theta_1^j}^{\theta_2^j} pdf_{\dot{\theta}}(\theta)\, d\theta \leq \frac{1}{\sqrt{2\pi}} \int_{\theta_1^j}^{\theta_2^j} \frac{m_x\cos(\theta) + m_y\sin(\theta)}{\sigma_N}\, e^{-\frac{\left(m_x\sin(\theta) - m_y\cos(\theta)\right)^2}{2\sigma_N^2}}\, d\theta$$

$$\leq \frac{1}{\sqrt{2\pi}} \int_{\frac{m_x\sin\theta_1^j - m_y\cos\theta_1^j}{\sigma_N}}^{\frac{m_x\sin\theta_2^j - m_y\cos\theta_2^j}{\sigma_N}} e^{-\frac{t^2}{2}}\, dt$$

$$\leq \Phi\left[\frac{m_x\sin\theta_2^j - m_y\cos\theta_2^j}{\sigma_N}\right] - \Phi\left[\frac{m_x\sin\theta_1^j - m_y\cos\theta_1^j}{\sigma_N}\right]. \tag{4.21}$$

Thus, we find the upper bound for the conditional probability of symbol error is given by

$$P_s(s_j|H_1,H_2,\tau_\Delta,I,f_\Delta,\phi) \le 1 - \sum_{i=1}^{M} \frac{1}{M} \left\{ \Phi\left[\frac{m_x \sin\theta_2^j - m_y \cos\theta_2^j}{\sigma_N}\right] - \Phi\left[\frac{m_x \sin\theta_1^j - m_y \cos\theta_1^j}{\sigma_N}\right]\right\} \tag{4.22}$$

where m_x and m_y are dependent on both the i and j index through the present and past symbols $s_{k-1} = s_i$ and $s_k = s_j$ and are given by eqs. (4.9) and (4.10). Using eq. (4.22) in eq. (4.6) we find that the average conditional probability of symbol error can be written as

$$P_s(H_1,H_2,\tau_\Delta,I,f_\Delta,\phi) \le 1 - \sum_{j=1}^{M} \sum_{i=1}^{M} \frac{1}{M^2} \left\{ \Phi\left[\frac{m_x \sin\theta_2^j - m_y \cos\theta_2^j}{\sigma_N}\right] - \Phi\left[\frac{m_x \sin\theta_1^j - m_y \cos\theta_1^j}{\sigma_N}\right]\right\} \tag{4.23}$$

Eqs. (4.23) and (4.22) are valid as long as $m_x\cos(\theta) + m_y\sin(\theta) > 0$ for all $\theta_1^j \le \theta \le \theta_2^j$. For M=2, eq. (4.23) can be shown to be exactly twice as large the exact BPSK expression derived in eq. (3.9).

4.2 TERMS IN EQS. (4.4) AND (4.5)

$a_k\, D(k)$ and $b_k\, D(k)$ are the desired in-phase and quadrature signal terms from the direct transmission path. $D(k)$ can be found from interpreting either arm of figure 4.1, for instance the quadrature gives

$$b_k\, D(k) = \int_0^T H_1 \sqrt{2S}\; a_k \sin(2\pi f_c t)\; 2\sin(2\pi f_c t)\; dt$$

for $P_T(t)$ equal to a rectangular pulse during the interval $[0,T]$. Solving for $D(k)$ we find

$$D(k) = H_1 \sqrt{2S}\, T \tag{4.24}$$

since the high-frequency terms are removed by the integration.

$a_k\, F_1(k)$, $b_k\, G_1(k)$, $a_{k-1}\, F_2(k)$, and $b_{k-1}\, G_2(k)$ are the in-phase interference terms (ISI) created by the multipath while $b_k\, F_1(k)$, $a_k\, G_1(k)$, $b_{k-1}\, F_2(k)$, and $a_{k-1}\, G_2(k)$ are the quadrature interference terms (ISI) created by the multipath. It is straightforward to show that

$$F_1(k) = H_2 \sqrt{2S}\; (T - \tau_\Delta)\; \cos(2\pi f_c \tau_\Delta) \tag{4.25}$$

$$F_2(k) = H_2 \sqrt{2S}\; (\tau_\Delta)\; \cos(2\pi f_c (\tau_\Delta - T)) \tag{4.26}$$

$$G_1(k) = H_2 \sqrt{2S}\; (T - \tau_\Delta)\; \sin(2\pi f_c \tau_\Delta) \tag{4.27}$$

$$G_2(k) = H_2 \sqrt{2S}\; (\tau_\Delta)\; \sin(2\pi f_c (\tau_\Delta - T)). \tag{4.28}$$

For the CW interference, $I_x(k)$ is given by

$$I_x(k) = \int_0^T \sqrt{2I}\cos(2\pi(f_c + f_\Delta)t + \phi)\ 2\cos(2\pi f_c t)\ dt$$
$$= \sqrt{2I}\ \frac{[\sin(2\pi f_\Delta T + \phi) - \sin(\phi)]}{2\pi f_\Delta} \tag{4.29}$$

and $I_y(k)$ is given by

$$I_y(k) = \int_0^T \sqrt{2I}\cos(2\pi(f_c + f_\Delta)t + \phi)\ 2\sin(2\pi f_c t)\ dt$$
$$= \sqrt{2I}\ \frac{[\cos(2\pi f_\Delta T + \phi) - \cos(\phi)]}{2\pi f_\Delta}. \tag{4.30}$$

$N_x(k)$ and $N_y(k)$ are the Gaussian noise terms defined as

$$N_x(k) = \int_0^T N(t)\ 2\cos(2\pi f_c t)\ dt \quad N_y(k) = \int_0^T N(t)\ 2\sin(2\pi f_c t)\ dt.$$

As was derived in eq. (3.14), it is straight forward to show that

$$E[N_x(k)] = E[N_y(k)] = E[N(t)] = 0$$
$$\sigma^2_{N_x} = \sigma^2_{N_y} = \sigma^2_N = N_0 T. \tag{4.31}$$

Thus, the conditional probability of symbol error for a M-PSK signal transmitted through a two-path channel with additive CW interference and AWGN is given by using eqs. (4.24) - (4.31) with eqs. (4.9) and (4.10) in either eqs. (4.16), (4.17), and (4.6) or in eq. (4.23).

4.3. MATCHED-FILTER DETECTION OF M-PSK WITH FINITE BANDWIDTH INTERFERENCE

The previous results are now extended to include a finite bandwidth interference. In particular, the interference is generated by passing white Gaussian noise through an ideal bandpass filter resulting in the spectrum displayed in figure 2.7. In this case, both the interference and the noise are assumed to be uncorrelated, Gaussian random variables. Thus, $\hat{s}_x(k)$ and $\hat{s}_y(k)$ are still conditionally Gaussian random variables as they were for the CW interference case, but with modified conditional mean and variance. In addition, the probability of symbol error is the same for each symbol, thus eq. (4.23) can be simplified to just that of eq. (4.22). Other than these modifications, all other previously derived results hold for finite bandwidth interference.

The statistics of $\hat{s}_x(k)$ and $\hat{s}_y(k)$ are given by

$$m_{\hat{s}_x} = a_k\, D(k) + a_k\, F_1(k) + b_k\, G_1(k) + a_{k-1}\, F_2(k) + b_{k-1}\, G_2(k)$$
$$\sigma^2_{\hat{s}_x} = \sigma^2_{N_x} + \sigma^2_{I_x} = \sigma^2_N + \sigma^2_I \tag{4.32}$$
$$m_{\hat{s}_y} = b_k\, D(k) + b_k\, F_1(k) - a_k\, G_1(k) + b_{k-1}\, F_2(k) - a_{k-1}\, G_2(k)$$
$$\sigma^2_{\hat{s}_y} = \sigma^2_{N_y} + \sigma^2_{I_y} = \sigma^2_N + \sigma^2_I. \tag{4.33}$$

All terms in eqs. (4.32) and (4.33) were previously derived in section 4.2 with the exception of $\sigma^2_{I_x}$ and $\sigma^2_{I_y}$, which will now be derived.

Let the received bandpass interference be written in terms of its in-phase baseband signal, $x(t)$, and its quadrature baseband signal, $y(t)$,

$$\begin{aligned} I(t) &= x(t)\cos(2\pi(f_c + f_\Delta)t) - y(t)\sin(2\pi(f_c + f_\Delta)t) \\ &= \left[x(t)\cos(2\pi f_\Delta t) - y(t)\sin(2\pi f_\Delta t)\right]\cos(2\pi f_c t) \\ &\quad -\left[x(t)\sin(2\pi f_\Delta t) + y(t)\cos(2\pi f_\Delta t)\right]\sin(2\pi f_c t). \end{aligned} \tag{4.34}$$

Then, the in-phase interference component can be written as

$$\begin{aligned} I_x(k) &= \int_0^T \left[x(t)\cos(2\pi f_\Delta t) - y(t)\sin(2\pi f_\Delta t)\right]\cos(2\pi f_c t)\, 2\cos(2\pi f_c t)\, dt \\ &\quad - \int_0^T \left[x(t)\sin(2\pi f_\Delta t) + y(t)\cos(2\pi f_\Delta t)\right]\sin(2\pi f_c t)\, 2\cos(2\pi f_c t)\, dt \\ &= \int_0^T \left[x(t)\cos(2\pi f_\Delta t) - y(t)\sin(2\pi f_\Delta t)\right] dt, \end{aligned} \tag{4.35}$$

and the quadrature interference component can be written as

$$\begin{aligned} I_y(k) &= \int_0^T \left[x(t)\cos(2\pi f_\Delta t) - y(t)\sin(2\pi f_\Delta t)\right]\cos(2\pi f_c t)\, 2\sin(2\pi f_c t)\, dt \\ &\quad - \int_0^T \left[x(t)\sin(2\pi f_\Delta t) + y(t)\cos(2\pi f_\Delta t)\right]\sin(2\pi f_c t)\, 2\sin(2\pi f_c t)\, dt \\ &= -\int_0^T \left[x(t)\sin(2\pi f_\Delta t) + y(t)\cos(2\pi f_\Delta t)\right] dt, \end{aligned} \tag{4.36}$$

since high frequency terms are removed by the integration. The mean of both eqs. (4.35) and (4.36) will be zero since $E[x(t)] = E[y(t)] = 0$. Following the same analysis as was done in section 3.3 it is apparent that $\sigma_{I_x}^2 = \sigma_{I_y}^2 = \sigma_I^2$, which was derived in eq. (3.23) and repeated here for convenience

$$\begin{aligned} \sigma_I^2 &= \frac{N_B}{\pi}\, T\left[Si(\pi(B - 2f_\Delta)T) + \frac{\cos(\pi(B - 2f_\Delta)T) - 1}{\pi(B - 2f_\Delta)T}\right] \\ &\quad + \frac{N_B}{\pi}\, T\left[Si(\pi(B + 2f_\Delta)T) + \frac{\cos(\pi(B + 2f_\Delta)T) - 1}{\pi(B + 2f_\Delta)T}\right]. \end{aligned} \tag{4.37}$$

4.4. SUMMARY AND EXAMPLES

The vector representation of the received baseband signal applied in section 3.4 for BPSK can also be applied for M-PSK. Figure 4.3 illustrates the vector diagram of the received baseband signal when the quadrature phase-shift-keyed (QPSK) (M=4) signal is transmitted through the time-invariant two-path channel with $\tau_\Delta \le T$. The direct path symbol vectors have length $H_1\sqrt{2S}$ while the two interfering symbol vectors have length $H_2\sqrt{2S}$ and phase relative to the direct path of $\theta_1 = 2\pi f_c \tau_\Delta$

and $\theta_2 = 2\pi f_c(\tau_\Delta - T)$. The received demodulated symbol can be found by vector addition resulting in a total of M (equal to four here) possible symbols demodulated in the interval $[0,T]$ for each transmitted symbol. Note that only one of the possible demodulated symbols represented in figure 4.3 exists at any one time. The duration of each symbol is defined in figure 3.2 as was the case for BPSK. For the case of $\tau_\Delta > T$, the first multipath symbol is no longer correlated with the transmitted direct path symbol, so it too will generate M vectors resulting in the demodulation of M^2 possible received symbols for each transmitted symbol.

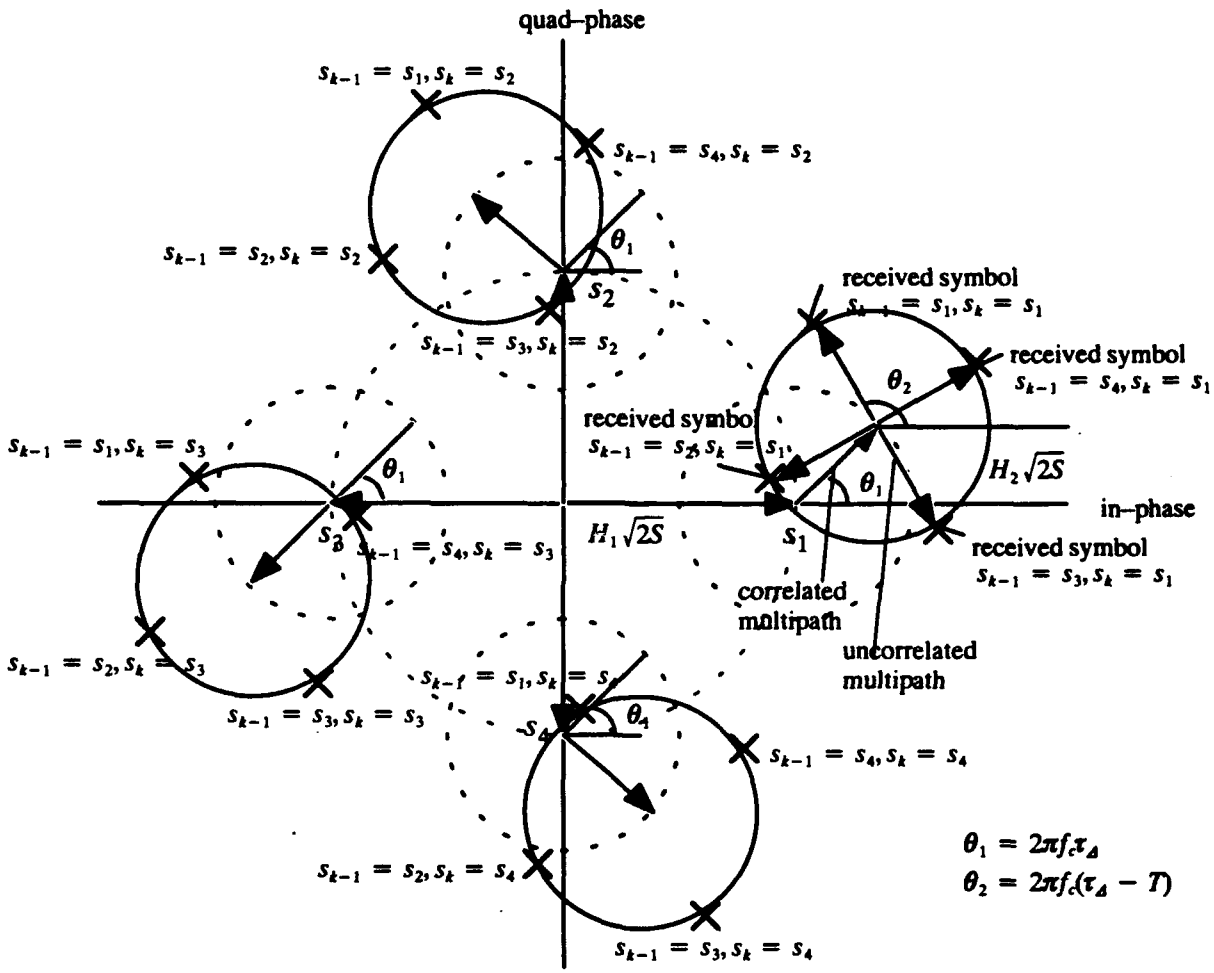

Figure 4.3. Possible demodulated symbols during the interval $[0, T]$ for a QPSK signal transmitted through a two-path channel with $0 \le \tau_\Delta \le T$.

It should be noted that while the exact relationship between the probability of bit error and the probability of symbol error is in general quite complicated, the relationship can be approximated by

$$P_e \approx \frac{1}{\log_2 M} P_s \tag{4.38}$$

where P_s is the average probability of symbol error and P_e is the average probability of bit error.

The following examples will exercise the average probability of symbol error equations derived in this chapter to highlight some of the characteristics exhibited by a multipath communication channel with additive interference. Figures 4.4, 4.6, and 4.7 summarize the equations required to compute the average probability of symbol error for the cases of no interference, CW interference, and finite bandwidth interference respectively for $0 \le \tau_\Delta \le T$. Appendix C presents results for $\tau_\Delta > T$.

Example 4.1 M-PSK Signal and AWGN

Consider first the simplified case of a M-PSK signal with AWGN. Figure 4.5 plots the probability of symbol error for both the exact value found by numerically integrating eq.(4.17) and the upper bound value given by reducing eq. (4.22) to obtain (see also eq. 4.2.109 of [3]),

$$P_s(H_1) \le 2\,\Phi\left[-\frac{m_x \sin\frac{\pi}{M}}{\sigma_N}\right]. \tag{4.39}$$

Note the expanded vertical axis highlights the tightness of the bound for large signal-to-noise levels. Also note that the bound improves as M increases. Under the worst case of BPSK, M=2, it is apparent that eq. (4.39) is equal to twice the exact value given by eq. (3.9). Due to the tightness of the upper bound, the following examples all plot the upper bound of the probability of symbol error for computational considerations.

$a_k = \cos(0) = 1$

$b_k = \sin(0) = 0$

$D(k) = H_1\sqrt{2S}\,T$

$F_1(k) = H_2\sqrt{2S}\;(T - \tau_\Delta)\cos(2\pi f_c \tau_\Delta)$

$F_2(k) = H_2\sqrt{2S}\;(\tau_\Delta)\cos(2\pi f_c(\tau_\Delta - T))$

$G_1(k) = H_2\sqrt{2S}\;(T - \tau_\Delta)\sin(2\pi f_c \tau_\Delta)$

$G_2(k) = H_2\sqrt{2S}\;(\tau_\Delta)\sin(2\pi f_c(\tau_\Delta - T))$

$\sigma_N = \sqrt{N_0 T}$

$P_c = 0$

For i = 1:M

$\theta = \frac{2\pi}{M}(i-1)$

$a_{k-1} = \cos(\theta)$

$b_{k-1} = \sin(\theta)$

$m_x = a_k D(k) + a_k F_1(k) + b_k G_1(k) + a_{k-1} F_2(k) + b_{k-1} G_2(k)$

$m_y = b_k D(k) + b_k F_1(k) - a_k G_1(k) + b_{k-1} F_2(k) - a_{k-1} G_2(k)$

$$P_c = P_c + \frac{1}{M}\left\{\Phi\left[\frac{m_x \sin\frac{\pi}{M} - m_y \cos\frac{\pi}{M}}{\sigma_N}\right] - \Phi\left[\frac{-m_x \sin\frac{\pi}{M} - m_y \cos\frac{\pi}{M}}{\sigma_N}\right]\right\}$$

EndFor

$P_s = 1 - P_c$

transmitted signal power $= S$

in-band noise power $= \left(\frac{2}{T}\right)\left(\frac{N_0}{2}\right) = \frac{N_0}{T}$

Figure 4.4. Generation of the average probability of symbol error for an M-PSK signal transmitted through a two-path channel model with $0 \le \tau_\Delta \le T$ and AWGN.

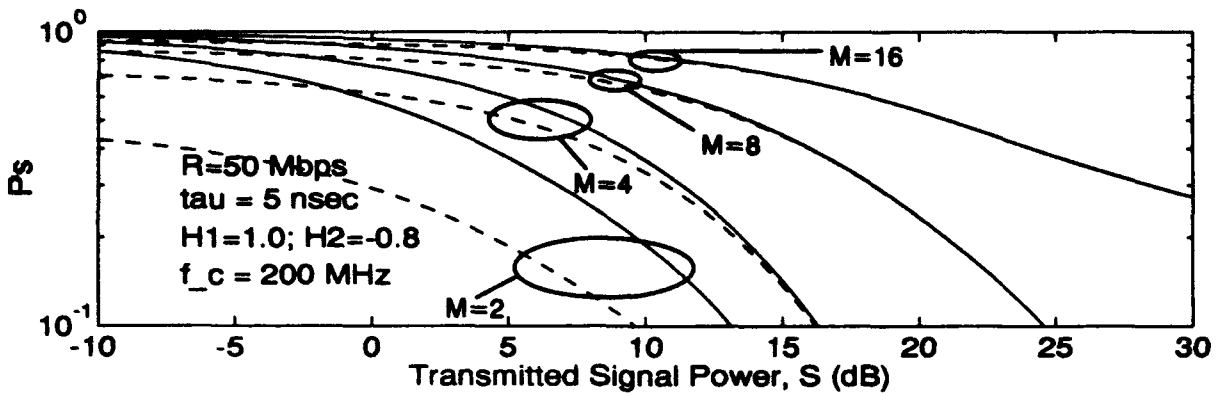

Figure 4.5. Comparison of exact (dashed) and upper bound (solid) expressions for probability of symbol error.

Example 4.2 M-PSK Signal, Multipath, and AWGN

Next, consider the case of an M-PSK signal transmitted through a time-invariant two-path channel with additive white Gaussian noise. Figure 4.4 summarizes the relevant equations. Figure 4.8 plots the system performance of M=4/ S=5 dB, M=8/ S=10 dB, M=16/ S=20 dB as a function of carrier frequency. All plots show the same carrier frequency dependence as did BPSK in example 3.1. This comes from the channel frequency response of the two-path channel given by eq. (2.9). In spectral nulls of the channel frequency response, the system performance degrades, corresponding to a reduction in received signal power due to the multipath and the direct path adding destructively. From the vector diagram in figure 4.3, this corresponds to the correlated multipath vector pointing toward the origin. In spectral peaks of the channel frequency response, the system performance improves, corresponding to an increase in received signal power due to the multipath and the direct path adding constructively. From the vector diagram in figure 4.3, this corresponds to the correlated multipath vector pointing away from the origin.

Figures 4.9 – 4.13 plot the performance of the M-PSK system for data rates given in table 4.1. These plots all have a carrier frequency of 200 MHz that centers the system in a spectral null of the channel frequency response when the multipath tap-gain coefficient is negative. Note that since the data rate remains constant in each plot, the symbol rate decreases as M increases and thus, the τ_Δ/T ratio changes. Table 4.1 summarizes the relationship between data rate, symbol rate, and τ_Δ/T for M=2,4,8,16 and $\tau_\Delta = 5\ \eta\,\text{sec}$. From the plots it is apparent that larger signal-to-noise ratios are required to maintain performance as M increases. Of course the benefit in increasing M is a reduced transmitted spectral bandwidth, which results in improved spectral efficiency. The interesting point is that for a multipath tap-gain coefficient $H_2 = -0.8$, 16-PSK becomes unusable (at least by the present system with practical signal levels) when $\tau_\Delta/T > 0.0625$ as shown in figure4.11c and 8-PSK becomes unusable when $\tau_\Delta/T > 0.333$ as shown by figure 4.13c. The reason for this is that as M increases the decision regions are reduced, which results in the system becoming more sensitive to channel nonidealities.

Table 4.1. Data rate, symbol rate, and τ_Δ/T for M=2,4,8,16 and $\tau = 5\ \eta$ sec.

Data Rate	Symbol Rate				τ_Δ/T			
	M=2	M=4	M=8	M=16	M=2	M=4	M=8	M=16
1.544 Mbps	1.544 Mbps	722 Ksps	514.7 Ksps	386 Ksps	0.0077	0.0036	0.0026	0.0019
10 Mbps	10 Mbps	5 Msps	33.3 Msps	2.5 Msps	0.05	0.025	0.0167	0.0125
50 Mbps	50 Mbps	25 Msps	16.7 Msps	12.5 Msps	0.25	0.125	0.083	0.0625
100 Mbps	100 Mbps	50 Msps	33.3 Msps	25 Msps	0.5	0.25	0.167	0.125
200 Mbps	200 Mbps	100 Msps	66.7 Msps	50 Msps	1.0	0.5	0.333	0.25

Example 4.3 M-PSK Signal, Interference, and AWGN

Figures 4.14 and 4.15 consider the case of M-PSK with additive interference, but no multipath. Both the deterministic CW interferer and the stochastic finite bandwidth interferer are considered. From the previous example, it was shown that the M-PSK system becomes more sensitive to nonidealities as M increases and the data rate is kept constant. Figures 4.14 and 4.15 also demonstrate this point.

Figure 4.15 plots system performance as a function of carrier offset frequency. As in example 3.2 for BPSK, performance is seen to be most severely affected when the interference carrier offset frequency is zero. Local minimum occur for stochastic narrowband interference in the nulls of the transmitted M-PSK signal spectrum, $f_\Delta = R, 2R, \ldots$, (note that R is different for each value of M since the data rate is a constant). Recall from chapter 3 that the deterministic CW interferer displayed additional offset frequencies, $f_\Delta = \frac{R}{2}, \frac{3R}{2}, \ldots$ where it had a minimum effect on the BPSK system performance. This was shown to be from the integration over the interval [0,T] of the deterministic, constant envelope, and constant phase CW interference. It is interesting to note that for M > 2 this effect does not appear to be exhibited. Figure 4.15c shows that as the bandwidth of the interference increases, the interference loses the ability to "hide" in the M–PSK signal spectral nulls.

$D(k) = H_1\sqrt{2S}\,T$

$F_1(k) = H_2\sqrt{2S}\ (T - \tau_\Delta)\cos(2\pi f_c \tau_\Delta)$

$F_2(k) = H_2\sqrt{2S}\ (\tau_\Delta)\cos(2\pi f_c(\tau_\Delta - T))$

$G_1(k) = H_2\sqrt{2S}\ (T - \tau_\Delta)\sin(2\pi f_c \tau_\Delta)$

$G_2(k) = H_2\sqrt{2S}\ (\tau_\Delta)\sin(2\pi f_c(\tau_\Delta - T))$

$I_x(k) = \sqrt{2I}\ \dfrac{[\sin(2\pi f_\Delta T + \phi) - \sin(\phi)]}{2\pi f_\Delta}$

$I_y(k) = \sqrt{2I}\ \dfrac{[\cos(2\pi f_\Delta T + \phi) - \cos(\phi)]}{2\pi f_\Delta}$

$\sigma_N = \sqrt{N_0 T}$

$P_c = 0$

For j = 1:M

$\theta = \dfrac{2\pi}{M}\ (j - 1)$

$a_k = \cos(\theta)$

$b_k = \sin(\theta)$

$\theta_2 = \dfrac{\pi}{M}\ (2j - 1)$

$\theta_1 = \dfrac{\pi}{M}\ (2j - 3)$

For i = 1:M

$\theta = \dfrac{2\pi}{M}\ (i - 1)$

$a_{k-1} = \cos(\theta)$

$b_{k-1} = \sin(\theta)$

$m_x = a_k\, D(k) + a_k\, F_1(k) + b_k\, G_1(k) + a_{k-1}\, F_2(k) + b_{k-1}\, G_2(k) + I_x(k)$

$m_y = b_k\, D(k) + b_k\, F_1(k) - a_k\, G_1(k) + b_{k-1}\, F_2(k) - a_{k-1}\, G_2(k) + I_y(k)$

$P_c = P_c + \dfrac{1}{M^2}\left\{\Phi\left[\dfrac{m_x \sin\theta_2 - m_y \cos\theta_2}{\sigma_N}\right] - \Phi\left[\dfrac{m_x \sin\theta_1 - m_y \cos\theta_1}{\sigma_N}\right]\right\}$

EndFor

EndFor

$P_s = 1 - P_c$

transmitted signal power = S

interference power = I

in-band noise power = $\left(\dfrac{2}{T}\right)\left(\dfrac{N_0}{2}\right) = \dfrac{N_0}{T}$

Figure 4.6. Generation of the average probability of symbol error for an M-PSK signal transmitted through a two-path channel model with $0 \le \tau_\Delta \le T$, additive CW interference and AWGN.

$a_k = \cos(0) = 1$

$b_k = \sin(0) = 0$

$D(k) = H_1\sqrt{2S}\,T$

$F_1(k) = H_2\sqrt{2S}\ (T - \tau_\Delta)\cos(2\pi f_c \tau_\Delta)$

$F_2(k) = H_2\sqrt{2S}\ (\tau_\Delta)\cos(2\pi f_c(\tau_\Delta - T))$

$G_1(k) = H_2\sqrt{2S}\ (T - \tau_\Delta)\sin(2\pi f_c \tau_\Delta)$

$G_2(k) = H_2\sqrt{2S}\ (\tau_\Delta)\sin(2\pi f_c(\tau_\Delta - T))$

transmitted signal power $= S$

interference power $= N_B B$

in-band noise power $= \left(\frac{2}{T}\right)\left(\frac{N_0}{2}\right) = \frac{N_0}{T}$

$\sigma_N^2 = N_0 T$

$$\sigma_I^2 = \frac{N_B}{\pi}\,T\left[Si(\pi(B - 2f_\Delta)T) + \frac{\cos(\pi(B - 2f_\Delta)T) - 1}{\pi(B - 2f_\Delta)T}\right] + \frac{N_B}{\pi}\,T\left[Si(\pi(B + 2f_\Delta)T) + \frac{\cos(\pi(B + 2f_\Delta)T) - 1}{\pi(B + 2f_\Delta)T}\right]$$

$\sigma_{I+N} = \sqrt{\sigma_N^2 + \sigma_I^2}$

$P_c = 0$

For i = 1:M

$\theta = \frac{2\pi}{M}(i - 1)$

$a_{k-1} = \cos(\theta)$

$b_{k-1} = \sin(\theta)$

$m_x = a_k D(k) + a_k F_1(k) + b_k G_1(k) + a_{k-1} F_2(k) + b_{k-1} G_2(k)$

$m_y = b_k D(k) + b_k F_1(k) - a_k G_1(k) + b_{k-1} F_2(k) - a_{k-1} G_2(k)$

$$P_c = P_c + \frac{1}{M}\left\{\Phi\left[\frac{m_x \sin\frac{\pi}{M} - m_y \cos\frac{\pi}{M}}{\sigma_{I+N}}\right] - \Phi\left[\frac{-m_x \sin\frac{\pi}{M} - m_y \cos\frac{\pi}{M}}{\sigma_{I+N}}\right]\right\}$$

EndFor

$P_s = 1 - P_c$

Figure 4.7 Generation of the average probability of symbol error for an M-PSK signal transmitted through a two-path channel model with $0 \le \tau_\Delta \le T$, additive finite bandwidth interference and AWGN.

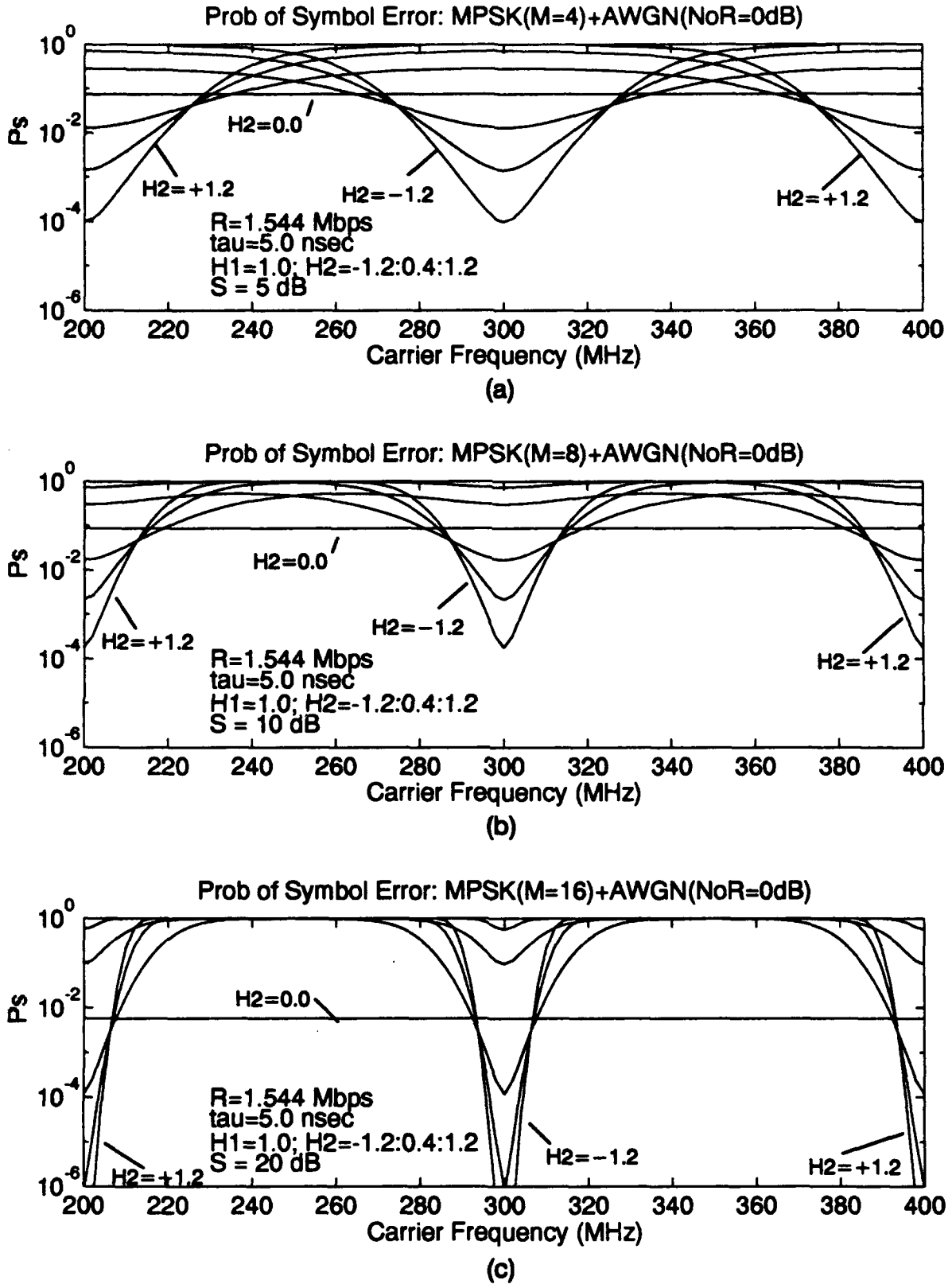

Figure 4.8. Effects of multipath as a function of carrier frequency for (a) QPSK S=5 dB, (b) 8–PSK S=10 dB, (c) 16–PSK S=20 dB and $\tau_{\Delta} = 0.0077\ T$.

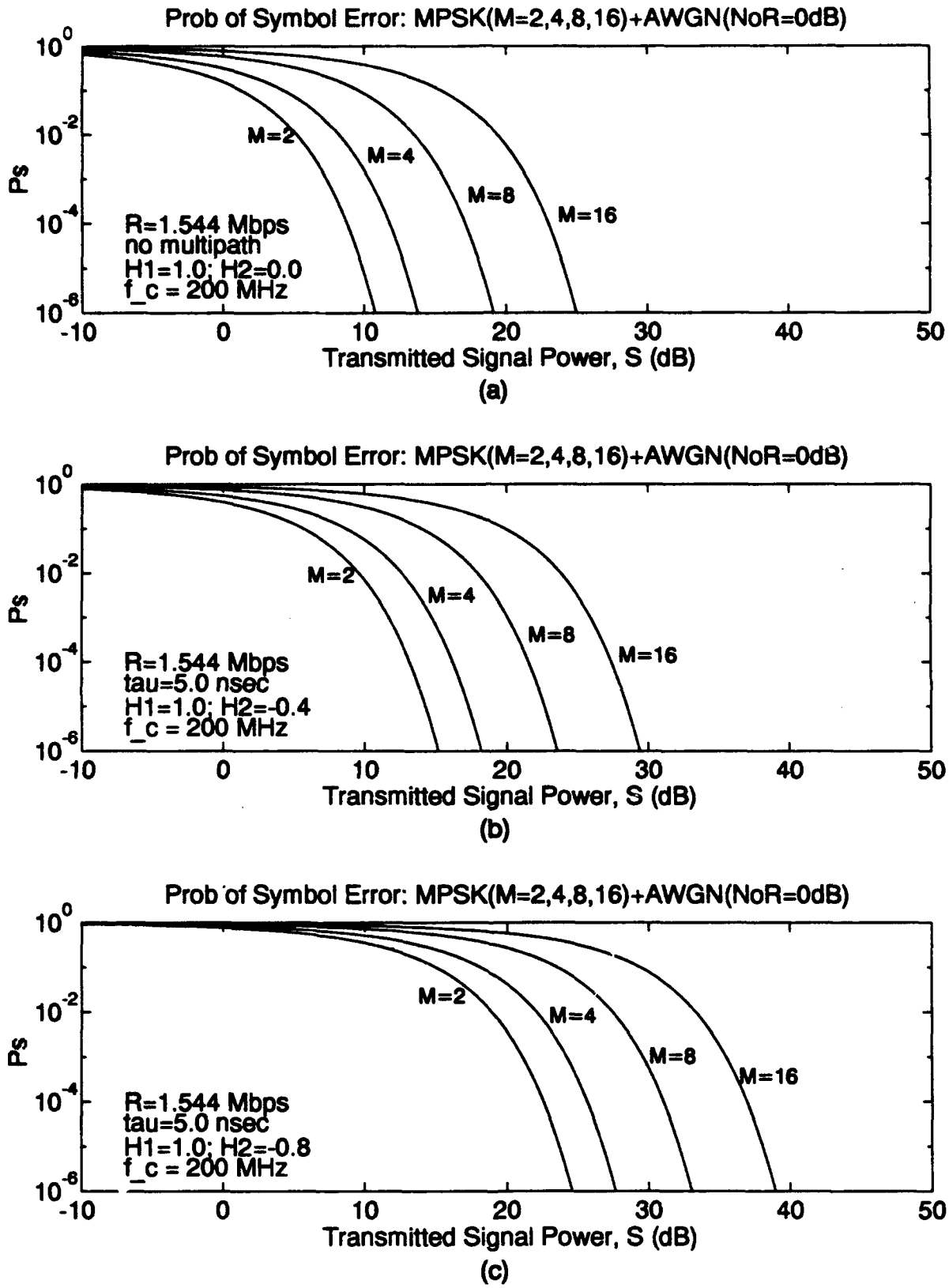

Figure 4.9. Performance of M-PSK for fixed data rate of 1.544 Mbps and (a) no multipath, (b) $H_2 = -0.4, \tau_\Delta = 5\ \eta$sec, (c) $H_2 = -0.8, \tau_\Delta = 5\ \eta$sec.

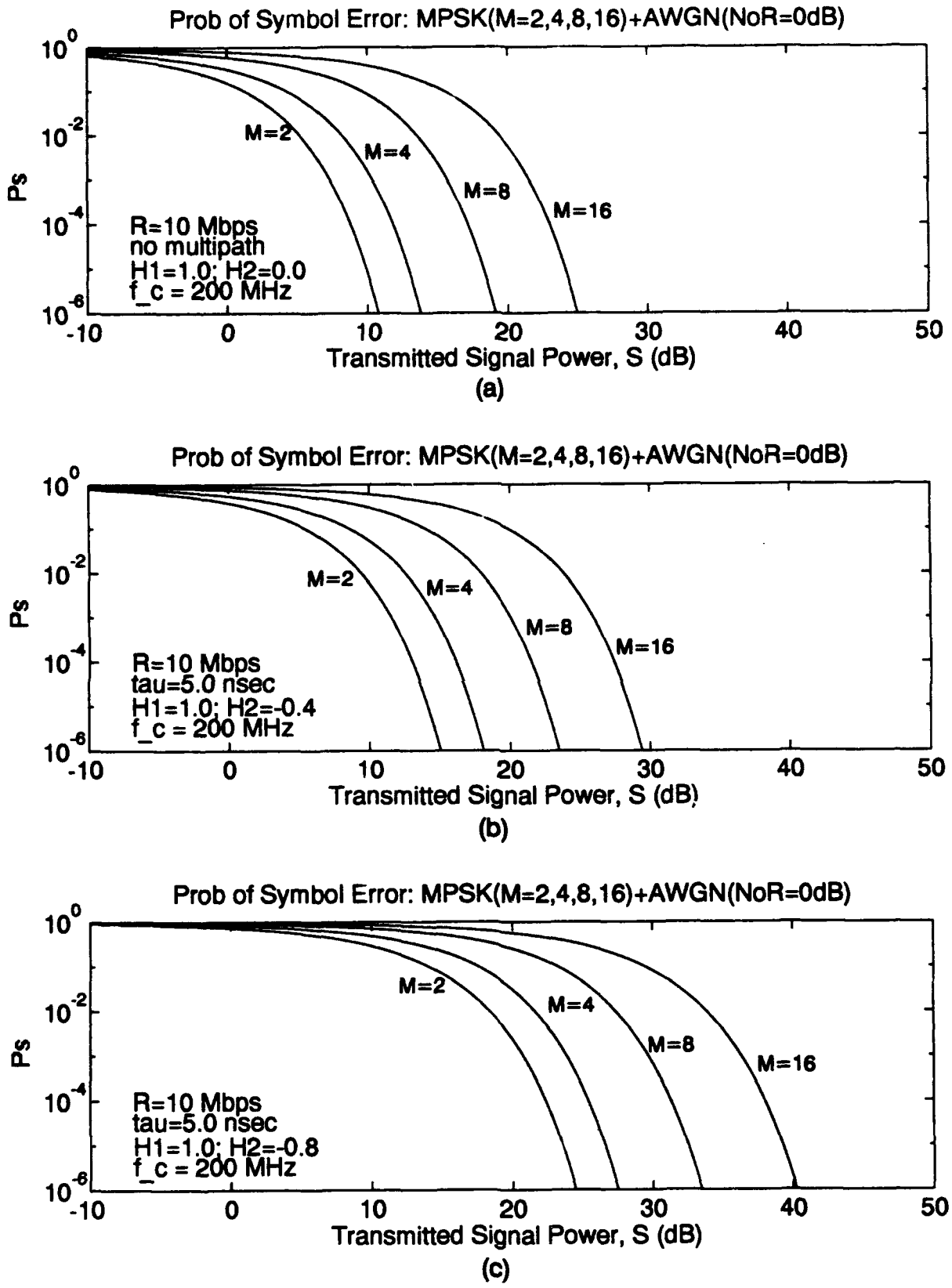

Figure 4.10. Performance of M-PSK for fixed data rate of 10 Mbps and (a) no multipath, (b) $H_2 = -0.4, \tau_\Delta = 5\ \eta$sec, (c) $H_2 = -0.8, \tau_\Delta = 5\ \eta$sec.

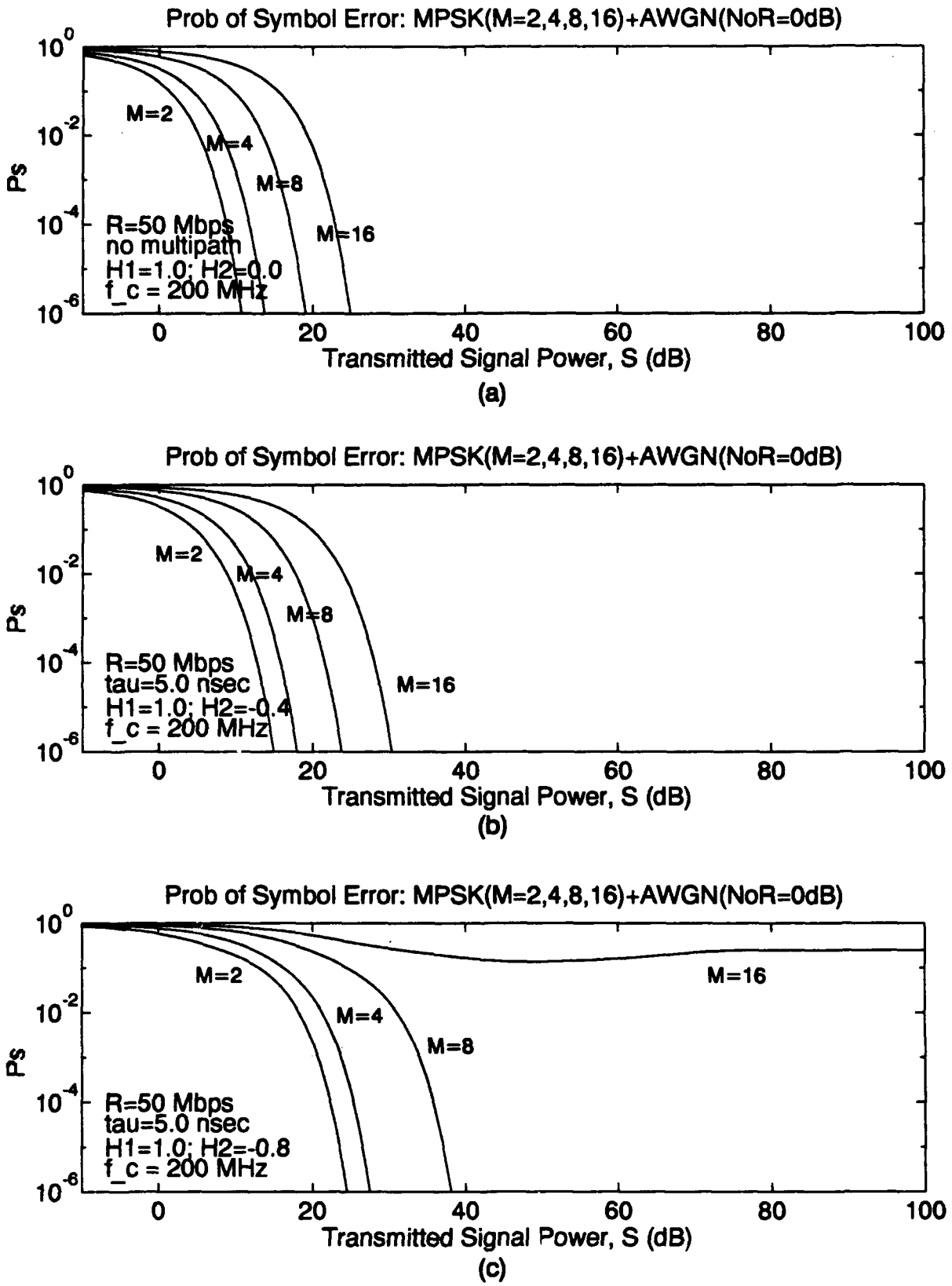

Figure 4.11. Performance of M-PSK for fixed data rate of 50 Mbps and (a) no multipath, (b) $H_2 = -0.4, \tau_\Delta = 5\ \eta$sec, (c) $H_2 = -0.8, \tau_\Delta = 5\ \eta$sec.

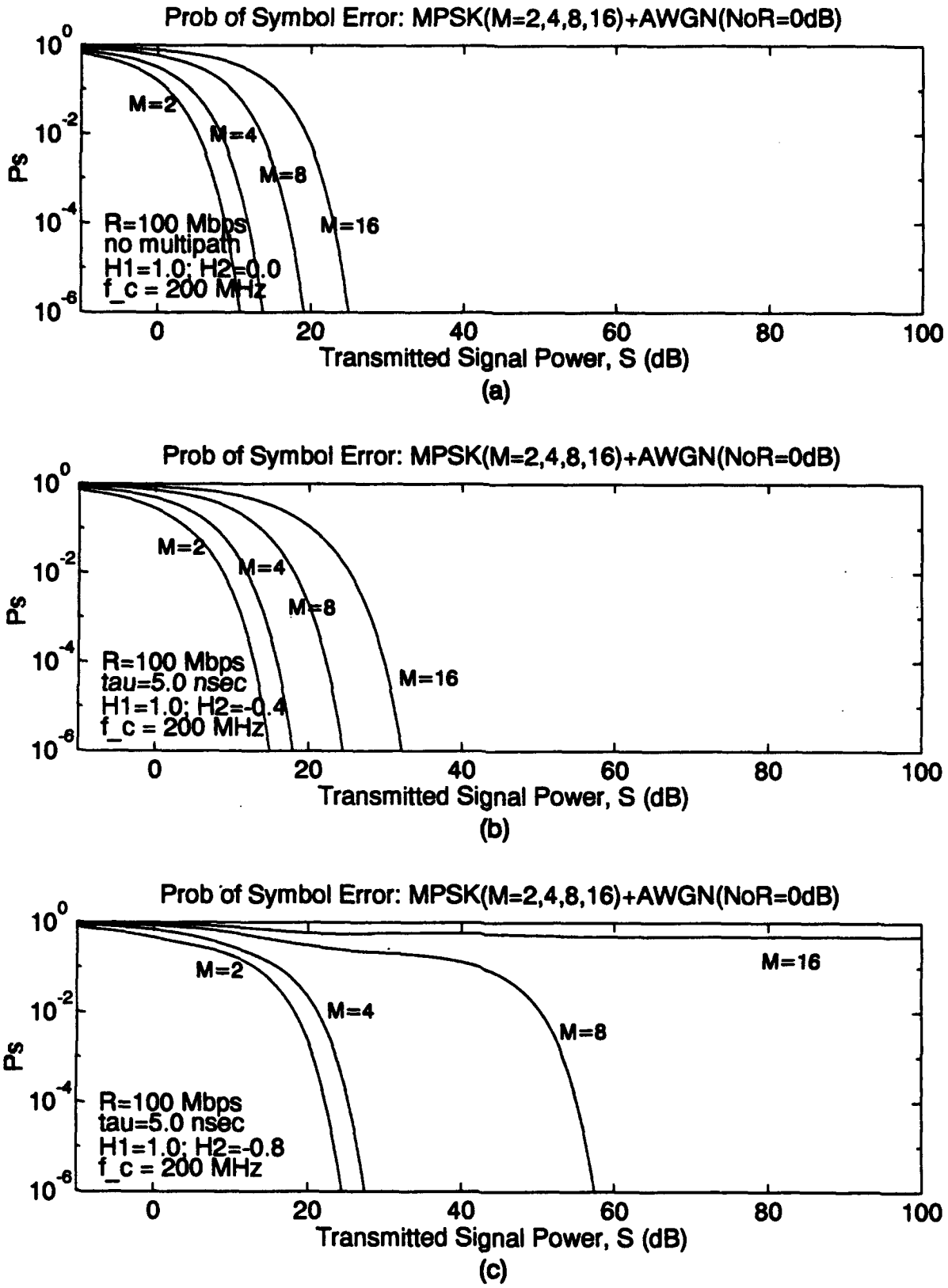

Figure 4.12. Performance of M-PSK for fixed data rate of 100 Mbps and (a) no multipath, (b) $H_2 = -0.4, \tau_\Delta = 5\ \eta$sec, (c) $H_2 = -0.8, \tau_\Delta = 5\ \eta$sec.

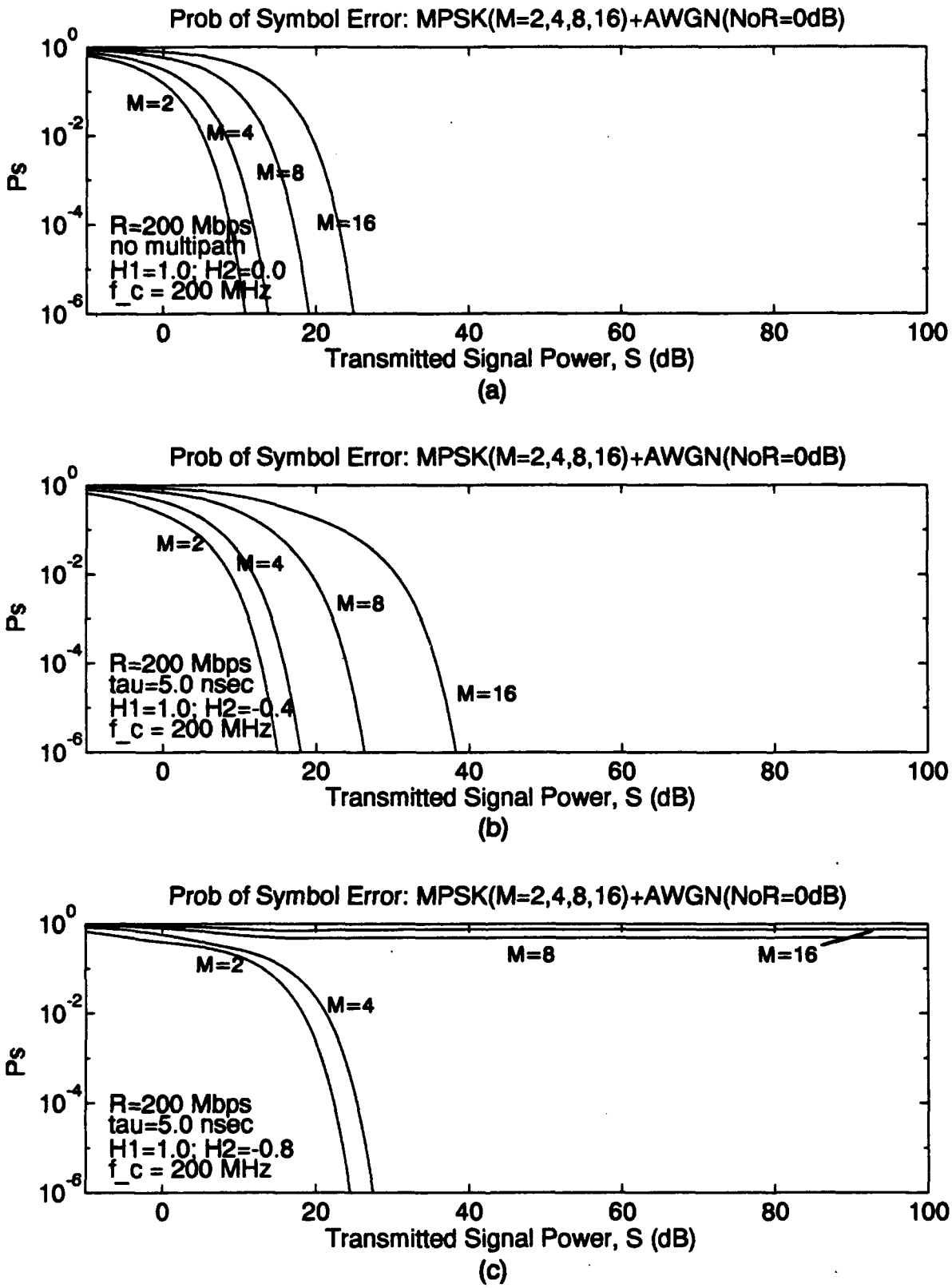

Figure 4.13. Performance of M-PSK for fixed data rate of 200 Mbps and (a) no multipath, (b) $H_2 = -0.4, \tau_\Delta = 5\ \eta$sec, (c) $H_2 = -0.8, \tau_\Delta = 5\ \eta$sec.

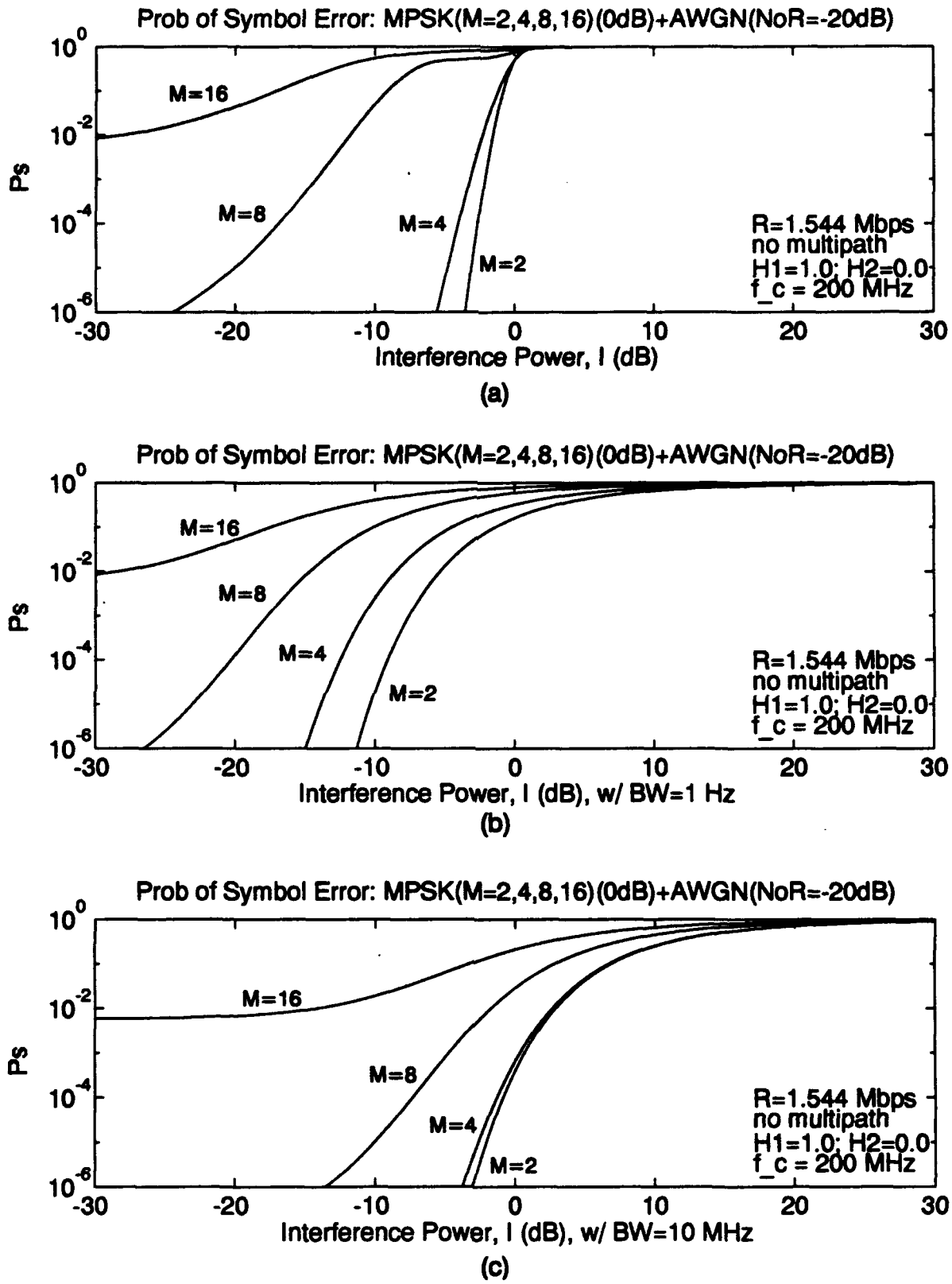

Figure 4.14. Performance of *M*-PSK for increasing interference power and –20-dB noise power (a) CW interference, (b) B = 1-Hz interference, (c) B = 10-MHz interference.

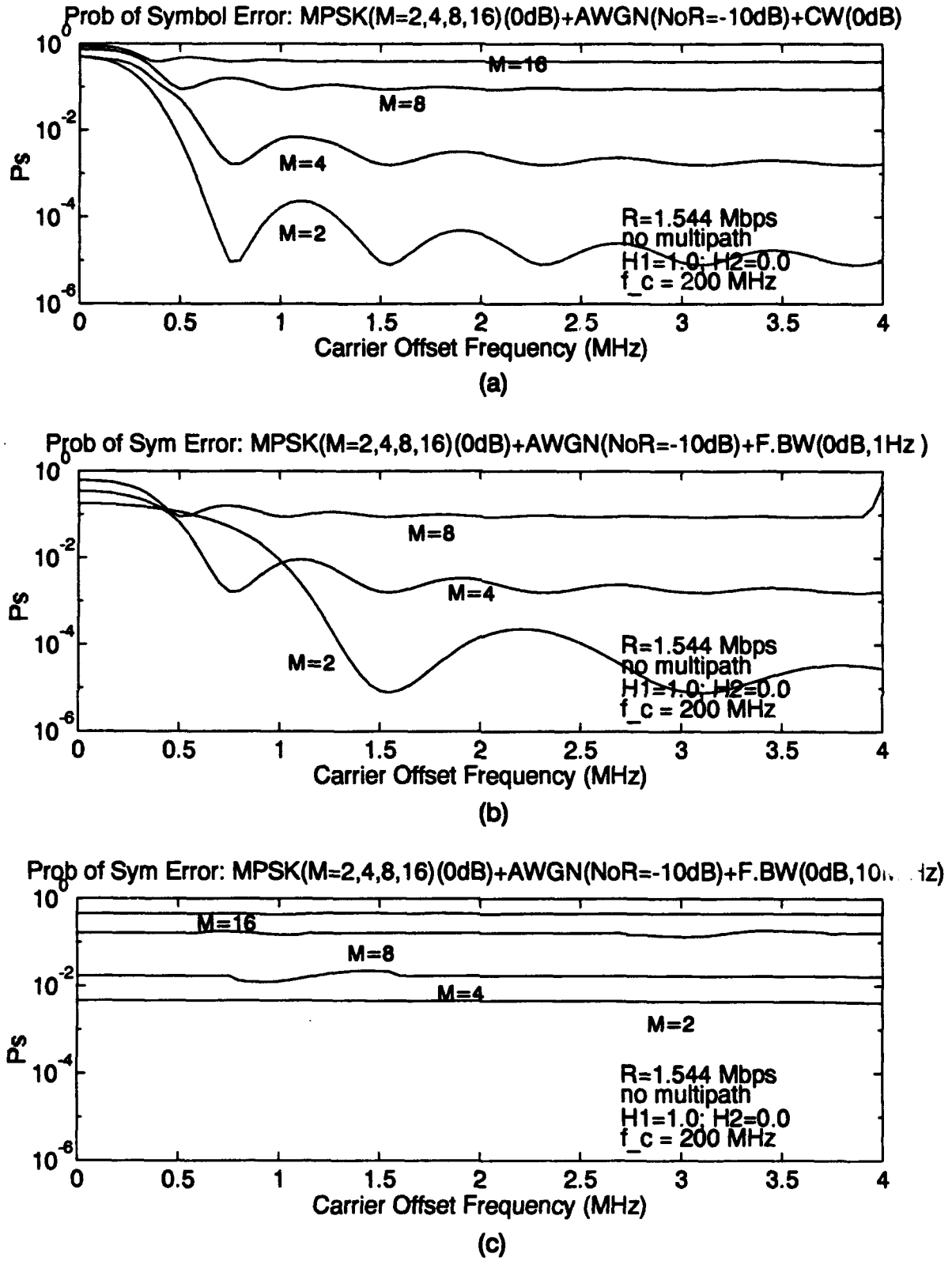

Figure 4.15. Performance of *M*-PSK for increasing carrier offset frequency (a) CW interference, (b) 1-Hz bandwidth interference, (c) 10-MHz bandwidth interference.

5. CONCLUSION

This report has presented derivations that describe the system performance of a coherent M-ary phase-shift-keyed (M-PSK) communication system in terms of the average probability of symbol error operating under the following nonideal conditions: (1) time-invariant two-path channel, (2) intentional/unintentional interference, and (3) AWGN. Two types of interference were considered, deterministic CW interference and stochastic finite bandwidth interference. The resulting derivations were consolidated in pseudocode for easy reference. All expressions are based on a simplified FIR channel model with two time-invariant propagation paths. While real channels will be time-variant, this model provides tractable solutions as well as being valid over short time intervals in a slowly fading channel. Future work will concentrate on removing the time-invariant channel restriction.

It is expected that the information contained in this report can be applied to any time-invariant two-path M-PSK communication channel with or without interference, for example HF, VHF, UHF, or SHF LOS communication systems. One particular example, LOS UHF radio, was used extensively to exercise the derived expressions and illustrate typical system performance. It was shown that:

1. for the "frequency nonselective multipath" condition (defined as the inverse of the channel delay spread (null-to-null separation) being approximately greater than the transmitted signal bandwidth, $\frac{1}{\tau_\Delta} \geq 2R$ or $\tau_\Delta \leq \frac{T}{2}$), the effects of the multipath on system performance oscillate between constructively adding with the direct path and destructively adding with the direct path and are described by $\cos(2\pi f_c \tau_\Delta)$,
2. for the "frequency selective multipath" condition (defined by the inverse of the channel delay spread (null-to-null separation) being approximately less than the transmitted signal bandwidth, $\frac{1}{\tau_\Delta} \leq 2R$ or $\tau_\Delta \geq \frac{T}{2}$), the effects of the multipath on system performance result in mostly destructive only addition with the direct path,
3. additive interference most severely degrades system performance when the interference carrier offset frequency is zero,
4. finite bandwidth stochastic interference can, under certain conditions, degrade system performance more than CW interference for the same signal-to- interference ratio, and
5. for constant data rates, the sensitivity to channel nonidealities increases dramatically as M increases even though the symbol rate decreases as M increases.

It should be emphasized that the results derived in this report pertain to a receiver with no means of compensation for the nonideal channel conditions. Methods of compensation for multipath and interference, like adaptive equalization, beamforming, spatial diversity, and multichannel adaptive equalization, are presently under investigation by the authors. The results in this report will help determine the performance gain offered by these methods of compensation.

6. REFERENCES

[1] Axford, R.A. "Effects of CW- and BPSK-Signal Interference on a Standard BPSK Digital Communications System," NRaD TR 1510. NCCOSC, RDT&E Division, San Diego, CA, August 1992.

[2] Rummler, W., R. Coutts, and M. Linger, "Multipath Fading Channel Models for Microwave Digital Radio," *IEEE Communications Magazine*, vol. 24, no. 11, pp. 30–42, Nov. 1986.

[3] Proakis, J. *Digital Communications* (2nd Ed.), McGraw Hill, New York, 1989.

[4] Saltzberg, B. "Intersymbol Interference Error Bounds with Application to Ideal Bandlimited Signaling," *IEEE Trans. on Information Theory*, vol. 14, no.4, pp. 563–568, 1968.

[5] Shimbo, O., and M. Celebiler. "Performance of M-Ary PSK Systems in Gaussian Noise and Intersymbol Interference," *IEEE Trans. on Info. Theory*, vol. 19, no. 1, pp. 44–58, Jan 1973.

[6] North, R.C. "The Simulation and Estimation of Digital Communications Channels," NRaD TN 1718. NCCOSC, RDT&E Division, San Diego, CA, January 1993.*

[7] Rummler, W. "A New Selective Fading Model: Application to Propagation Data," *The Bell System Technical Journal*, vol. 58, no. 5, pp. 1037–1071, May 1979.

[8] Wang J., and L.B. Milstein, "On the use of Suppression Filters for CDMA Overlay Situations," submitted to *IEEE Trans. on Comm*, 1993.

[9] Milstein, L.B. *"Lecture Notes for ECE 258: Digital Communications,"* Department of Electrical and Computer Engineering, University of California at San Diego, 1992.

[10] Stark H., and J. Woods, *Probability, Random Processes, and Estimation Theory for Engineers*, Prentice-Hall, Englewood Cliffs, New Jersey, 1986.

* NRaD Technical Notes are working documents and do not represent an official policy statement of Naval Command, Control and Ocean Surveillance Center, RDT&E Division. For further information, contact the author.

APPENDIX A - COMPLEX BASEBAND REPRESENTATION

Many of the simulations and analyses presented in the literature use a complex baseband representation to model the complete communication system (see for example [1]). This report derived its results based on a real bandpass signal representation. This appendix relates the real bandpass signals in this report to their equivalent complex baseband representations. Related future work will primarily use this complex baseband representation. The notation will use capitals letters for real bandpass signals and small letters for complex baseband signals.

A.1 BASEBAND SIGNAL AND CHANNEL MODEL

The real bandpass received signal, $R(t)$, can be written as

$$R(t) = H(t) * S(t) + I(t) + N(t) \tag{A.1}$$

where $H(t)$, $S(t)$, $I(t)$, and $N(t)$ are the bandpass channel impulse response, transmitted signal, interference signal, and additive noise respectively. Real bandpass signals that are narrowband can be represented by an equivalent complex baseband representation that can simplify simulation and analysis without loss of generality. For example, the real bandpass transmitted signal is written as

$$S(t) = a(t)\ cos(2\pi f_c t + \theta(t)) \tag{A.2}$$

where the real envelope of $S(t)$, $a(t)$, and the phase of $S(t)$, $\theta(t)$, bear the transmitted information and f_c is the carrier frequency. Eq. (A.2) can be rewritten using a trigonometric identity as

$$\begin{aligned} S(t) &= a(t)\ cos(\theta(t))\ cos(2\pi f_c t) - a(t)\ sin(\theta(t))\ sin(2\pi f_c t) \\ &= x(t)\ cos(2\pi f_c t) - y(t)\ sin(2\pi f_c t) \end{aligned} \tag{A.3}$$

where $x(t) = a(t)\cos(\theta(t))$ is called the in-phase component and $y(t) = a(t)\sin(\theta(t))$ is called the quadrature component. Both $x(t)$ and $y(t)$ are real baseband signals, that is, each has a spectrum that is symmetric about $f=0$. Eq. (A.3) can be generated by the block diagram in figure 2.1. The spectrum-shaping filter is typically a Nyquist pulse shaping filter like the raised-cosine filter, the cube filter, or the double-jump filter [2]. (Recall that a Nyquist pulse-shaping filter has the property that at the ideal sampling instants, there are no contributions from data pulses other than the one being detected [3]). Returning to eq. (A.3), it can be written as

$$\begin{aligned} S(t) &= \mathrm{Re}\left[\{x(t) + j\ y(t)\}\ e^{j2\pi f_c t}\right] \\ S(t) &= \mathrm{Re}\left[s(t)\ e^{j2\pi f_c t}\right] \end{aligned} \tag{A.4}$$

where $s(t) = x(t) + j\ y(t)$ represents the equivalent complex baseband signal.

To see how the convolution of real bandpass signals in eq. (A.1) can also be rewritten in complex baseband representation, lets expand the bandpass convolution using the two-path channel model, $H(t) = H_1\delta(t) + H_2\delta(t - \tau_\Delta)$. Thus,

$$\begin{aligned} H(t) * S(t) &= H_1[x(t)cos(2\pi f_c t) - y(t)\sin(2\pi f_c t)] \\ &\quad + H_2[x(t-\tau_\Delta)cos(2\pi f_c(t-\tau_\Delta)) - y(t-\tau_\Delta)\sin(2\pi f_c(t-\tau_\Delta))] \\ &= [H_1 x(t) + H_2 x(t-\tau_\Delta)cos(2\pi f_c \tau_\Delta) - H_2 y(t-\tau_\Delta)sin(2\pi f_c \tau_\Delta)]\ cos(2\pi f_c t) \\ &\quad - [H_1 y(t) + H_2 x(t-\tau_\Delta)sin(2\pi f_c \tau_\Delta) + H_2 y(t-\tau_\Delta)cos(2\pi f_c \tau_\Delta)]\ sin(2\pi f_c t). \end{aligned} \tag{A.5}$$

Eq. (A.5) can be shown to be equal to

$$\begin{aligned} H(t) * S(t) &= \mathrm{Re}\Big[\big([h_1 x(t) + h_2 x(t-\tau_\Delta)] + j\,[h_1 y(t) + h_2 y(t-\tau_\Delta)]\big)\, e^{j2\pi f_c t}\Big] \\ &= \mathrm{Re}\Big[(h(t) * s(t))\, e^{j2\pi f_c t}\Big] \end{aligned} \tag{A.6}$$

where $h(t) = h_1\delta(t) + h_2\delta(t-\tau_\Delta)$, $h_1 = H_1$, and $h_2 = H_2 e^{-j2\pi f_c \tau_\Delta}$. Thus, $h(t)$ is the complex, baseband channel impulse response (see section 7.1 of [1] for more general expressions relating the complex baseband channel impulse response to the real bandpass channel impulse response). In general, it can be shown that for linear filters, $H(t) * S(t) = \mathrm{Re}\big[h(t)\, e^{j2\pi f_c t}\big] * \mathrm{Re}\big[s(t)\, e^{j2\pi f_c t}\big] = \mathrm{Re}\big[(h(t) * s(t))\, e^{j2\pi f_c t}\big]$.

Finally, we see how eq. (A.1) can be rewritten in its equivalent baseband representation

$$r(t) = h(t) * s(t) + i(t) + n(t). \tag{A.7}$$

Eq. (A.7) describes the complex baseband communication system described in this appendix and figure A.1 shows the complex baseband communication channel model.

For digital communication, the complex baseband transmitted signal is described by

$$s(t) = \sqrt{2S} \sum_k s_k\, P_T(t - kT) \tag{A.8}$$

where S is the average transmitted signal power, $\{s_k\}$ represents a sequence of symbols transmitted at the symbol rate of $R = 1/T$ symbols per second, and $P_T(t)$ is a pulse with band-limited baseband frequency response. The binary data sequence is encoded to form the symbol sequence, $\{s_k\}$, by any of numerous digital modulation techniques like M-ary Phase-Shift Key (M-PSK) and M-ary Quadrature Amplitude Modulation (M-QAM). Each modulation technique is defined by its discrete alphabet (or constellation) of complex numbers.

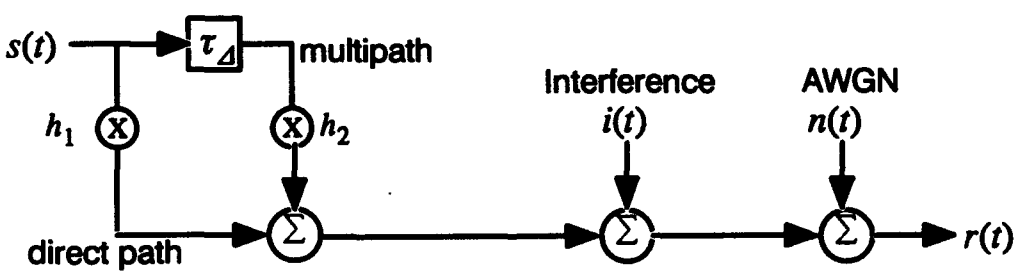

Figure A.1. Continuous-time, complex baseband model of the communication channel.

A.2 BASEBAND SIGNAL STATISTICS

The autocorrelation of eq. (A.7) can be written as

$$\phi_{r,r}(\tau) \equiv \frac{1}{2}\, E\Big[r(t)\, r^*(t-\tau)\Big] = \phi_{h*s,h*s}(\tau) + \phi_{i,i}(\tau) + \phi_{n,n}(\tau) \tag{A.9}$$

where it has been assumed that each signal component is mutually uncorrelated. The factor of $\frac{1}{2}$ in the definition of the autocorrelation function of a *complex-valued* stochastic process is an arbitrary

but mathematically convenient normalization factor frequently used in the literature (see for example section 1.2 and 3.1 of [1]). For example, if $s(t)$ is a zero-mean, complex-valued stochastic process written in terms of its in-phase and quadrature components, $s(t) = x(t) + j\,y(t)$, then the autocorrelation function of $s(t)$ is written as

$$\begin{aligned}\phi_{s,s}(\tau) &\equiv \frac{1}{2}E\left[s(t)\,s^*(t-\tau)\right] \\ &= \frac{1}{2}\left\{E[x(t)x(t-\tau)] + E[y(t)y(t-\tau)] + j\left(E[y(t)x(t-\tau)] - E[x(t)y(t-\tau)]\right)\right\} \\ &= \frac{1}{2}\left\{\phi_{x,x}(\tau) + \phi_{y,y}(\tau) + j\left(\phi_{y,x}(\tau) - \phi_{x,y}(\tau)\right)\right\}.\end{aligned} \tag{A.10}$$

Notice that the factor of $\frac{1}{2}$ is missing from the definition of the correlation function of *real-valued* stochastic processes, consistent with previous definitions given for bandpass signals. Eq. (A.10) can be further reduced if $s(t)$ is from a wide sense stationary stochastic process. Under these conditions, $\phi_{x,x}(\tau) = \phi_{y,y}(\tau)$ and $\phi_{x,y}(\tau) = -\phi_{y,x}(\tau)$ (see section 3.1 of [1]), and eq. (A.10) reduces to

$$\phi_{s,s}(\tau) = \phi_{x,x}(\tau) + j\,\phi_{y,x}(\tau). \tag{A.11}$$

Thus, the relationship between the autocorrelation of the real bandpass signal and the autocorrelation of the complex baseband signal can be easily shown to be

$$\phi_{S,S}(\tau) = \mathrm{Re}\left[\phi_{s,s}(\tau)\,e^{j2\pi f_c\tau}\right]. \tag{A.12}$$

The aesthetically pleasing form of eq. (A.12) is the reason for including the arbitrary $\frac{1}{2}$ factor in the definition of the correlation function for complex processes.

To proceed in evaluating eq. (A.9) requires that some assumptions be made about the components of the received signal. The channel impulse response considered in this paper consists of two, time-invariant, discrete paths, normalized to the delay of the direct path. With this channel model, it can be shown that

$$\phi_{h^*s,h^*s}(\tau) = \left(h_1h_2^*\right)\phi_{s,s}(\tau+\tau_\Delta) + \left(|h_1|^2 + |h_2|^2\right)\phi_{s,s}(\tau) + \left(h_1^*h_2\right)\phi_{s,s}(\tau-\tau_\Delta) \tag{A.13}$$

where for $P_T(t) = 1$ in the interval [0,T] and 0 elsewhere,

$$\phi_{s,s}(\tau) = \phi_{x,x}(\tau) = \begin{cases} S\left(1-\frac{|\tau|}{T}\right) & -T \le \tau \le T \\ 0 & \text{otherwise} \end{cases}. \tag{A.14}$$

Eq. (A.14) has explicitly assumed that the power spectra of $S(t)$ is symmetric about $f = f_c$ (as is typical for double-sideband communication systems) and thus, $\phi_{x,y}(\tau) = 0 = \phi_{y,x}(\tau)$.

Two types of interference are analyzed in this paper. The first is a CW interference given by, $i(t) = \sqrt{2I}\;e^{j(2\pi f_\Delta t+\phi)}$, where I, f_Δ, ϕ are the power, carrier offset frequency, and phase of the interference respectively. The autocorrelation of the CW interference is found to be

$$\phi_{i,i}(\tau) = I\,e^{+j2\pi f_\Delta\tau}. \tag{A.15}$$

The second type of interference is bandpass white Gaussian noise with power spectra shown in figure A.2 and defined by

$$PSD_i(f) = \begin{cases} N_B & f_\Delta - \frac{B}{2} \le f \le f_\Delta + \frac{B}{2} \\ 0 & \text{otherwise} \end{cases}. \tag{A.16}$$

Its autocorrelation can be computed by taking the inverse Fourier transform of eq. (A.16),

$$\phi_{i,i}(\tau) = N_B B \left(\frac{\sin(\pi B \tau)}{\pi B \tau}\right) e^{+j2\pi f_\Delta \tau}. \tag{A.17}$$

This interference model encompasses both narrowband and broadband interference with a single parameter, the bandwidth B. For very small but finite B, eq. (A.17) reduces to eq. (A.15) where $I = N_B B$ is equal to the total baseband interferer power.

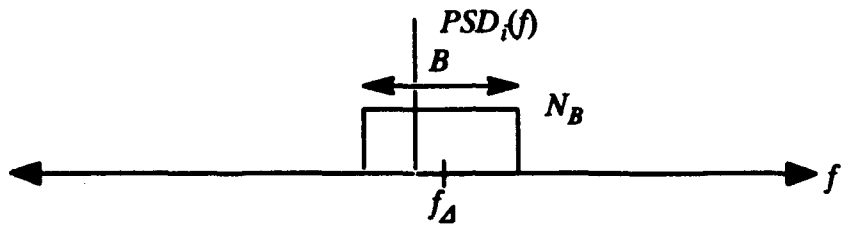

Figure A.2. Spectrum of finite bandwidth interference at baseband.

Finally, the additive noise is assumed to come from a white Gaussian process with power spectral density $PSD_n(f) = N_0$ for all frequency resulting in its autocorrelation function being $\phi_{n,n}(\tau) = \sigma_n^2\, \delta(\tau) = N_0\, \delta(\tau)$.

REFERENCES

[1] Proakis, J. *Digital Communications* (2nd Ed.), McGraw Hill, New York. 1989.

[2] Tugbay, N., and E. Panayirci. "Energy Optimization of Ban," *IEEE Trans. on Comm.*, April 1987.

[3] Noguchi, T., Y. Daido, and J. Nossek. "Modulation techniques for Microwave Digital Radio," *IEEE Communications Magazine*, vol. 24, no. 10, pp. 21–30, Oct 1986.

APPENDIX B – PERFORMANCE ANALYSIS OF BPSK SIGNAL FOR $\tau_\Delta > T$

This appendix augments chapter 3 by presenting an analysis of the average probability of bit error for a BPSK signal transmitted through the two-path channel with $\tau_\Delta > T$. All other assumption are the same as in chapter 3.

Using the two-path multipath channel model described in section 2.3, $H(t) = H_1\delta(t) + H_2\,\delta(t - \tau_\Delta)$, the received signal can be expressed as

$$R(t) = H_1 S(t) + H_2 S(t-\tau_\Delta) + I(t) + N(t), \tag{B.1}$$

where

$$S(t) = \sqrt{2S}\,\sum_k a_k\,P_T(t - kT)\,\cos(2\pi f_c t) \tag{B.2}$$

is the BPSK transmitted bandpass signal, $a_k \in \{+1, -1\}$ is the *kth* bit, S is the transmitted signal power, and $P_T(t)$ the symbol pulse waveform. At most, one-bit transition of the multipath signal can take place in the interval [0, T] of the direct path signal. The following analysis will consider the case of $\gamma\,T \le \tau_\Delta \le (\gamma + 1)T$ where $\gamma \in \{1, 2, 3, ...\}$ as shown in figure B.1. For $\tau_\Delta = T$, $\gamma = 1$ and the results in this appendix reduce to those in chapter 3. The received signal during the interval $[0,T]$ can be written as

$$\begin{aligned}
R(t) &= H_1\sqrt{2S}\;a_k\,P_T(t)\,\cos(2\pi f_c t)\\
&\quad + H_2\sqrt{2S}\;a_{k-\gamma}\,P_T\big(t-(\tau_\Delta-\gamma T)\big)\,\cos\big(2\pi f_c(t-(\tau_\Delta-\gamma T))\big)\\
&\quad + H_2\sqrt{2S}\;a_{k-(\gamma+1)}\,P_T\big(t-(\tau_\Delta-(\gamma+1)T)\big)\,\cos\big(2\pi f_c(t-(\tau_\Delta-(\gamma+1)T))\big)\\
&\quad + I(t) + N(t)\\
&= \Big[H_1\sqrt{2S}\;a_k\,P_T(t) + H_2\sqrt{2S}\;a_{k-\gamma}\,P_T\big(t-(\tau_\Delta-\gamma T)\big)\,\cos\big(2\pi f_c(\tau_\Delta-\gamma T)\big)\\
&\quad + H_2\sqrt{2S}\;a_{k-(\gamma+1)}\,P_T\big(t-(\tau_\Delta-(\gamma+1)T)\big)\,\cos\big(2\pi f_c(\tau_\Delta-(\gamma+1)T)\big)\Big]\,\cos(2\pi f_c t)\\
&\quad + I(t) + N(t)
\end{aligned} \tag{B.3}$$

using trigonometric identities and neglecting $\sin(2\pi f_c t)$ terms since they will be eliminated by the coherent BPSK demodulator shown in figure 3.1. Note that for $\tau_\Delta > T$, the multipath looks like an uncorrelated BPSK interference with equal data rate and zero offset frequency since the two multipath bits are uncorrelated with the direct path bit in the interval $[0,T]$. This case was treated in section 4.2 of [1]. It will be seen that the results do not depend on the actual value of γ, but rather on the multipath bit durations in the interval $[0,T]$ given by $\tau_\Delta - \gamma T$ and $(\gamma + 1)T - \tau_\Delta$ as shown in figure 3.1.

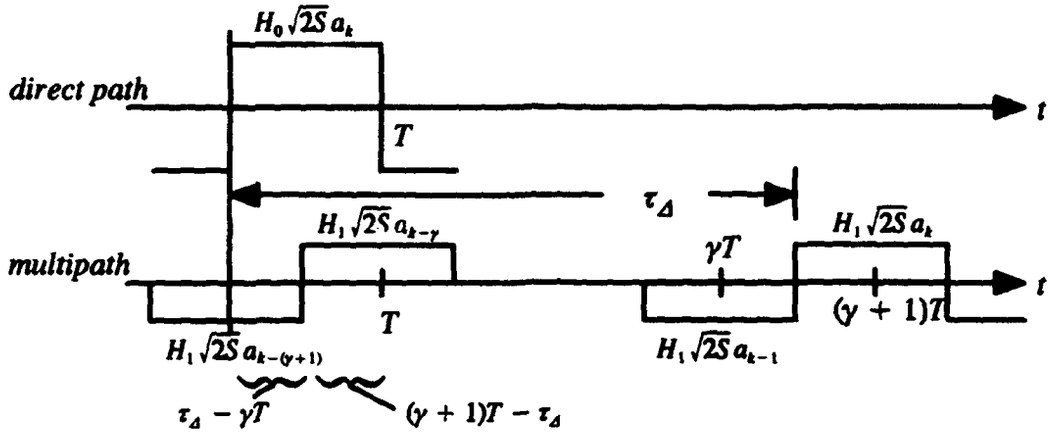

Figure B.1. Desired and interfering baseband signals in $[0, T]$, $\gamma T \le \tau_\Delta \le (\gamma+1)T$, $a_{k-\gamma} = +1, a_{k-(\gamma+1)} = -1$.

B.1 MATCHED-FILTER DETECTION OF BPSK WITH CW INTERFERENCE

This section derives the probability of bit error for the received signal given by eq. (B.3) with CW interference, $I(t) = \sqrt{2I}\,\cos(2\pi(f_c + f_\Delta)t + \phi)$. Without loss of generality, consider the interval $[0,T]$. The decision variable, $\hat{s}(k)$, can be written as

$$\hat{s}(k) = \int_0^T R(t)\; 2\cos(2\pi f_c t)\; dt \;= a_k\, D(k) + a_{k-\gamma}\, K_1(k) + a_{k-(\gamma+1)}\, K_2(k) + I(k) + N(k). \quad \text{(B.4)}$$

The only random term in eq. (B.4) that is not being conditioned on is the Gaussian random variable, $N(k)$. Thus, the decision variable, $\hat{s}(k)$, will be a conditionally Gaussian random variable with variance

$$\sigma_N^2 = N_0 T \quad \text{(B.5)}$$

as was derived in section 3.2. The deterministic terms in eq. (B.4) can be shown to be equal to

$$D(k) = H_1\sqrt{2S}\,T \quad \text{(B.6)}$$

$$K_1(k) = H_2\sqrt{2S}\;\big((\gamma+1)T - \tau_\Delta\big)\cos\big(2\pi f_c(\tau_\Delta - \gamma T)\big) \quad \text{(B.7)}$$

$$K_2(k) = H_2\sqrt{2S}\;\big(\tau_\Delta - \gamma T\big)\cos\big(2\pi f_c(\tau_\Delta - (\gamma+1)T)\big) \quad \text{(B.8)}$$

$$I(k) = \sqrt{2I}\;\frac{\big[\sin(2\pi f_\Delta T + \phi) - \sin(\phi)\big]}{2\pi f_\Delta}. \quad \text{(B.9)}$$

The conditional probability of bit error, given the parameters of the channel model and interference parameters, is given by,

$$P_e(H_1,H_2,\tau_\Delta,I,f_\Delta,\phi) = \tfrac{1}{2}P_e(+1|H_1,H_2,\tau_\Delta,I,f_\Delta,\phi) + \tfrac{1}{2}P_e(-1|H_1,H_2,\tau_\Delta,I,f_\Delta,\phi) \quad \text{(B.10)}$$

for equal probabilities of transmitting +1 and -1 bits. For the case when $\tau_\Delta > T$,

$$
\begin{aligned}
P_e(+1|H_1,H_2,\tau_\Delta,I,f_\Delta,\phi) = {} & \tfrac{1}{4}\Pr\Big(\hat{s}(k) < 0 \mid a_{k-(\gamma+1)} = -1, a_{k-\gamma} = +1, a_k = +1\Big) \\
& + \tfrac{1}{4}\Pr\Big(\hat{s}(k) < 0 \mid a_{k-(\gamma+1)} = -1, a_{k-\gamma} = -1, a_k = +1\Big) \\
& + \tfrac{1}{4}\Pr\Big(\hat{s}(k) < 0 \mid a_{k-(\gamma+1)} = +1, a_{k-\gamma} = +1, a_k = +1\Big) \\
& + \tfrac{1}{4}\Pr\Big(\hat{s}(k) < 0 \mid a_{k-(\gamma+1)} = +1, a_{k-\gamma} = -1, a_k = +1\Big)
\end{aligned} \tag{B.11}
$$

$$
\begin{aligned}
P_e(-1|H_1,H_2,\tau_\Delta,I,f_\Delta,\phi) = {} & \tfrac{1}{4}\Pr\Big(\hat{s}(k) > 0 \mid a_{k-(\gamma+1)} = -1, a_{k-\gamma} = +1, a_k = -1\Big) \\
& + \tfrac{1}{4}\Pr\Big(\hat{s}(k) > 0 \mid a_{k-(\gamma+1)} = -1, a_{k-\gamma} = -1, a_k = -1\Big) \\
& + \tfrac{1}{4}\Pr\Big(\hat{s}(k) > 0 \mid a_{k-(\gamma+1)} = +1, a_{k-\gamma} = +1, a_k = -1\Big) \\
& + \tfrac{1}{4}\Pr\Big(\hat{s}(k) > 0 \mid a_{k-(\gamma+1)} = +1, a_{k-\gamma} = -1, a_k = -1\Big).
\end{aligned} \tag{B.12}
$$

Rewriting eqs. (B.11) and (B.12) so that the Gaussian random variable has zero mean and unity variance, we find that eq. (B.10) can be written in terms of eq. (3.8) as,

$$
\begin{aligned}
P_e(H_1,H_2,\tau_\Delta,I,f_\Delta,\phi) = {} & \tfrac{1}{8}\Phi\left(-\frac{+D(k)+K_1(k)-K_2(k)+I(k)}{\sigma_N}\right) \\
& + \tfrac{1}{8}\Phi\left(-\frac{+D(k)-K_1(k)-K_2(k)+I(k)}{\sigma_N}\right) \\
& + \tfrac{1}{8}\Phi\left(-\frac{+D(k)+K_1(k)+K_2(k)+I(k)}{\sigma_N}\right) \\
& + \tfrac{1}{8}\Phi\left(-\frac{+D(k)-K_1(k)+K_2(k)+I(k)}{\sigma_N}\right) \\
& + \tfrac{1}{8}\Phi\left(\frac{-D(k)+K_1(k)-K_2(k)+I(k)}{\sigma_N}\right) \\
& + \tfrac{1}{8}\Phi\left(\frac{-D(k)-K_1(k)-K_2(k)+I(k)}{\sigma_N}\right) \\
& + \tfrac{1}{8}\Phi\left(\frac{-D(k)+K_1(k)+K_2(k)+I(k)}{\sigma_N}\right) \\
& + \tfrac{1}{8}\Phi\left(\frac{-D(k)-K_1(k)+K_2(k)+I(k)}{\sigma_N}\right)
\end{aligned} \tag{B.13}
$$

where the components of eq. (B.13) are given by eqs. (B.5) - (B.9).

B.2 MATCHED-FILTER DETECTION OF BPSK WITH FINITE BANDWIDTH INTERFERENCE

The previous results are now extended to include a finite bandwidth interference. In particular the interference is generated by passing white Gaussian noise through an ideal bandpass filter resulting in the spectrum displayed in figure 2.7. In this case, both the interference and the noise are assumed to be uncorrelated, Gaussian random variables. Thus, eq. (B.13) can be modified to find the

conditional probability of bit error, given the parameters of the channel model and interference parameters, as

$$
\begin{aligned}
P_e(H_1, H_2, \tau_\Delta, N_B, f_\Delta, B) = {} & \frac{1}{4}\Phi\left(-\frac{+D(k) + K_1(k) - K_2(k)}{\sigma_{I+N}}\right) \\
& + \frac{1}{4}\Phi\left(-\frac{+D(k) - K_1(k) - K_2(k)}{\sigma_{I+N}}\right) \\
& + \frac{1}{4}\Phi\left(-\frac{+D(k) + K_1(k) + K_2(k)}{\sigma_{I+N}}\right) \\
& + \frac{1}{4}\Phi\left(-\frac{+D(k) - K_1(k) + K_2(k)}{\sigma_{I+N}}\right)
\end{aligned}
\tag{B.14}
$$

where

$$
\sigma_{I+N}^2 = \sigma_I^2 + \sigma_N^2. \tag{B.15}
$$

Recall that σ_I^2 was previously computed in section 3.3 and found to be

$$
\begin{aligned}
\sigma_I^2 = {} & \frac{N_B}{\pi}\, T\left[Si\big(\pi(B - 2f_\Delta)T\big) + \frac{\cos\big(\pi(B - 2f_\Delta)T\big) - 1}{\pi(B - 2f_\Delta)T}\right] \\
& + \frac{N_B}{\pi}\, T\left[Si\big(\pi(B + 2f_\Delta)T\big) + \frac{\cos\big(\pi(B + 2f_\Delta)T\big) - 1}{\pi(B + 2f_\Delta)T}\right].
\end{aligned}
\tag{B.16}
$$

Thus, all components in eq. (B.14) are known. Figures B.2 and B.3 summarize the equations derived in this appendix.

$$D(k) = H_1\sqrt{2S}\,T$$
$$K_1(k) = H_2\sqrt{2S}\;((\gamma+1)T - \tau_\Delta)\cos(2\pi f_c(\tau_\Delta - \gamma T))$$
$$K_2(k) = H_2\sqrt{2S}\;(\tau_\Delta - \gamma T)\cos(2\pi f_c(\tau_\Delta - (\gamma+1)T))$$

transmitted signal power = S
interference power = I
in-band noise power = $\left(\frac{2}{T}\right)\left(\frac{N_0}{2}\right) = \frac{N_0}{T}$

$$I(k) = \sqrt{2I}\,\frac{[\sin(2\pi f_\Delta T + \phi) - \sin(\phi)]}{2\pi f_\Delta}$$
$$\sigma_N = \sqrt{N_0 T}$$
$$P_e = \frac{1}{8}\Phi\left(-\frac{+D(k)+K_1(k)-K_2(k)+I(k)}{\sigma_N}\right) + \frac{1}{8}\Phi\left(-\frac{+D(k)-K_1(k)-K_2(k)+I(k)}{\sigma_N}\right)$$
$$+\frac{1}{8}\Phi\left(-\frac{+D(k)+K_1(k)+K_2(k)+I(k)}{\sigma_N}\right) + \frac{1}{8}\Phi\left(-\frac{+D(k)-K_1(k)+K_2(k)+I(k)}{\sigma_N}\right)$$
$$+\frac{1}{8}\Phi\left(\frac{-D(k)+K_1(k)-K_2(k)+I(k)}{\sigma_N}\right) + \frac{1}{8}\Phi\left(\frac{-D(k)-K_1(k)-K_2(k)+I(k)}{\sigma_N}\right)$$
$$+\frac{1}{8}\Phi\left(\frac{-D(k)+K_1(k)+K_2(k)+I(k)}{\sigma_N}\right) + \frac{1}{8}\Phi\left(\frac{-D(k)-K_1(k)+K_2(k)+I(k)}{\sigma_N}\right)$$

Figure B.2. Generation of the average probability of bit error for a transmitted BPSK signal through the two-path channel model with $\tau_\Delta > T$ and additive CW interference and AWGN.

$$D(k) = H_1\sqrt{2S}\,T$$
$$K_1(k) = H_2\sqrt{2S}\;((\gamma+1)T - \tau_\Delta)\cos(2\pi f_c(\tau_\Delta - \gamma T))$$
$$K_2(k) = H_2\sqrt{2S}\;(\tau_\Delta - \gamma T)\cos(2\pi f_c(\tau_\Delta - (\gamma+1)T))$$
$$\sigma_N^2 = N_0 T$$

transmitted signal power = S
interference power = $N_B B$
in-band noise power = $\left(\frac{2}{T}\right)\left(\frac{N_0}{2}\right) = \frac{N_0}{T}$

$$\sigma_I^2 = \frac{N_B}{\pi}\,T\left[Si(\pi(B-2f_\Delta)T) + \frac{\cos(\pi(B-2f_\Delta)T)-1}{\pi(B-2f_\Delta)T}\right]$$
$$+\frac{N_B}{\pi}\,T\left[Si(\pi(B+2f_\Delta)T) + \frac{\cos(\pi(B+2f_\Delta)T)-1}{\pi(B+2f_\Delta)T}\right]$$
$$\sigma_{I+N} = \sqrt{\sigma_N^2 + \sigma_I^2}$$
$$P_e = \frac{1}{4}\Phi\left(-\frac{+D(k)+K_1(k)-K_2(k)}{\sigma_N}\right) + \frac{1}{4}\Phi\left(-\frac{+D(k)-K_1(k)-K_2(k)}{\sigma_N}\right)$$
$$+\frac{1}{4}\Phi\left(-\frac{+D(k)+K_1(k)+K_2(k)}{\sigma_N}\right) + \frac{1}{4}\Phi\left(-\frac{+D(k)-K_1(k)+K_2(k)}{\sigma_N}\right)$$

Figure B.3. Generation of the average probability of bit error for a transmitted BPSK signal through the two-path channel model with $\tau_\Delta > T$ and additive finite bandwidth interference and AWGN.

REFERENCE

[1] Axford, R.A. "Effects of CW- and BPSK-Signal Interference on a Standard BPSK Digital Communications System," NRaD Technical Report 1510. NCCOSC, RDT&E Division, San Diego, CA, August 1992.

APPENDIX C - PERFORMANCE ANALYSIS OF M-PSK SIGNAL FOR $\tau_\Delta > T$

This appendix augments chapter 4 by presenting an analysis of the average probability of symbol error for a M-PSK signal transmitted through the two-path channel with $\tau_\Delta > T$. All other assumption are the same as in chapter 4.

Using the two-path multipath channel model described in section 2.3, $H(t) = H_1\delta(t) + H_2\,\delta(t - \tau_\Delta)$, the received signal can be expressed as

$$R(t) = H_1 S(t) + H_2 S(t-\tau_\Delta) + I(t) + N(t). \tag{C.1}$$

The M-PSK transmitted bandpass signal can be written as

$$S(t) = \sqrt{2S} \sum_k \left[a_k \cos(2\pi f_c t) - b_k \sin(2\pi f_c t)\right] P_T(t - kT) \tag{C.2}$$

where $\theta_k \in \left\{\frac{2\pi}{M}\ (i-1)\right\}$ for $i = 1,\ldots,M$ is the phase of the kth M-PSK symbol, $a_k = \cos(\theta_k)$, $b_k = \sin(\theta_k)$, S is the transmitted signal power, and $P_T(t)$ the symbol pulse waveform. At most, one-symbol transition of the multipath signal can take place in the interval $[0, T]$ of the direct path signal. The following analysis will consider the case of $\gamma\ T \le \tau_\Delta \le (\gamma + 1)T$ where $\gamma \in \{1, 2, 3, \ldots\}$ as shown in figure B.1. For $\tau_\Delta = T$ and $\gamma = 1$, the results in this appendix reduce to those in chapter 4. To simplify the notation in the following let $\tau_1 = \tau_\Delta - \gamma T$ and $\tau_2 = (\gamma + 1)T - \tau_\Delta$, which corresponds to the duration of the $s_{k-(\gamma+1)}$ and $s_{k-\gamma}$ multipath symbols in the interval $[0,T]$ respectively. The received signal during the interval [0,T] can be written as,

$$\begin{aligned}
R(t) &= H_1\sqrt{2S}\left[a_k\cos(2\pi f_c t) - b_k\sin(2\pi f_c t)\right] P_T(t) \\
&\quad + H_2\sqrt{2S}\left[a_{k-\gamma}\cos(2\pi f_c(t-\tau_1)) - b_{k-\gamma}\sin(2\pi f_c(t-\tau_1))\right] P_T(t-\tau_1) \\
&\quad + H_2\sqrt{2S}\left[a_{k-(\gamma+1)}\cos(2\pi f_c(t-\tau_2)) - b_{k-(\gamma+1)}\sin(2\pi f_c(t-\tau_2))\right] P_T(t-\tau_2) \\
&\quad + I(t) + N(t), \\
&= \Big[H_1\sqrt{2S}\ a_k P_T(t) + H_2\sqrt{2S}\left\{a_{k-\gamma}\cos(2\pi f_c\tau_1) + b_{k-\gamma}\sin(2\pi f_c\tau_1)\right\} P_T(t-\tau_1) \\
&\quad + H_2\sqrt{2S}\left\{a_{k-(\gamma+1)}\cos(2\pi f_c\tau_2) + b_{k-(\gamma+1)}\sin(2\pi f_c\tau_2)\right\} P_T(t-\tau_2)\Big]\cos(2\pi f_c t) \\
&\quad - \Big[H_1\sqrt{2S}\ b_k P_T(t) + H_2\sqrt{2S}\left\{-a_{k-\gamma}\sin(2\pi f_c\tau_1) + b_{k-\gamma}\cos(2\pi f_c\tau_1)\right\} P_T(t-\tau_1) \\
&\quad + H_2\sqrt{2S}\left\{-a_{k-(\gamma+1)}\sin(2\pi f_c\tau_2) + b_{k-(\gamma+1)}\cos(2\pi f_c\tau_2)\right\} P_T(t-\tau_2)\Big]\sin(2\pi f_c t) \\
&\quad + I(t) + N(t)
\end{aligned} \tag{C.3}$$

using trigonometric identities. Note that for $\tau_\Delta > T$, the multipath looks like an uncorrelated M-PSK interference with equal data rate and zero offset frequency since the two multipath bits are uncorrelated with the direct path bit in the interval $[0,T]$.

C.1 MATCHED-FILTER DETECTION OF M-PSK WITH CW INTERFERENCE

This section derives the probability of symbol error for the received signal given by eq. (C.3) with CW interference, $I(t) = \sqrt{2I}\ \cos(2\pi(f_c + f_\Delta)t + \phi)$. Without loss of generality, consider the

interval $[0,T]$. The output of the in-phase integrator, $\hat{s}_x(k)$, and the output of the quadrature-phase integrator, $\hat{s}_y(k)$, in figure 4.1 can be written as,

$$\begin{aligned}\hat{s}_x(k) &= \int_0^T R(t)\ 2\cos(2\pi f_c t)\ dt \\ &= a_k\, D(k) + a_{k-\gamma}\, K_1(k) + b_{k-\gamma}\, L_1(k) + a_{k-(\gamma+1)}\, K_2(k) + b_{k-(\gamma+1)}\, L_2(k) + I_x(k) + N_x(k)\end{aligned} \tag{C.4}$$

$$\begin{aligned}\hat{s}_y(k) &= \int_0^T R(t)\ 2\sin(2\pi f_c t)\ dt \\ &= b_k\, D(k) + b_{k-\gamma}\, K_1(k) - a_{k-\gamma}\, L_1(k) + b_{k-(\gamma+1)}\, K_2(k) - a_{k-(\gamma+1)}\, L_2(k) + I_y(k) + N_y(k)\end{aligned} \tag{C.5}$$

The only random term in eq. (C.4) (eq. (C.5)) that is not being conditioned on is the Gaussian random variable, $N_x(k)$ ($N_y(k)$). Thus, $\hat{s}_x(k)$ and $\hat{s}_y(k)$ will be uncorrelated, conditionally Gaussian random variables with variance

$$\sigma^2_{\hat{s}_x} = \sigma^2_{\hat{s}_y} = \sigma^2_N = N_0 T \tag{C.6}$$

as was derived in section 4.2 and mean

$$m_{\hat{s}_x} = a_k\, D(k) + a_{k-\gamma}\, K_1(k) + b_{k-\gamma}\, L_1(k) + a_{k-(\gamma+1)}\, K_2(k) + b_{k-(\gamma+1)}\, L_2(k) + I_x(k) \tag{C.7}$$

$$m_{\hat{s}_y} = b_k\, D(k) + b_{k-\gamma}\, K_1(k) - a_{k-\gamma}\, L_1(k) + b_{k-(\gamma+1)}\, K_2(k) - a_{k-(\gamma+1)}\, L_2(k) + I_y(k). \tag{C.8}$$

The deterministic terms in eqs.(C.4) and (C.5) can be shown to be equal to

$$D(k) = H_1 \sqrt{2S}\, T \tag{C.9}$$

$$K_1(k) = H_2 \sqrt{2S}\ \big((\gamma+1)T - \tau_\Delta\big) \cos\big(2\pi f_c(\tau_\Delta - \gamma T)\big) \tag{C.10}$$

$$K_2(k) = H_2 \sqrt{2S}\ \big(\tau_\Delta - \gamma T\big) \cos\big(2\pi f_c(\tau_\Delta - (\gamma+1)T)\big) \tag{C.11}$$

$$L_1(k) = H_2 \sqrt{2S}\ \big((\gamma+1)T - \tau_\Delta\big) \sin\big(2\pi f_c(\tau_\Delta - \gamma T)\big) \tag{C.12}$$

$$L_2(k) = H_2 \sqrt{2S}\ \big(\tau_\Delta - \gamma T\big) \sin\big(2\pi f_c(\tau_\Delta - (\gamma+1)T)\big) \tag{C.13}$$

$$I_x(k) = \sqrt{2I}\ \frac{\big[\sin(2\pi f_\Delta T + \phi) - \sin(\phi)\big]}{2\pi f_\Delta} \tag{C.14}$$

$$I_y(k) = \sqrt{2I}\ \frac{\big[\cos(2\pi f_\Delta T + \phi) - \cos(\phi)\big]}{2\pi f_\Delta}. \tag{C.15}$$

The conditional probability of symbol error, given the parameters of the channel model and interference parameters, is given by

$$P_s(H_1, H_2, \tau_\Delta, I, f_\Delta, \phi) = \sum_{j=1}^{M} \frac{1}{M}\ P_s(s_j \mid H_1, H_2, \tau_\Delta, I, f_\Delta, \phi) \tag{C.16}$$

for equal probabilities of transmitting each of the M symbols. Recall that the probability of detecting a symbol error, P_s, is equal to one minus the probability of detecting a correct symbol, P_c. Thus, for the case when $\tau_\Delta > T$, we can express the conditional probability of symbol error given that the symbol s_j was transmitted as

$$P_s(s_j|H_1,H_2,\tau_\Delta,I,f_\Delta,\phi) = 1-P_c(s_j|H_1,H_2,\tau_\Delta,I,f_\Delta,\phi),$$

$$= 1 - \sum_{l=1}^{M}\sum_{i=1}^{M}\frac{1}{M^2}\Pr\left(\theta_1^j < \hat{\theta}(k) \le \theta_2^j \mid s_{k-(\gamma+1)} = s_i\ ,\ s_{k-\gamma} = s_l\ ,\ s_k = s_j\right) \quad \text{(C.17)}$$

where θ_1^j and θ_2^j are the angles of the lower and upper decision boundaries respectively for s_j. Using the same techniques as was used in chapter 4, eq. (C.17) can be written as

$$P_s(s_j|H_1,H_2,\tau_\Delta,I,f_\Delta,\phi) = 1 - \sum_{l=1}^{M}\sum_{i=1}^{M}\frac{1}{M^2}\int_{\theta_1^j}^{\theta_2^j} pdf_{\hat{\theta}}\left(\theta \mid s_{k-(\gamma+1)} = s_i\ ,\ s_{k-\gamma} = s_l\ ,\ s_k = s_j\right) d\theta \quad \text{(C.18)}$$

where

$$pdf_{\hat{\theta}}(\theta) = \frac{1}{2\pi}\, e^{-\frac{m_x^2+m_y^2}{2\sigma_N^2}} + \frac{m_x\cos(\theta) + m_y\sin(\theta)}{\sqrt{2\pi}\,\sigma_N}\, e^{-\frac{(m_x\sin(\theta)-m_y\cos(\theta))^2}{2\sigma_N^2}}\,\Phi\left(\frac{m_x\cos(\theta) + m_y\sin(\theta)}{\sigma_n}\right). \quad \text{(C.19)}$$

By using an upper bound for the phi function, eq. (C.19) was bounded in chapter 4, which can then be used to find the following upper bound of eq. (C.18),

$$P_s(s_j|H_1,H_2,\tau_\Delta,I,f_\Delta,\phi) \le 1 - \sum_{l=1}^{M}\sum_{i=1}^{M}\frac{1}{M^2}\left\{\Phi\left[\frac{m_x\sin\theta_2^j - m_y\cos\theta_2^j}{\sigma_N}\right] - \Phi\left[\frac{m_x\sin\theta_1^j - m_y\cos\theta_1^j}{\sigma_N}\right]\right\} \quad \text{(C.20)}$$

where m_x and m_y are dependent on both the l, i and j index through the present direct path symbol $s_k = s_j$ and the past multipath symbols $s_{k-(\gamma+1)} = s_i$ and $s_{k-\gamma} = s_l$ and are given by eqs. (C.7) and (C.8). Using eq. (C.20) in eq. (C.16), we find that the average conditional probability of symbol error can be written as,

$$P_s(H_1,H_2,\tau_\Delta,I,f_\Delta,\phi) \le 1 - \sum_{j=1}^{M}\sum_{l=1}^{M}\sum_{i=1}^{M}\frac{1}{M^3}\left\{\Phi\left[\frac{m_x\sin\theta_2^j - m_y\cos\theta_2^j}{\sigma_N}\right] - \Phi\left[\frac{m_x\sin\theta_1^j - m_y\cos\theta_1^j}{\sigma_N}\right]\right\} \quad \text{(C.21)}$$

where m_x and m_y are given by eqs. (C.7) and (C.8) using eqs. (C.9)–(C.14) and σ_N is given by eq. (C.6). Eqs. (C.21) and (C.20) are valid as long as $m_x\cos(\theta) + m_y\sin(\theta) > 0$ for all $\theta_1^j \le \theta \le \theta_2^j$.

C.2 MATCHED-FILTER DETECTION OF *M*-PSK WITH FINITE BANDWIDTH INTERFERENCE AND SUMMARY

When the probability of symbol error is the same for each symbol eq. (C.16) can be simplified to

$$P_s(H_1,H_2,\tau_\Delta,I,f_\Delta,\phi) = P_s(s_1 \mid H_1,H_2,\tau_\Delta,I,f_\Delta,\phi) \quad \text{(C.22)}$$

This can be shown to be true for either the case of multipath and additive white noise or the case of multipath with additive white noise and additive finite bandwidth interference. Under these cases

$$P_s(H_1,H_2,\tau_\Delta,I,f_\Delta,\phi) \le 1 - \sum_{l=1}^{M}\sum_{i=1}^{M}\frac{1}{M^2}\left\{\Phi\left[\frac{m_x\sin\theta_2^j - m_y\cos\theta_2^j}{\sigma_N}\right] - \Phi\left[\frac{m_x\sin\theta_1^j - m_y\cos\theta_1^j}{\sigma_N}\right]\right\} \quad \text{(C.23)}$$

where for finite bandwidth interference σ_N is replaced by σ_{I+N} given by

$$\sigma_{I+N}^2 = \sigma_I^2 + \sigma_N^2. \quad \text{(C.24)}$$

Recall that σ_I^2 was previously computed in section 3.3 and found to be

$$\sigma_I^2 = \frac{N_B}{\pi}\, T \left[Si\big(\pi(B - 2f_\Delta)T\big) + \frac{\cos\big(\pi(B - 2f_\Delta)T\big) - 1}{\pi(B - 2f_\Delta)T} \right] + \frac{N_B}{\pi}\, T \left[Si\big(\pi(B + 2f_\Delta)T\big) + \frac{\cos\big(\pi(B + 2f_\Delta)T\big) - 1}{\pi(B + 2f_\Delta)T} \right]. \tag{C.25}$$

Thus, all components in eq. (C.23) are known. Figures C.1 – C.3 summarize the equations derived in this appendix.

$D(k) = H_1 \sqrt{2S}\, T$ — transmitted signal power $= S$

$K_1(k) = H_2 \sqrt{2S}\ ((\gamma + 1)T - \tau_\Delta) \cos(2\pi f_c(\tau_\Delta - \gamma T))$

$K_2(k) = H_2 \sqrt{2S}\ (\tau_\Delta - \gamma T) \cos(2\pi f_c(\tau_\Delta - (\gamma + 1)T))$ — in-band noise power $= \left(\frac{2}{T}\right)\left(\frac{N_0}{2}\right) = \frac{N_0}{T}$

$L_1(k) = H_2 \sqrt{2S}\ ((\gamma + 1)T - \tau_\Delta) \sin(2\pi f_c(\tau_\Delta - \gamma T))$

$L_2(k) = H_2 \sqrt{2S}\ (\tau_\Delta - \gamma T) \sin(2\pi f_c(\tau_\Delta - (\gamma + 1)T))$

$a_k = \cos(0) = 1$

$b_k = \sin(0) = 0$

$\theta_2 = \frac{\pi}{2}$

$\theta_1 = -\frac{\pi}{2}$

$\sigma_N = \sqrt{N_0 T}$

$P_c = 0$

For l = 1:M

  $\theta = \frac{2\pi}{M}\ (l - 1)$

  $a_{k-\gamma} = \cos(\theta)$

  $b_{k-\gamma} = \sin(\theta)$

  For i = 1:M

    $\theta = \frac{2\pi}{M}\ (i - 1)$

    $a_{k-(\gamma+1)} = \cos(\theta)$

    $b_{k-(\gamma+1)} = \sin(\theta)$

    $m_x = a_k\, D(k) + a_{k-\gamma}\, K_1(k) + b_{k-\gamma}\, L_1(k) + a_{k-(\gamma+1)}\, K_2(k) + b_{k-(\gamma+1)}\, L_2(k)$

    $m_{i_y} = b_k\, D(k) + b_{k-\gamma}\, K_1(k) - a_{k-\gamma}\, L_1(k) + b_{k-(\gamma+1)}\, K_2(k) - a_{k-(\gamma+1)}\, L_2(k)$

    $P_c = P_c + \frac{1}{M^2} \left\{ \Phi\left[\frac{m_x \sin\theta_2 - m_y \cos\theta_2}{\sigma_N}\right] - \Phi\left[\frac{m_x \sin\theta_1 - m_y \cos\theta_1}{\sigma_N}\right] \right\}$

  EndFor

EndFor

$P_s = 1 - P_c$

Figure C.1. Generation of the average probability of symbol error for a transmitted M-PSK signal through the two-path channel model with $\tau_\Delta > T$ and AWGN.

$D(k) = H_1\sqrt{2S}\,T$

$K_1(k) = H_2\sqrt{2S}\ ((\gamma + 1)T - \tau_\Delta)\cos(2\pi f_c(\tau_\Delta - \gamma T))$

$K_2(k) = H_2\sqrt{2S}\ (\tau_\Delta - \gamma T)\cos(2\pi f_c(\tau_\Delta - (\gamma + 1)T))$

$L_1(k) = H_2\sqrt{2S}\ ((\gamma + 1)T - \tau_\Delta)\sin(2\pi f_c(\tau_\Delta - \gamma T))$

$L_2(k) = H_2\sqrt{2S}\ (\tau_\Delta - \gamma T)\sin(2\pi f_c(\tau_\Delta - (\gamma + 1)T))$

$I_x(k) = \sqrt{2I}\ \dfrac{[\sin(2\pi f_\Delta T + \phi) - \sin(\phi)]}{2\pi f_\Delta}$

$I_y(k) = \sqrt{2I}\ \dfrac{[\cos(2\pi f_\Delta T + \phi) - \cos(\phi)]}{2\pi f_\Delta}$

$\sigma_N = \sqrt{N_0 T}$

$P_c = 0$

For j = 1:M

$\theta = \dfrac{2\pi}{M}\ (j - 1)$

$a_k = \cos(\theta)$

$b_k = \sin(\theta)$

$\theta_2 = \dfrac{\pi}{M}\ (2j - 1)$

$\theta_1 = \dfrac{\pi}{M}\ (2j - 3)$

For l = 1:M

$\theta = \dfrac{2\pi}{M}\ (l - 1)$

$a_{k-\gamma} = \cos(\theta)$

$b_{k-\gamma} = \sin(\theta)$

For i = 1:M

$\theta = \dfrac{2\pi}{M}\ (i - 1)$

$a_{k-(\gamma+1)} = \cos(\theta)$

$b_{k-(\gamma+1)} = \sin(\theta)$

$m_x = a_k\, D(k) + a_{k-\gamma}\, K_1(k) + b_{k-\gamma}\, L_1(k) + a_{k-(\gamma+1)}\, K_2(k) + b_{k-(\gamma+1)}\, L_2(k) + I_x(k)$

$m_{i_y} = b_k\, D(k) + b_{k-\gamma}\, K_1(k) - a_{k-\gamma}\, L_1(k) + b_{k-(\gamma+1)}\, K_2(k) - a_{k-(\gamma+1)}\, L_2(k) + I_y(k)$

$P_c = P_c + \dfrac{1}{M^3}\left\{\Phi\left[\dfrac{m_x \sin\theta_2 - m_y \cos\theta_2}{\sigma_N}\right] - \Phi\left[\dfrac{m_x \sin\theta_1 - m_y \cos\theta_1}{\sigma_N}\right]\right\}$

EndFor

EndFor

EndFor

$P_s = 1 - P_c$

transmitted signal power = S

interference power = I

in-band noise power = $\left(\dfrac{2}{T}\right)\left(\dfrac{N_0}{2}\right) = \dfrac{N_0}{T}$

Figure C.2. Generation of the average probability of symbol error for a transmitted M-PSK signal through the two-path channel model with $\tau_\Delta > T$, additive C interference and AWGN.

$D(k) = H_1\sqrt{2S}\,T$

$K_1(k) = H_2\sqrt{2S}\ ((\gamma + 1)T - \tau_\Delta)\cos(2\pi f_c(\tau_\Delta - \gamma T))$

$K_2(k) = H_2\sqrt{2S}\ (\tau_\Delta - \gamma T)\cos(2\pi f_c(\tau_\Delta - (\gamma + 1)T))$

$L_1(k) = H_2\sqrt{2S}\ ((\gamma + 1)T - \tau_\Delta)\sin(2\pi f_c(\tau_\Delta - \gamma T))$

$L_2(k) = H_2\sqrt{2S}\ (\tau_\Delta - \gamma T)\sin(2\pi f_c(\tau_\Delta - (\gamma + 1)T))$

transmitted signal power $= S$

interference power $= N_B B$

in-band noise power $= \left(\frac{2}{T}\right)\left(\frac{N_0}{2}\right) = \frac{N_0}{T}$

$a_k = \cos(0) = 1$

$b_k = \sin(0) = 0$

$\theta_2 = \frac{\pi}{2}$

$\theta_1 = -\frac{\pi}{2}$

$\sigma_N^2 = N_0 T$

$$\sigma_I^2 = \frac{N_B}{\pi}\,T\left[Si(\pi(B - 2f_\Delta)T) + \frac{\cos(\pi(B - 2f_\Delta)T) - 1}{\pi(B - 2f_\Delta)T}\right] + \frac{N_B}{\pi}\,T\left[Si(\pi(B + 2f_\Delta)T) + \frac{\cos(\pi(B + 2f_\Delta)T) - 1}{\pi(B + 2f_\Delta)T}\right]$$

$\sigma_{I+N} = \sqrt{\sigma_N^2 + \sigma_I^2}$

$P_c = 0$

For l = 1:M

$\theta = \frac{2\pi}{M}\,(l - 1)$

$a_{k-\gamma} = \cos(\theta)$

$b_{k-\gamma} = \sin(\theta)$

For i = 1:M

$\theta = \frac{2\pi}{M}\,(i - 1)$

$a_{k-(\gamma+1)} = \cos(\theta)$

$b_{k-(\gamma+1)} = \sin(\theta)$

$m_x = a_k\,D(k) + a_{k-\gamma}\,K_1(k) + b_{k-\gamma}\,L_1(k) + a_{k-(\gamma+1)}\,K_2(k) + b_{k-(\gamma+1)}\,L_2(k)$

$m_{i_y} = b_k\,D(k) + b_{k-\gamma}\,K_1(k) - a_{k-\gamma}\,L_1(k) + b_{k-(\gamma+1)}\,K_2(k) - a_{k-(\gamma+1)}\,L_2(k)$

$$P_c = P_c + \frac{1}{M^2}\left\{\Phi\left[\frac{m_x\sin\theta_2 - m_y\cos\theta_2}{\sigma_{I+N}}\right] - \Phi\left[\frac{m_x\sin\theta_1 - m_y\cos\theta_1}{\sigma_{I+N}}\right]\right\}$$

EndFor

EndFor

$P_s = 1 - P_c$

Figure C.3. Generation of the average probability of symbol error for a transmitted M-PSK signal through the two-path channel model with $\tau_\Delta > T$, additive finite bandwidth interference and AWGN.

APPENDIX D – DERIVATIONS

DERIVATION OF EQ. (2.10)

Recall that the group delay is defined as $G(f) = -\frac{1}{2\pi}\frac{d\measuredangle H(f)}{df}$, thus we have

$$G(f) = -\frac{1}{2\pi}\frac{d}{df}\left\{\tan^{-1}\left[\frac{-H_2\sin(2\pi f\tau_\Delta)}{H_1 + H_2\cos(2\pi f\tau_\Delta)}\right]\right\}. \tag{D.1}$$

Letting $\omega = 2\pi f$, and recalling that

$$\frac{d\tan^{-1}(x)}{dx} = \frac{1}{1+x^2} \qquad \frac{d\sin(x)}{dx} = \cos(x) \qquad \frac{d\cos(x)}{dx} = -\sin(x)$$

we find,

$$G(f) = \frac{1}{1 + \frac{H_2^2\sin^2(\omega\tau_\Delta)}{[H_1 + H_2\cos(\omega\tau_\Delta)]^2}}\ \frac{d}{d\omega}\left\{\frac{H_2\sin(\omega\tau_\Delta)}{H_1 + H_2\cos(\omega\tau_\Delta)}\right\}. \tag{D.2}$$

It can be shown with some elementary calculus that,

$$\frac{d}{d\omega}\left\{\frac{H_2\sin(\omega\tau_\Delta)}{H_1 + H_2\cos(\omega\tau_\Delta)}\right\} = H_2\,\Delta\tau\,\frac{H_2 + H_1\cos(\omega\tau_\Delta)}{\left[H_1 + H_2\cos(\omega\tau_\Delta)\right]^2}. \tag{D.3}$$

Thus, we find by using eq. (D.3) in eq. (D.2),

$$\boxed{G(f) = H_2\,\Delta\tau\left[\frac{H_2 + H_1\cos(2\pi f\tau_\Delta)}{H_1^2 + H_2^2 + 2H_1H_2\cos(2\pi f\tau_\Delta)}\right]} \tag{D.4}$$

DERIVATION OF CHERNOFF BOUND FOR COMPARISON TO EQ. (4.18)

The Chernoff bound of the phi function is defined as

$$\begin{aligned}\Phi(-x) &\equiv \frac{1}{\sqrt{2\pi}}\int_x^\infty e^{-t^2/2}\,dt \\ &\le E\left[e^{\lambda(X-x)}\right]\end{aligned} \tag{D.5}$$

for X equal to a zero mean, unity variance Gaussian random variable. The tightest upper bound is obtained by finding λ that minimizes $E\left[e^{\lambda(X-x)}\right]$. This is found by setting the derivative of $E\left[e^{\lambda(X-x)}\right]$ with respect to λ to zero and solving for λ. The resulting equation to be solved is

$$E\left[X\,e^{\lambda X}\right] - x\,E\left[e^{\lambda X}\right] = 0. \tag{D.6}$$

This can be solved by noting that (see for example section 3.1 of [1]).

$$E\left[X\, e^{\lambda X}\right] = \int_{-\infty}^{\infty} t\, e^{\lambda t} \frac{1}{\sqrt{2\pi}}\, e^{-t^2/2}\, dt$$

$$= \frac{e^{\lambda^2/2}}{\sqrt{2\pi}} \left\{ \int_{-\infty}^{\infty} (y + \lambda)\, e^{-y^2/2} \right\} dy \tag{D.7}$$

by first completing the square in the exponent and then letting $y = t - \lambda$. The first term is an odd function and thus, its integral is equal to zero. The second term is just the integral of the Gaussian probability density function and so is equal to unity. Thus, we find

$$E\left[X\, e^{\lambda X}\right] = \lambda\, e^{\lambda^2/2}. \tag{D.8}$$

Similarly, it can be shown that

$$E\left[e^{\lambda X}\right] = e^{\lambda^2/2}. \tag{D.9}$$

Using eqs.(D.8) and (D.9) in eq. (D.6), we find that the value of λ that minimizes the bound is $\lambda_{\min} = x$. Thus, with this value of λ in eq. (D.5) and using the result of eq. (D.9), we find the Chernoff Bound of the phi function is

$$\Phi(-x) \le e^{-\frac{x^2}{2}}. \tag{D.10}$$

REFERENCE

[1] Stark, H., and J. Woods. *Probability, Random Processes, and Estimation Theory for Engineers,* Prentice-Hall, Englewood Cliffs, New Jersey. 1986.

REPORT DOCUMENTATION PAGE

Form Approved
OMB No. 0704-0188

Public reporting burden for this collection of information is estimated to average 1 hour per response, including the time for reviewing instructions, searching existing data sources, gathering and maintaining the data needed, and completing and reviewing the collection of information. Send comments regarding this burden estimate or any other aspect of this collection of information, including suggestions for reducing this burden, to Washington Headquarters Services, Directorate for Information Operations and Reports, 1215 Jefferson Davis Highway, Suite 1204, Arlington, VA 22202-4302, and to the Office of Management and Budget, Paperwork Reduction Project (0704-0188), Washington, DC 20503.

1. AGENCY USE ONLY *(Leave blank)*	2. REPORT DATE November 1993	3. REPORT TYPE AND DATES COVERED Final: Oct 1992 – Sep 1993
4. TITLE AND SUBTITLE THE EFFECTS OF A MULTIPATH CHANNEL AND INTERFERENCE ON COHERENT *M*-PSK DIGITAL COMMUNICATION SYSTEMS		5. FUNDING NUMBERS PE: 0602232N, 0602234N PROJ: RC32W11 SUBPROJ: 82-CHB5-06 ACC: DN300107
6. AUTHOR(S) R. C. North, R. A. Axford, and D. Bryan		
7. PERFORMING ORGANIZATION NAME(S) AND ADDRESS(ES) Naval Command, Control and Ocean Surveillance Center (NCCOSC) RDT&E Division San Diego, CA 92152-5001		8. PERFORMING ORGANIZATION REPORT NUMBER TR 1636
9. SPONSORING/MONITORING AGENCY NAME(S) AND ADDRESS(ES) Office of the Chief of Naval Research 800 N. Quincy Street Arlington, VA 22217-5660		10. SPONSORING/MONITORING AGENCY REPORT NUMBER
11. SUPPLEMENTARY NOTES		
12a. DISTRIBUTION/AVAILABILITY STATEMENT Approved for public release; distribution is unlimited.		12b. DISTRIBUTION CODE

13. ABSTRACT *(Maximum 200 words)*

This report derives expressions for the average probability of symbol error of a coherent *M*-ary phase-shift-keyed (*M*-PSK) communication system operating under the following nonideal conditions: (1) time-invariant multipath channel consisting of a direct path and a single multipath, (2) intentional/unintentional interference consisting of either a continuous wave (CW) signal or a bandpass filtered white Gaussian noise signal (bandwidth is variable), and (3) additive white Gaussian noise. Exact solutions are derived for coherent binary phase shift-keyed (BPSK) while both exact and upper bound solutions (shown to be tighter than the Chernoff bound) are derived for coherent *M*-PSK. One particular example, line-of-sight ultrahigh frequency (LOS UHF) radio, is used extensively to exercise the derived expressions and illustrate typical system performance.

These results pertain to a receiver with no means of compensation for the nonideal channel conditions. Methods of compensation for multipath and interference, like adaptive equalization, beamforming, spatial diversity, and multichannel adaptive equalization, are presently under investigation by the authors. The results in this report will help determine the performance gain offered by these methods of compensation.

14. SUBJECT TERMS *M*-PSK digital radio probability of symbol error multipath interference			15. NUMBER OF PAGES 83 16. PRICE CODE
17. SECURITY CLASSIFICATION OF REPORT UNCLASSIFIED	18. SECURITY CLASSIFICATION OF THIS PAGE UNCLASSIFIED	19. SECURITY CLASSIFICATION OF ABSTRACT UNCLASSIFIED	20. LIMITATION OF ABSTRACT SAME AS REPORT

21a. NAME OF RESPONSIBLE INDIVIDUAL	21b. TELEPHONE (Include Area Code)	21c. OFFICE SYMBOL
Richard C. North	(619) 553-4323	Code 824

INITIAL DISTRIBUTION

Code 0012	Patent Counsel	(1)
Code 0274B	Library	(2)
Code 0275	Archive/Stock	(6)
Code 563	D. Bryan	(10)
Code 80	K. D. Regan	(1)
Code 804	J. R. Zeidler	(1)
Code 802	R. D. Peterson	(1)
Code 824	P. D. Donich	(1)
Code 824	C. S. Fuzak	(1)
Code 824	R. J. Kochanski	(1)
Code 824	J. B. Rhode	(1)
Code 824	R. C. North	(10)
Code 844	R. A. Axford	(10)

Defense Technical Information Center
Alexandria, VA 22304–6145 (4)

NCCOSC Washington Liaison Office
Washington, DC 20363–5100

Center for Naval Analyses
Alexandria, VA 22302–0268

Navy Acquisition, Research and Development
Information Center (NARDIC)
Arlington, VA 22244–5114

GIDEP Operations Center
Corona, CA 91718–8000

NCCOSC Division Detachment
Warminster, PA 18974–5000

Office of Naval Research
Arlington, VA 22217–5000 (2)